

# ACTA GEO TECHNICA S LOVENICA

2013/2

**g. dolinar & s. škrabl**  
ATTERBERG LIMITS IN RELATION TO OTHER  
PROPERTIES OF FINE-GRAINED SOILS

**v. jagodnik et al.**  
ON THE APPLICATION OF A MIXED FINITE-ELEMENT APPROACH TO  
BEAM-SOIL INTERACTION

**o. sivrikaya et al.**  
PREDICTION OF THE COMPACTION PARAMETERS FOR COARSE-GRAINED  
SOILS WITH FINES CONTENT BY MLR AND GEP

**g. ebrahimian & a. nazari**  
EVOLUTIONARY-BASED PREDICTION OF  $\epsilon_{50}$  FOR THE LATERAL  
LOAD-DISPLACEMENT BEHAVIOR OF PILES IN CLAYS

**s. kadali et al.**  
INVESTIGATIONS TO ESTABLISH THE INFLUENCE OF THE THERMAL  
ENERGY FIELD ON SOIL PROPERTIES



**ustanovitelji** **founders**

Univerza v Mariboru, Fakulteta za gradbeništvo  
University of Maribor, Faculty of Civil Engineering

Univerza v Ljubljani, Fakulteta za gradbeništvo in geodezijo  
University of Ljubljana, Faculty of Civil and Geodetic Engineering

Univerza v Ljubljani, Naravoslovnotehniška fakulteta  
University of Ljubljana, Faculty of Natural Sciences and Engineering

Slovensko geotehniško društvo  
Slovenian Geotechnical Society

Društvo za podzemne in geotehniške konstrukcije  
Society for Underground and Geotechnical Constructions

**izdajatelj** **publisher**

Univerza v Mariboru, Fakulteta za gradbeništvo  
University of Maribor, Faculty of Civil Engineering

**odgovorni urednik** **editor-in-chief**

Ludvik Trauner University of Maribor

**uredniki** **co-editors**

Bojana Dolinar University of Maribor  
Borut Macuh University of Maribor  
Stanislav Škrabl University of Maribor  
Helena Vrecl Kojc University of Maribor  
Bojan Žlender University of Maribor

**posvetovalni uredniki** **advisory editors**

Darinka Battelino University of Trieste  
Heinz Brandl Vienna University of Technology  
Chandrakant. S. Desai University of Arizona  
Pedro Seco e Pinto National Laboratory of Civil Engineering

**lektor** **proof-reader**

Paul McGuiness

**naklada** **circulation**

300 izvodov - issues

**cena** **price**

25 EUR/izvod - 25 EUR/issue; (50 EUR for institutions/za institucije)

**tisk** **print**

ROLGRAF tiskarna Medvode d.o.o.

Revija redno izhaja dvakrat letno. Članki v reviji so recenzirani s strani priznanih mednarodnih strokovnjakov. Baze podatkov v katerih je revija indeksirana: SCIE - Science Citation Index Expanded, JCR - Journal Citation Reports / Science Edition, ICONDA - The international Construction database, GeoRef. Izid publikacije je finančno podprla Javna agencija za raziskovalno dejavnost Republike Slovenije iz naslova razpisa za sofinanciranje domačih periodičnih publikacij.

**uredniški odbor** **editorial board**

Amin Barari Aalborg University  
Theodoros Hatzigogos Aristotle University of Thessaloniki  
Vojkan Jovičič IRGO-Ljubljana, President of the SloGeD  
Rolf Katzenbach Technical University Darmstadt  
Nasser Khalili The University of New South Wales, Sydney  
Jakob Likar University of Ljubljana  
Janko Logar University of Ljubljana  
Bojan Majes University of Ljubljana  
Milan Maksimović University of Belgrade  
Borut Petkovšek Slovenian National Building and Civil Engineering Institute  
Mihael Ribičič University of Ljubljana  
César Sagaseta University of Cantabria  
Patrick Selvadurai McGill University  
Stephan Semprich University of Technology Graz  
Devendra Narain Singh Indian Institute of Technology, Bombay  
Abdul-Hamid Soubra University of Nantes  
Kiirchi Suzuki Saitama University  
Antun Szavits-Nossan University of Zagreb  
Ivan Vaniček Czech Technical University in Prague  
Jianhua Yin The Hong Kong Polytechnic University

**naslov uredništva** **address**

ACTA GEOTECHNICA SLOVENICA  
Univerza v Mariboru, Fakulteta za gradbeništvo  
Smetanova ulica 17, 2000 Maribor, Slovenija  
Telefon / Telephone: +386 (0)2 22 94 300  
Faks / Fax: +386 (0)2 25 24 179  
E-pošta / E-mail: ags@uni-mb.si

**spletni naslov** **web address**

<http://www.fg.uni-mb.si/journal-ags/>

The journal is published twice a year. Papers are peer reviewed by renowned international experts. Indexation data bases of the journal: SCIE - Science Citation Index Expanded, JCR - Journal Citation Reports / Science Edition, ICONDA - The international Construction database, GeoRef. The publication was financially supported by Slovenian Research Agency according to the Tender for co-financing of domestic periodicals.

## VSEBINA

2	Ludvik Trauner UVODNIK
4	bojana dolinar in stanislav škrabl SOODVISNOSTI MED ATTERBERGOVIMI MEJAMI IN DRUGIMI FIZIKALNIMI LASTNOSTMI VEZLJIVIH ZEMLJIN
14	vedran jagodnik in drugi UPORABA MEŠANE METODE KONČNIH ELEMENTOV PRI INTERAKCIJI NOSILEC-TLA
28	osman sivrikaya in drugi NAPOVED PARAMETROV KOMPRESIJE GROBO ZANATIH ZEMLJIN Z VSEBNOSTJO DROBNIH DELCEV Z UPORABO MLR IN GEP
42	babak ebrahimian in aida nazari EVOLUCIJSKA-OSNOVNA NAPOVED $\epsilon_{50}$ PRI POMIKIH PILOTOV V GLINI ZARADI BOČNE OBREMENITVE
58	srinivas kadali in drugi PREISKAVE VPLIVA TOPLOTNO ENERGETSKIH POLJ NA LASTNOSTI ZEMLJIN
78	NAVODILA AVTORJEM

## CONTENTS

Ludvik Trauner EDITORIAL	3
bojana dolinar and stanislav škrabl ATTERBERG LIMITS IN RELATION TO OTHER PROPERTIES OF FINE-GRAINED SOILS	5
vedran jagodnik et al. ON THE APPLICATION OF A MIXED FINITE-ELEMENT APPROACH TO BEAM-SOIL INTERACTION	15
osman sivrikaya et al. PREDICTION OF THE COMPACTION PARAMETERS FOR COARSE-GRAINED SOILS WITH FINES CON- TENT BY MLR AND GEP	29
babak ebrahimian and aida nazari EVOLUTIONARY-BASED PREDICTION OF $\epsilon_{50}$ FOR THE LATERAL LOAD-DISPLACEMENT BEHAVIOR OF PILES IN CLAYS	43
srinivas kadali et al. INVESTIGATIONS TO ESTABLISH THE INFLUENCE OF THE THERMAL ENERGY FIELD ON SOIL PROPERTIES	59
INSTRUCTIONS FOR AUTHORS	79

---

# UVODNIK

---

V letu 2004 je bila Republika Slovenija sprejeta v Evropsko Unijo. Takrat je izšla prva številka mednarodne revije Acta Geotechnica Slovenica (AGS). Samostojno jo izdaja Katedra za geotehniko pod streho Fakultete za gradbeništvo Univerze v Mariboru. Sedaj slavimo njeno 10. obletnico; prehojeno dolgo pot, ki je bila včasih težavna. A s priznanimi domačimi in tujimi souredniki ter recenzenti smo uspeli vse težave premagati in doseči primerljivo kakovostno raven, kar izkazuje tudi bibliografska baza podatkov SCIE in JCR. Vsako leto izideta dve redni številki. S pričujočo izdajo je bilo doslej natisnjenih 19 števil AGS, v katerih je izšlo že 88 znanstvenih člankov, ki dajejo široki strokovni sferi geotehnike precejšen doprinos znanja. Letno narašča interes avtorjev za objavo prispevkov v AGS (letos smo jih dobili že 65). Zato želimo prihodnje leto pričeti z izdajo dodatnih izbranih publikacij. Ob 10-letnem jubileju ima revija AGS optimistično prihodnost.

V tej številki objavljamo pet znanstvenih prispevkov:

V prvem članku avtorja, Bojana Dolinar in Stanislav Škrabl, pojasnjujeta najpomembnejše razloge zakaj za nabreklijve in ne-nabreklijve koherentne zemljine ne morejo obstajati enotna razmerja med Atterbergovimi konsistenčnimi mejami (ki predstavljajo skupno količino porne in adsorbirane vode) in drugimi fizikalnimi lastnostmi. V prispevku so predstavljene nekatere možnosti uporabe mej židkosti in plastičnosti pri napovedovanju fizikalnih lastnosti tal.

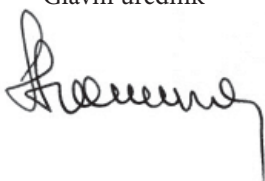
V drugem članku avtorji, Vedran Jagodnik, Gordan Jelenic in Željko Arbanas, podajajo pregled deformacij Bernoullijevega nosilca na Winklerjevi zemljini z uporabo mešane metode končnih elementov. Članek pokaže, da je najmanj konvergenten element z enim poljem, ki temelji na pomikih, medtem ko je element mešanega tipa s štirimi interpoliranimi polji najbolj konvergenten.

V tretjem članku avtorji, Osman Sivrikaya, Cafer Kayadelen in Emre Cecen, podajajo korelacije za ocenitev parametrov komprimiranja v odvisnosti od energije stiskanja grobo zrnatih zemljin z različno vsebnostjo drobnih delcev. Rezultati raziskave prikazujejo, da so modeli GEP (genetsko programiranje) in MLR (multi-linerna regresivna analiza) precej uporabni za napovedovanje največje suhe prostorninske mase in optimalne vlažnosti nekohezijskih zemljin z različno vsebnostjo drobnih delcev pri energiji stiskanja s standardnimi (SP) in modificiranimi (MP) Proctorjevimi preizkusi.

V četrtem članku avtorja, Babak Ebrahimian in Aida Nazari, analizirata pilote, ki so izpostavljeni bočnim obremenitvam in njihovo obnašanje je odvisno od odpornosti tal, kot funkcija odklona pilota. Preučevala sta učinke nedrenirane strižne trdnosti, normalizirane odpornosti zemljine pri penetracijskem preizkusu, presežnega pritiska, indeksa plastičnosti in prekonsolidacijskega razmerja na deformacijo zemljin pri 50% maksimalnem deviatornem pritisku v morskih glinah. Dokazala sta, da privede normalizirana odpornost zemljin pod konico pilota do realnejših vrednosti, v primerjavi z laboratorijsko dobljenim parametrom nedrenirane strižne trdnosti.

V petem članku avtorji, Srinivas Kadali, Susha Lekshmi S.U., Susmita Sharma in Devendra Narain Singh, opisujejo podrobnosti študije o preiskavah zemljin in njihovih spremembah pri povišanih temperaturah. Na osnovi kritične sinteze rezultatov so dokazali, da povišane temperature povzročijo fizikalne, kemične in mineraloške spremembe zemljin: (i) spremembo barve, (ii) povečanje specifične teže, velikosti delcev in izgubo teže, (iii) zmanjšanje specifične površine, sposobnosti kationske izmenjave in zeta potenciala in (iv) strukturne spremembe zemljin.

Ludvik Trauner  
Glavni urednik



---

# EDITORIAL

---

In 2004 Slovenia was accepted into the European Union. At the same time the first issue of the international journal of Acta Geotechnica Slovenica (AGS) was published by the Chair of Geotechnical Engineering as part of the Faculty of Civil Engineering, University of Maribor. We are now celebrating our 10-year anniversary; it has been a long and sometimes difficult journey. However, with recognized domestic and foreign co-editors and reviewers, we managed to overcome all the difficulties and to achieve a level of quality that is demonstrated by the bibliographic database SCIE and JCR. Each year of publication brings two regular editions. With the present edition we have now printed 19 editions of AGS, which means 88 scientific articles. This means that across a wide professional sphere Geotechnics has made a significant contribution to knowledge. Each year there is a growing interest by authors to publish contributions to the AGS (this year we already have 65). Therefore, next year we want to start issuing additional selected publications. So, on this 10-year anniversary, AGS is optimistic about the future.

In this edition there are five scientific contributions:

In the first article, the authors Bojana Dolinar and Stanislav Škrabl explain the main reasons why in swelling and non-swelling coherent soils there can be no uniform relationship between Atterberg's consistency limits (representing the total quantity of pore and adsorbed water) and other physical properties. This paper presents some possibilities for using the limits of viscosity and plasticity in predicting the physical properties of soils.

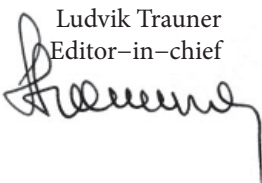
In the second article, the authors Vedran Jagodnik, Gordan Jelenic and Zeljko Arbanas provide an overview of the deformation of a Bernoulli beam resting on Winkler's soil using a mixed finite-element method. The article shows that the displacement-based one-field element is the least convergent, while the mixed-type element with four interpolated fields is the most convergent.

In the third article, the authors Osman Sivrikaya, Cafer Kayadelen and Emre Chechnya give correlations to estimate the parameters of compression, depending on the energy of compression for coarse-grained soils with various fines contents. The survey results show that GEP (genetic programming) and MLR (multi-linear regression analysis) models are quite useful for predicting the maximum unit weight of the dry and optimum water content of non-cohesion soils with different contents of fine particles during energy compression with standard (SP) and modified (MP) Proctor tests.

In the fourth article, the authors Babak Ebrahimian and Aida Nazari analyse pilots that are exposed to lateral loads and their behaviour depends on the resistance of soils as a function of the pile's deflection. They studied the effects of the undrained shear strength, the normalized tip resistance of the cone-penetration test, the over-burden pressure, the plasticity index and the over-consolidation ratio on the deformation of soils at 50% maximum deviatoric stress in marine clays. It was shown to result in the normalized resistance of soil under the pile tip to a more realistic value, compared with laboratory parameters obtained for the undrained shear strength.

In the fifth article, the authors Srinivas Kadali, Susha Lekshmi S.U., Susmita Sharma and Devendra Narain Singh describe the details of investigations of soils and their changes at elevated temperatures. Based on a critical synthesis of the results they have demonstrated that the elevated temperature causes physical, chemical and mineralogical changes in the soil: (i) a colour change, (ii) an increase of the specific gravity, particle size, and weight loss, (iii) a reduction of the specific surface area, an ability for cation exchange and the zeta-potential, and (iv) the structural transformation of the soil.

Ludvik Trauner  
Editor-in-chief



---

# SOODVISNOSTI MED ATTERBERGOVIMI MEJAMI IN DRUGIMI FIZIKALNIMI LASTNOSTMI VEZLJIVIH ZEMLJIN

---

BOJANA DOLINAR IN STANISLAV ŠKRABL

---

## o avtorjih

### vodilni avtor

Bojana Dolinar  
University of Maribor,  
Faculty of Civil Engineering  
Smetanova ul. 17, 2000 Maribor, Slovenija  
E-pošta: bojana.dolinar@um.si

Stanislav Škrabl  
University of Maribor,  
Faculty of Civil Engineering  
Smetanova ul. 17, 2000 Maribor, Slovenija  
E-pošta: stanislav.skrabl@um.si

---

## izvleček

*V mehaniki tal so Atterbergove konsistenčne meje najbolj prepoznavna in najlažje merljiva lastnost vezljivih zemljin. Ker so vrednosti teh mej odvisne od nekaterih istih dejavnikov kot vrednosti drugih fizikalnih lastnosti tal, bi lahko bili mejni židkosti in plastičnosti zelo uporabni za njihovo napoved. O tem obstajajo številne študije, vendar pa se rezultati precej razlikujejo in niso splošno uporabni. V članku so pojasnjeni najpomembnejši razlogi za ta neskladja, nanašajo pa se predvsem na neupoštevanje sledečih dejstev: a) v vezljivih zemljinah se pojavlja porna voda, ki se nahaja med zrni in v agregatih glin in adsorbirana voda, ki je trdno vezana na zunanje in notranje površine glinenih mineralov; b) fizikalne lastnosti vezljivih zemljin so odvisne samo od proste porne vode, kajti adsorbirana voda, ki je trdno povezana z glinenimi zrni, nanje ne more vplivati; c) količina adsorbirane vode na zunanje površine glinenih mineralov je odvisna od velikosti in količine le teh, medtem ko je količina adsorbirane vode na notranje površine glinenih zrn odvisna predvsem od količine in vrste nabreklih glinenih mineralov in njihovih izmenjalnih kationov. Iz tega sledi, da za nabreklih in ne-nabreklih zemljine ne morejo obstajati enotna razmerja med Atterbergovimi mejami (ki predstavljajo skupno količino porne in adsorbirane vode) in drugimi fizikalnimi lastnostmi. V prispevku so predstavljene nekatere možnosti uporabe mej židkosti in plastičnosti pri napovedovanju fizikalnih lastnosti tal, nanašajo pa se na ne-nabreklih in omejeno nabreklih zemljine*

---

## ključne besede

Atterbergove meje; specifična površina; nedrenirana strižna trdnost, stisljivosti, vodoprepustnost

---

# ATTERBERG LIMITS IN RELATION TO OTHER PROPERTIES OF FINE-GRAINED SOILS

---

BOJANA DOLINAR and STANISLAV ŠKRABL

---

## about the authors

### corresponding author

Bojana Dolinar  
University of Maribor,  
Faculty of Civil Engineering  
Smetanova ul. 17, 2000 Maribor, Slovenia  
E-mail: bojana.dolinar@um.si

Stanislav Škrabl  
University of Maribor,  
Faculty of Civil Engineering  
Smetanova ul. 17, 2000 Maribor, Slovenia  
E-mail: stanislav.skrabl@um.si

---

## abstract

*In soil mechanics the Atterberg limits are the most distinctive and the easiest property of fine-grained soils to measure. As they depend on the same physical factors as the other mechanical properties of soils, the values of the liquid and plastic limits would be a very convenient basis for their prediction. There are many studies concerning the use of the Atterberg limits in soil mechanics; however, their results vary considerably and are not generally applicable. This paper explains the main reasons for the different conclusions in these studies, which do not take into account the following: a) the water in fine-grained soils appears as interparticle and interaggregate pore water as well as adsorbed water onto the surfaces of clay minerals; b) the physical properties of fine-grained soils depend on the quantity of pore water only, because the adsorbed water is tightly tied on the clay's external and internal surfaces and thus cannot influence them; c) the quantity of adsorbed water on the external surfaces of the clay minerals in soils depends mostly on the size and the quantity of the clay minerals, while the interlayer water quantity depends mostly on the quantity and the type of the swelling clay minerals in the soil composition and their exchangeable cations. From this it follows that for swelling and non-swelling soils, the uniform relationships between the Atterberg limits (which represent the total quantity of pore water and the adsorbed water onto the external and internal surfaces of clay minerals) and other physical prop-*

*erties does not exist. This paper presents some possibilities for the use of the Atterberg limits in predicting the soil's other properties for non-swelling and limited-swelling soils.*

---

## keywords

Atterberg limits; specific surface area; undrained shear strength; compressibility; hydraulic conductivity

---

## 1 INTRODUCTION

The Atterberg limits represent the water content where the consistence of a fine-grained soil is transformed from a plastic state (plastic limit  $PL$ ) to a liquid state (liquid limit  $LL$ ) and from a semi-solid state (shrinkage limit  $SL$ ) to a plastic state, as well as the water content at which different fine-grained soils have an approximately equal undrained shear strength, which is 1.7–2.7 kPa at the  $LL$  (depending on the method of measurement) and about 100 times greater at the  $PL$ . The quantity of water at the Atterberg limits and for the other physical properties depends on the same, mostly compositional factors, such as the type of minerals, the amount of each mineral, the shapes and size distribution of the particles and the pore-water composition [1], which leads to the conclusion that the exactly defined relationships between the values of the Atterberg limits and the soil's other properties must exist. Several researchers have tried to find the generally valid relationships between the quantity of water at the  $LL$ , the  $PL$  or at the plasticity index ( $PI=LL-PL$ ) and various physical properties. The results of these studies, however, varied considerably and were valid in most cases for the investigated soils only. The main reasons for the different conclusions in these studies are explained in Section 2. The next section shows the empirically obtained relationships between the Atterberg limits and some other properties of the soil with an explanation about the limitations of their use. The comparison between the measured and the calculated values from the proposed correlations for different properties of the soils are shown in Section 4.

This paper briefly summarizes all our already-published and new findings with the intention to understand more easily the impact of the mineralogical composition on the physical properties of fine-grained soils, the basic mechanisms that determine the physical properties, and thus the possible correlations between them. As an example, the possibilities of using the Atterberg limits to predict the soil's other properties are shown.

## 2 BASIC ASSUMPTIONS

Fine-grained soils contain both clay minerals and associated minerals, and the interactions between the clay minerals and water affect the soil's water-holding capacity. Water is strongly adsorbed onto the external surfaces of hydrophilic non-swelling clay minerals, whereas water adsorbs onto both the external and internal surfaces of swelling clay minerals. Besides the adsorbed water soils also contain free interparticle and interaggregate pore water [2]. It was found also that:

1. most of the water in soils is associated with clay minerals [3];
2. the pore sizes that effectively control fluid flow at the liquid limit are the same size for all soils [1] and, hence, the quantity of free pore water at the liquid limit is a constant;
3. soils have similar pore water suction at the liquid limit [4-6]. This means that the ratio of adsorbed water to clay surface area should be about the same at the liquid limit;
4. at the liquid limit, different fine-grained soils have approximately equal undrained shear strength [7-9];
5. at the plastic limit the undrained shear strength is about 100 times the undrained shear strength at the liquid limit [10 and numerous subsequent authors];
6. the quantity of interlayer water in swelling clays is mostly dependent on the type of the clay minerals, the exchangeable cations and the chemical composition of the pore water [11, 12].

On the basis of the above findings, Dolinar and Trauner [13, 14] assumed that the quantity of free pore water and external surface water at the liquid limit  $w_{e|LL}$  and the plastic limit  $w_{e|PL}$  can be expressed in terms of the external specific surface area and the clay minerals content by Eqs. (1) and (2).

$$w_{e|LL} = p \cdot (w_{ef|LL} + w_{ea|LL}) = p \cdot (w_{ef|LL} + t_{a|LL} \cdot A_{SCe}) \quad (1)$$

$$w_{e|PL} = p \cdot (w_{ef|PL} + w_{ea|PL}) = p \cdot (w_{ef|PL} + t_{a|PL} \cdot A_{SCe}) \quad (2)$$

where  $w_{ef|LL}$  and  $w_{ef|PL}$  are the quantities of free pore water. These quantities are constant at the liquid and

plastic limits (according to item 2, 4 and 5).  $w_{ea|LL}$  and  $w_{ea|PL}$  are the quantities of firmly adsorbed water on the clay's external surfaces. These quantities of water depend on the size of the external surfaces of the clay mineral particles  $A_{SCe}$  because the thicknesses  $t_{a|LL}$ ,  $t_{a|PL}$  of the firmly adsorbed water on the external surfaces are, for most clay minerals, constant at the liquid and plastic limits (according to item 3). The water content (pore water and external surface water) depends on the quantity of clay minerals in the soil, assuming that all the water in the soil is associated with the clay minerals (according to item 1).

The experimental tests on artificial mono-mineral clay mixtures confirmed the above assumptions (Fig.1). For non-swelling soils the liquid limit  $LL_e$  (%) and plastic limit  $PL_e$  (%) can thus be expressed as:

$$LL_e = 31.90 \cdot p + 0.81 \cdot A_{Se} \quad (3)$$

$$PL_e = 23.16 \cdot p + 0.27 \cdot A_{Se} \quad (4)$$

where  $A_{Se} = p \cdot A_{SCe}$  ( $m^2/g$ ) is the external specific surface area of the soil and  $p$  is the content (%) of clay minerals in the soil divided by 100 ( $0 < p \leq 1$ ). Note that  $LL = LL_e$  for non-swelling soils and  $LL = LL_e + w_i$  for swelling soils ( $w_i$  is the quantity of interlayer water).

The above findings can be summarized in the following conclusions:

- for non-swelling soils the water content at the  $LL$  and  $PL$  depends mostly on the specific surface area  $A_{Se}$  and the content of clay minerals  $p$  in the soil composition;
- for swelling soils the quantity of free pore water and adsorbed water on the clay's external surfaces depend on  $A_{Se}$  and  $p$ , while the interlayer water content  $w_i$  is mostly dependent on the quantity and type of the swelling clay minerals, exchangeable cations and the chemical composition of the pore water. This explains why a general criterion cannot be found relating the water content at the Atterberg limits to the total specific surface area  $A_S = A_{Se} + A_{Si}$  ( $A_{Si}$  is internal specific surface area) for soils with and without swelling clay minerals. It should be noted that using a standard method for measuring the water content  $w$ , the total quantity of free pore water  $w_{ef}$  and strongly adsorbed water on the external  $w_{ea}$  and internal  $w_i$  clay surfaces can always be determined by drying at a temperature of 100–110°C;
- the physical properties of fine-grained soils depend only on the free pore water because the adsorbed water is tightly tied on the clay's external and internal surfaces.



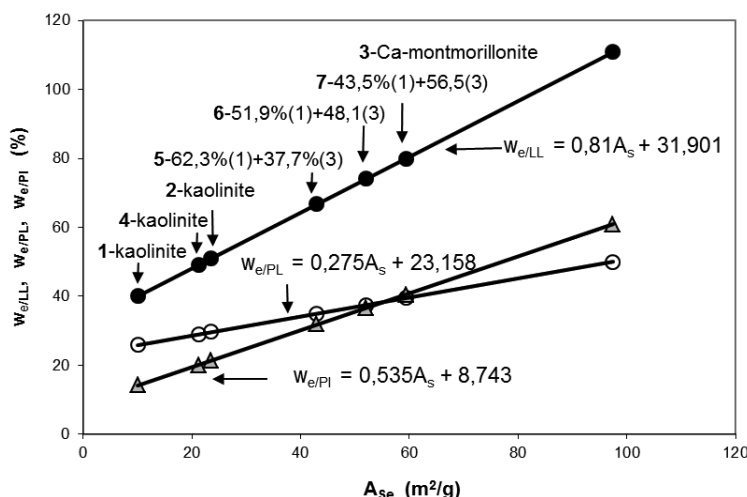


Figure 1. Quantity of pore water plus the external surface water at the liquid limit  $w_{e|LL}$  (%), plastic limit  $w_{e|PL}$  (%) and plasticity index  $w_{e|PI}$  (%) as a function of the specific surface area  $A_{Se}$  ( $m^2/g$ ) for clay minerals ( $p=1$ ).

The above findings allow us to better understand the relationships between the quantity of water at the liquid and plastic limits and other properties of the soil and hence their proper use in predicting other physical properties of fine-grained soils.

### 3 CORRELATION OF THE ATTERBERG LIMITS WITH THE SOIL'S OTHER PROPERTIES

#### 3.1 DETERMINATION OF THE EXTERNAL SPECIFIC SURFACE AREA

For non-swelling soils, which only contain pore water and adsorbed water on the external surfaces of clay minerals, the specific surface area  $A_{Se}$  ( $m^2/g$ ) can be expressed with Eqs. (3) and (4), depending on the  $LL$  and  $PL$ . The portion of clay minerals  $p$  could be equalled with the grain quantity  $< \mu 2m$ , determined using a hydrometer method.

For soils that contain limited-swelling clay minerals, the quantity of interlayer water ( $w_i$ ) at the  $LL$  and  $PL$  is approximately the same ( $w_{i|LL} \approx w_{i|PL} \rightarrow PI \approx PI_e$ ), and the external specific surface area  $A_{Se}$  ( $m^2/g$ ) can be expressed with Eq. (5), depending on the plasticity index  $PI$  (%).

$$PI = LL - PL \Rightarrow A_{Se} = (PI - 8.74p)/0.54 \quad (5)$$

For soils with other swelling clay minerals a correlation between the specific surface area and the Atterberg limits does not exist [15, 16].

#### 3.2 DETERMINATION OF THE UNDRAINED SHEAR STRENGTH

Koumoto and Houlsby [9] present a relationship between the water content  $w$  and the undrained shear strength  $s_u$  using the following equation

$$w = a \cdot s_u^{-b} \quad (6)$$

where  $a$  and  $b$  are soil-dependent parameters.  $a$  (%) is the water content at the undrained shear strength  $s_u = 1kPa$ , and  $b$  is the slope of the linear function that represents the ratio between the water content  $w(\%)$  logarithm and the the undrained shear strength  $s_u(kPa)$  logarithm. According to Koumoto and Houlsby [9] the parameters  $a$  and  $b$  can only be obtained experimentally, while Trauner et al. [17] found that for non-swelling soils these parameters ( $a_e$ ,  $b_e$ ) depend mainly on the external specific surface area  $A_{Se}$  ( $m^2/g$ ) of soils and the content of clay minerals  $p$  in the soil's composition and can be expressed by Eqs. (7) and (8).  $A_{Se}$  in the equations can be determined experimentally or calculated using Eqs. (3), (4) or (5), while  $p$  can be estimated from a particle size analysis.

$$a_e = 33.70 \cdot p + 0.99 \cdot A_{Se} = 1.22 \cdot LL_e - 5.29 \cdot p \quad (7)$$

$$b_e = 0.05 \cdot (A_{Se}/p)^{0.27} = 0.05 \cdot \left( \frac{LL_e - 31.90 \cdot p}{0.81 \cdot p} \right)^{0.27} \quad (8)$$

For both the swelling and non-swelling fine-grained soils, the undrained shear strength could be determined using the Atterberg limits and a modified plasticity index or modified consistency index. Equations (10)

and (11), which show these relationships, are derived as follows:

The undrained shear strength of the soils at the liquid limit  $s_{uLL}$ , determined by the fall cone test, can be calculated using Eq. (9)

$$s_u = K \cdot \frac{W}{h^2} \quad (9)$$

where  $K$  is a constant depending on the type of cone and  $W$  is the cone mass. The theoretically determined value of the constant is  $K = 1.33$  for the British cone [9] and the mass of the cone is  $W = 80$  g. The depth of cone penetration that corresponds to the water content at the  $LL$  is  $h = 20$  mm. The undrained shear strength is  $s_{uLL} = 2.66$  kPa. The data of Skempton and Northey [10] and numerous subsequent authors show that the undrained shear strength at the  $PL$  is about 100 times the undrained shear strength at the  $LL$  ( $s_{uPL} = 266$  kPa). Considering the above findings the water content at the  $LL$  and  $PL$  can be expressed as  $LL = a \cdot 2.66^{-b}$  (%) and  $PL = a \cdot 266^{-b}$  (%). The form of these expressions suggests that it would be convenient to define a modified plasticity index as  $PI_M = \log LL - \log PL$ , which makes it possible to express the parameters  $a$  and  $b$  in terms of  $PI_M$  as follows [9]:  $b = \log LL - \log PL / \log s_{uLL} - \log s_{uPL} = PI_M / -2$  and  $a = LL / s_{uLL}^{-b} = LL / 2.66^{-PI_M / -2}$ . At the selected water content  $w$  (%) the undrained shear strength  $s_{uw}$  (kPa) of the soils can thus be determined in terms of the liquid limit  $LL$  (%) and the modified plasticity index  $PI_M$  by Eq. (10).

$$s_{uw} = 2.66 \cdot LL^{2/PI_M} \cdot w^{-2/PI_M} \quad (10)$$

The consistency index ( $CI$ ) is defined as the ratio of the difference between the  $LL$  and the natural water content ( $w$ ) to the plasticity index ( $PI$ ) of a soil ( $CI = (LL - w) / PI$ ). Consistent with the above discussion of the variation of strength with water content, it would be appropriate to define a new, modified consistency index as  $CI_M = (\log LL - \log w) / PI_M$ . By considering that  $\log LL = \log a - b \cdot \log s_{uLL}$ ,  $\log PL = \log a - b \cdot \log s_{uPL}$  and  $\log w = \log a - b \cdot \log s_{uw}$ , the modified consistency index  $CI_M$  can be written in the form  $CI_M = (\log s_{uLL} - \log s_{uw}) / (\log s_{uLL} - \log s_{uPL}) = -0.212 + 0.5 \log s_{uw}$  which makes it possible to express the undrained shear strength at a particular water content as:

$$s_{uw} = 10^{(CI_M + 0.212) / 0.5} \quad (11)$$

### 3.3 DETERMINATION THE WATER CONTENT - EFFECTIVE STRESS RELATIONSHIP

In a compressibility test of saturated soils the quantity of free pore water and adsorbed water on external clay

surfaces depends on the stress state and the physico-chemical properties of the clay minerals. It is known that the interlayer water cannot be drained from an expanding mineral under usual stresses, which leads to the conclusion that in the case of swelling soils a generally applicable relationship between the total water content and the effective stress does not exist.

On the basis of experimental tests Dolinar [18] found that the relationship between the free pore water plus the adsorbed water on the external clay surfaces  $w_e$  (%) and the effective stress  $\sigma'$  (kPa) is completely linear when both variables are shown in a double logarithmic scale and can be expressed as:

$$\log w_e = \log i_e - j_e \log \sigma' \Rightarrow w_e = i_e \cdot (\sigma')^{-j_e} \quad (12)$$

where  $i_e$  (the water content in the soil at  $\sigma' = 1$  kPa) and  $j_e$  (the slope of the linear function that represents the ratio between the water content  $w$  (%) logarithm and the effective stress  $\sigma'$  (kPa) logarithm) are soil-dependent parameters. It was also found that these parameters depend mainly on the external surface area  $A_{Se}$  (m<sup>2</sup>/g) and the content of clay minerals  $p$  in the soil's composition and can be expressed as:

$$i_e = 33.46 \cdot p + 1.39 \cdot A_{Se} \quad (13)$$

$$j_e = 0.05 \cdot (A_{Se} / p)^{0.27} \quad (14)$$

The known relationship between  $A_{Se}$  (m<sup>2</sup>/g) and the Atterberg limits (Eqs. (3), (4) and (5)) makes it possible to express both parameters using the  $LL_e$  (%), the  $PL_e$  (%) or the  $PI$  (%) in the case of limited-swelling soils. The portion of clay minerals  $p$  in the soil composition can be estimated from the particle size analysis.

$$i_e = 2.57 \cdot PI + 10.96 \cdot p \quad (15)$$

$$j_e = 0.05 \cdot \left( \frac{PI - 8.7 \cdot p}{0.54 \cdot p} \right)^{0.27} \quad (16)$$

### 3.4 PREDICTING THE NORMALIZED UNDRAINED SHEAR STRENGTH

It is evident from Section 2 that the normalized undrained shear strength can only be correlated with the  $PI$  in the case of non-swelling soils. It means that there is no uniform criterion to determine the normalized undrained shear strength from the plasticity index for all fine-grained soils.

The dependence of the undrained shear strength  $s_u$  on the vertical effective stress  $\sigma'_v$  at which the soils were previously consolidated can be expressed by considering Eq. (6) and (12), [19]. Note that the parameter  $j_e = b_e$ .

$$s_u = b_e \sqrt{\frac{a_e}{i_e}} \cdot \sigma_v' \quad (17)$$

Equation (17) shows that the value  $s_u / \sigma_v'$  is constant and determined for different soils with the material parameters  $a_e$ ,  $b_e$  ( $j_e$ ) and  $i_e$ . Because these parameters depend on the external surface of soils  $A_{Se}$  and the portion of clay minerals  $p$  in the soil composition, Eq. (17) can be written as:

$$\frac{s_u}{\sigma_v'} = b_e \sqrt{\frac{a_e}{i_e}} = b_e \sqrt{\frac{33.70 \cdot p + 0.99 \cdot A_{Se}}{33.46 \cdot p + 1.39 \cdot A_{Se}}}; \quad (18)$$

$$b_e = 0.05 \cdot (A_{Se}/p)^{0.27}$$

The known relationships between  $A_{Se}$  ( $m^2/g$ ) and the values of the Atterberg limits make it possible to express the  $s_u / \sigma_v'$  value in terms of the  $LL_e$  (%), the  $PL_e$  (%) or the  $PI$  (%) in the case of limited-swelling soils (Eq. (19)).

$$\frac{s_u}{\sigma_v'} = b_e \sqrt{\frac{17.68 \cdot p + 1.83 \cdot PI}{10.96 \cdot p + 2.57 \cdot PI}}; \quad (19)$$

$$b_e = 0.05 \cdot ((PI - 8.74)p / 0.54p)^{0.27}$$

### 3.5 PREDICTING THE HYDRAULIC CONDUCTIVITY OF SATURATED CLAYS

The experimental data of Dolinar [20] and many other researchers [21-24] indicate that a power equation of the form (20) can be employed to describe the variation of the hydraulic conductivity  $k$  (m/s) with the void ratio  $e$  of soils. In the equation  $\alpha$  and  $\beta$  are soil-dependent parameters.

$$k = \alpha e^\beta \quad (20)$$

The parameters  $\alpha$  and  $\beta$ , which reflect the tortuosity of the flow path and the cross-sectional characteristics of the flow conduit, depend on the shape and the size of the particles. Dolinar [20] found that for plate-like clay particles these parameters can be expressed with Eqs. (21) and (22), depending on the external specific surface area  $A_{Se}$  ( $m^2/g$ ).

$$\alpha = 4.08 \cdot 10^{-6} A_{Se}^{-3.03} \quad (21)$$

$$\beta = 2.30 A_{Se}^{0.234} \quad (22)$$

Taking into account Eqs. (20), (21) and (22), the hydraulic conductivity  $k$  (m/s) of the clays can be expressed as follows:

$$k = 4.08 \cdot 10^{-6} A_{Se}^{-3.03} e^{2.30 A_{Se}^{0.234}} \quad (23)$$

Combining Eq. (23) with Eq. (5) leads to Eq. (24), which allows us to predict the hydraulic conductivity  $k$  (m/s) of non-swelling or limited-swelling clays using the plasticity index  $PI$  (%).

$$k = \frac{6.31 \cdot 10^{-7}}{(PI - 8.74)^{3.03}} e^{2.66 (PI - 8.74)^{0.234}} \quad (24)$$

## 4 PRACTICAL EXAMPLES

The use of the proposed equations for predicting different properties of soils from the values of their Atterberg limits are presented in data taken from the literature. The first five samples in Table 1 belong to heterogeneous fine-grained soils from different locations in which the mineralogical and chemical compositions and the size of the grains were investigated [15, 19]. The bulk mineral composition and the clay fraction of the samples were determined using the X-ray diffraction technique (Table 1 and 2). The results of chemical analyses were used to check the quantity of individual minerals in the soils. The grain size distribution was determined using a hydrometer method (Table 3). The external specific surface areas of the investigated soils were measured using a five-point BET method with  $N_2$ , (Table 3). The liquid limits of the samples were determined by the fall-cone test and the plastic limits by the rolling-thread test in accordance with the standard BSI [28], (Table 4). A more detailed description of the used methods can be found in the cited literature. The data for the pure clay samples of kaolinite (sample 6) and illite (sample 7) arise from the paper of Mesri and Olson [25], and were used for the comparison between the measured and calculated values of the hydraulic conductivity of clays (Table 9).

The mineralogical analyses indicate that heterogeneous soils contain montmorillonite in I/M, K/M, and Ch/M mixed layered minerals or as Ca-montmorillonite. This means that the quantities of water at the liquid and plastic limits consist of pore water  $w_{ef}$ , adsorbed water on external clay surfaces  $w_{ea}$  and interlayer water  $w_i$ ; therefore, these limits cannot be used directly for predicting the mechanical properties of investigated soils. In this case it was necessary to decrease the total water content  $w$  at the  $LL$  and  $PL$  for the interlayer water portion  $w_i$  in the expanding soils. The interlayer water quantity  $w_i$  was calculated with Eq. (25), [26].

$$w_i = \frac{A_{Si}(d_2 - d_1)}{2 \cdot 10^3} \cdot p_m \quad (\%) \quad (25)$$

The basal spacing (the distance between layers) in the  $c$  direction in the crystal structure, which is  $d_1 = 0.96$  nm for calcium montmorillonite (dried at  $105^\circ\text{C}$ ), increased to  $d_2 \sim 1.54$  nm at a relative humidity of 80% and to  $d_2 = 1.9$  nm in water [27]. In the case of exchangeable calcium ions in montmorillonite, the adsorption of water between the layers was then completed and the basal spacing remained practically constant. When calculating the interlayer water quantity  $w_i$  with Eq. (25), consideration was given to the internal specific surface area  $A_{si} = 626.80$   $\text{m}^2/\text{g}$  (the adopted value from the literature [13]) and appropriate mass portions of montmorillonite  $p_m$  in the individual soils (Table 4). The assumed basal spacings ( $d_2$ ) of the montmorillonite at the  $PL$  and  $LL$  were, respectively, 1.54 and 1.90 nm.

**Table 1.** Mineralogical composition of the whole soil samples.

Mineral. composition (% mass)	Sample						
	1	2	3	4	5	6	7
Muscovite /Illite	25	35	28	35	34		100
Chlorite	8	14	16	0	18		
Kaolinite	5	0	0	12	0	100	
Ca-montmorillonite	14	0	0	34	0		
Quartz	34	25	42	19	43		
Plagioclase	9	3	9	0	3		
Microcline	5	0	4	0	3		
Calcite	0	23	0	0	0		

**Table 2.** The mineralogical composition of the clay fraction  $< 2 \mu\text{m}$ .

Mineral. composition (% mass)	Sample				
	1	2	3	4	5
Illite (I)	11	12	6	13	12
Chlorite (Ch)	0	3	7	0	0
Kaolinite (K)	4	3	0	5	7
Ca-montmorillonite	14	4	2	34	0
Mixed layer	10	19	14	19	25

**Table 3.** Particle size distribution and external specific surface area of the soil samples.

Sample	% Clay	% Silt	% Sand	$A_{se}$ $\text{m}^2/\text{g}$
1	39.1	58.1	2.8	$30.1 \pm 0.4$
2	40.7	56.9	2.4	$28.5 \pm 0.4$
3	29.2	60.6	10.2	$16.7 \pm 0.1$
4	70.7	27.2	2.1	$54.1 \pm 0.3$
5	44.2	53.9	1.9	$32.6 \pm 0.2$

**Table 4.** Soil clay fraction ( $p$ ), % Ca-montmorillonite ( $p_m$ ), interlayer water contents at the liquid and plastic limits ( $w_{iLL}$ ,  $w_{iPL}$ ), intergrain water contents at the liquid and plastic limits and plasticity index ( $LL_e$ ,  $PL_e$ ,  $PI_e$ ), the liquid limit ( $LL$ ), the plastic limit ( $PL$ ), and the plasticity index ( $PI$ ).

Physical properties	Sample						
	1	2	3	4	5	6	7
$p$	0.39	0.41	0.29	0.71	0.44	1.00	1.00
$p_m$ (%)	14	4	2	34	0	0	0
$w_{iLL}$ (%)	4.12	1.18	0.59	10.02	0	0	0
$w_{iPL}$ (%)	2.54	0.72	0.36	6.18	0	0	0
$LL$ (%)	47.2	44.0	31.2	82.1	43.1	50	104
$LL_e$ (%)	43.1	42.9	30.6	72.7	43.1	50	104
$PL$ (%)	24.3	22.7	18.7	44.9	22.0	31	32
$PL_e$ (%)	21.7	22.0	18.3	39.1	22.0	31	32
$PI$ (%)	22.9	21.3	12.5	37.2	21.1	19	72
$PI_e$ (%)	21.4	20.9	12.3	33.6	21.1	19	72

#### 4.1 EXPERIMENTALLY DETERMINED AND CALCULATED EXTERNAL SPECIFIC SURFACE AREA

Due to the presence of Ca-montmorillonite in the investigated soils the external specific surface area was calculated with Eq. (5) using the data of the plasticity index  $PI$  (%) and the portion  $p$  of clay minerals in the soil's composition ( $p$  is the content (%) of clay minerals in the soil divided by 100 ( $0 < p \leq 1$ )). The experimentally determined and calculated values are shown in Table 5.

**Table 5.** Measured and calculated values of the external specific surface area  $A_{se}$  (Dolinar, 2012).

Input data	Sample				
	1	2	3	4	5
Content of clay minerals $p$	0.39	0.41	0.29	0.71	0.44
$PI$ (%)	22.9	21.3	12.5	37.2	21.1
$A_{se}$ ( $\text{m}^2/\text{g}$ ) measured by BET method	30.1	28.5	16.7	54.1	32.6
$A_{se}$ ( $\text{m}^2/\text{g}$ ) calculated by Eq. (5)	36.1	32.8	18.4	57.4	32.0

#### 4.2 EXPERIMENTALLY DETERMINED AND CALCULATED UNDRAINED SHEAR STRENGTH

The undrained shear strength of selected samples was tested with a laboratory vane test [28]. The disturbed samples with the water content near the liquid limit were previously consolidated at  $\sigma'_v = 50$  kPa. The most appropriate way to calculate the undrained shear strength is the use of equations (10) or (11) due to the presence of

**Table 6.** Measured and calculated values of the undrained shear strength  $s_u$ .

Input data	Sample				
	1	2	3	4	5
Content of clay minerals $p$	0.39	0.41	0.29	0.71	0.44
$LL$ (%)	47.2	44.0	31.2	82.1	43.1
$LL_e = LL - w_{iLL}$ (%)	43.1	42.9	30.6	72.7	43.1
Parameter $a$ calculated by Eq. (7)	50.49	50.07	35.81	84.18	50.25
Parameter $b$ calculated by Eq. (8)	0.1719	0.1683	0.1689	0.1664	0.1641
$PI_M = \log LL - \log PL$	0.2883	0.2874	0.2223	0.2621	0.2921
$CI_M = (\log LL - \log w) / PI_M$	0.3477	0.2311	0.2697	0.3606	0.3214
$w$ (%)	37.47	37.76	25.82	66.04	34.72
$w_i^*$ (%)	3.33	0.95	0.47	8.10	0
$w_e = w - w_i^*$ (%)	34.14	36.81	25.35	57.94	34.72
Measured $s_{uw}$ (kPa)	11.3	10.8	9.4	10.9	10.1
Calculated $s_{uw}$ (kPa) by Eq. (6)	9.7	6.2	7.7	9.4	9.5
Calculated $s_{uw}$ (kPa) by Eq. (10) or (11)	13.2	7.7	14.6	14.0	11.7

$w_i^*$  - The average quantity of interlayer water in the plasticity range of the soils is considered.

Ca-montmorillonite in the soils. When using Eq. (6) it is necessary to calculate both parameters  $a_e$  and  $b_e$  from the intergrain water content and to decrease the total water quantity  $w$  of the soils for the interlayer water portion  $w_i^*$ . The quantity of interlayer water can only be calculated for limited-swelling clay minerals (Table 6). This procedure is given as an example only and it is not useful in practice because it requires precise knowledge of the qualitative and quantitative mineral composition of the soils.

#### 4.3 EXPERIMENTALLY DETERMINED AND CALCULATED WATER CONTENT-EFFECTIVE STRESS RELATIONSHIP

The quantity of water in the saturated soils was measured under an effective stress  $\sigma' = 50$  kPa using

an oedometer consolidation test. The initial moisture content in the samples was near the liquid limit. The quantities of free pore water and external surface water at the selected axial stress were calculated using Eq. (12). To calculate the parameters  $i_e$  and  $j_e$  the equations (15) and (16) were chosen due to the presence of limited-swelling mineral in the soils (Table 7). Note that  $PI \approx PI_e$  for limited-swelling soils.

#### 4.4 EXPERIMENTALLY DETERMINED AND CALCULATED NORMALIZED UNDRAINED SHEAR STRENGTH

The undrained shear strength of selected samples was tested with a laboratory vane test [28]. The saturated disturbed samples were previously consolidated at

**Table 7.** Measured and calculated water content-effective stress relationship.

Input data	Sample				
	1	2	3	4	5
Content of clay minerals $p$	0.39	0.41	0.29	0.71	0.44
$PI$ (%)	22.9	21.3	12.5	37.2	21.1
$w_i^*$ (%)	3.33	0.95	0.47	8.10	0
Parameter $i$ calculated by Eq. (15)	63.17	59.28	35.33	103.46	59.09
Parameter $j$ calculated by Eq. (16)	0.1698	0.1633	0.1535	0.1637	0.1591
Measured $w$ at $\sigma_v' = 50$ kPa	37.5	37.7	25.8	66.0	34.7
Calculated $w_e$ at $\sigma_v' = 50$ kPa by Eq. (12)	32.5	31.3	19.4	54.5	31.7
$w_e = w - w_i^*$ (%)	35.8	32.2	19.9	62.6	31.7

$w_i^*$  - The average quantity of interlayer water in the plasticity range of the soils is considered.

**Table 8.** Measured and calculated normalized undrained shear strength  $s_u / \sigma_v'$ .

Input data	Sample				
	1	2	3	4	5
Content of clay minerals $p$	0.39	0.41	0.29	0.71	0.44
$PI$ (%)	22.9	21.3	12.5	37.2	21.1
Measured $s_u$ (kPa) at $\sigma_v' = 50$ kPa	11.3	10.8	9.4	10.9	10.1
Measured $s_u / \sigma_v'$	0.23	0.22	0.19	0.22	0.20
Calculated $s_u / \sigma_v'$ by Eq. (19)	0.24	0.24	0.24	0.24	0.24

$\sigma_v' = 50$  kPa. Measured and calculated values of the normalized undrained shear strength are shown in Table 8. More examples with a precise explanation of the proposed procedure are given in the paper of Dolinar [19].

#### 4.5 EXPERIMENTALLY DETERMINED AND CALCULATED HYDRAULIC CONDUCTIVITY OF SATURATED CLAYS

A comparison between the measured and calculated values of the hydraulic conductivity using Eq. (24) was made using data from the literature [25]. The shown samples belong to sodium kaolinite with the plasticity index  $PI = 19$  % and sodium illite with the  $PI = 72$  %.

## 5 CONCLUSION

The first part of this paper discussed recent findings that show how the soil composition influences the water content at the liquid and plastic limits. It was found that the quantity of water at the Atterberg limits depends mostly on the size and the portion of clay minerals in non-swelling soils, while in swelling soils it also depends on the quantity of interlayer water, which is mostly

dependent on the type of clay minerals, exchangeable cations and the chemical composition of the pore water. This means that there is no uniform criterion for determining the interdependence of the liquid and plastic limit values and the mineralogical properties of different soils. Considering that the mechanical properties of fine-grained soils depend on the free pore water only because the adsorbed water is tightly tied on the clay external and internal surfaces, that the relationship between the quantity of free pore water and the adsorbed water on the external clay surfaces is exactly defined, while it is not true for the free pore water–interlayer water relationship and that Atterberg limits always show the total water content, leads to the conclusion that for swelling and non-swelling fine-grained soils, a uniform relationship between the Atterberg limits and other mechanical properties does not exist.

The above findings have allowed us to derive generally valid relationships between the water content and the different physical properties and thus also between the quantity of water at the Atterberg limits and other physical properties for non-swelling soils and in some cases for limited-swelling soils. The parameters in the equations were determined by testing artificially prepared samples of mono-mineral clay mixtures and are valid for soils without organic matter.

**Table 9.** Measured and calculated values of hydraulic conductivity.

Sample	Void ratio $e$				
	1.90	1.80	1.70	1.50	1.30
Kaolinite $PI = 72$ %					
Measured $k$ (m/s)	$1.13 \cdot 10^{-8}$	$8.09 \cdot 10^{-9}$	$5.78 \cdot 10^{-9}$	$2.95 \cdot 10^{-9}$	$1.51 \cdot 10^{-9}$
Calculated $k$ (m/s) by Eq. (24)	$1.03 \cdot 10^{-8}$	$9.07 \cdot 10^{-9}$	$6.21 \cdot 10^{-9}$	$3.49 \cdot 10^{-9}$	$1.81 \cdot 10^{-9}$
Illite $PI = 72$ %					
Measured $k$ (m/s)	$2.68 \cdot 10^{-10}$	$1.93 \cdot 10^{-10}$	$1.39 \cdot 10^{-10}$	$7.19 \cdot 10^{-11}$	$3.73 \cdot 10^{-11}$
Calculated $k$ (m/s) by Eq. (24)	$1.99 \cdot 10^{-10}$	$1.36 \cdot 10^{-10}$	$9.12 \cdot 10^{-11}$	$3.79 \cdot 10^{-11}$	$1.39 \cdot 10^{-11}$

## REFERENCES

- [1] Mitchell, J. K. (1993). *Fundamentals of Soil Behaviour*. John Wiley&Sons, Inc., New York.
- [2] Fripiat, J.J., Letellier, M., Levitz, P. (1984). Interaction of water with clay surface. *Philosophical Transactions of the Royal Society of London*, A311, 287-299.
- [3] Seed, H.B., Woodward, R.J., Lundgren, R. (1964). Clay mineralogical aspects of Atterberg limits. *Journal of Soil Mechanics and Foundations Division* 90, 4, 107-131.
- [4] Russell, E.R., Mickle, J.L. (1970). Liquid limit values of soil moisture tension. *Journal of soil mechanics and Foundations Division* 96, 967-987.
- [5] Tuller, M., Or, D. (2005). Water films and scaling of soil characteristic curves at low water contents. *Water Resources Research* 41:WO9403.
- [6] Dolinar, B., Škrabl, S. (2012). The matrix potential of fine-grained soils at the liquid limit. *Eng. geol.* 135-136, 48-51, doi: 10.1016/j.enggeo.2012.03.003.
- [7] Casagrande, A. (1932). Research on the Atterberg limits of soils. *Public Roads*, 13, 121-136.
- [8] Wroth, C.P., Wood, D.W. (1978). The correlation of index properties with some basic engineering properties of soils. *Canadian Geotechnical Journal* 15, 2, 137-145.
- [9] Koumoto, T., and Houlsby, G.T. (2001). Theory and practice of the fall cone test. *Geotechnique* 51, 8, 701-712.
- [10] Skempton, A., Northey R.D. (1953). The sensitivity of clays. *Geotechnique* 3, 1, 30-53.
- [11] Grim, R.E. (1962). *Applied Clay Mineralogy*. McGraw-Hill Company, USA.
- [12] Bergaya, F., Theng, B.K.G., Lagaly, G. (2006). *Handbook of clay science*, first ed. Elsevier Science, Netherlands.
- [13] Dolinar, B., and Trauner, L. (2004). Liquid limit and specific surface of clay particles. *Geotechnical Testing Journal* 27, 580-584.
- [14] Dolinar, B., and Trauner, L. (2005). Impact of Soil Composition on fall Cone test Results. *Journal of Geotechnical and Geoenvironmental Engineering* 131, 1, 126-130.
- [15] Dolinar, B., Mišič, M., Trauner, L. (2007). Correlation between surface area and Atterberg Limits of fine-grained soils. *Clays and clay miner.*, 55, 5, 519-523.
- [16] Dolinar, B. (2012). A simplified method for determining the external specific surface area of non-swelling fine-grained soils. *Applied clay science*, 64, 34-37, doi: 10.1016/j.clay.2009.12.013.
- [17] Trauner, L., Dolinar, B., Mišič, M. (2005). Relationship between the undrained shear strength, water content, and mineralogical properties of fine-grained soils. *International journal of geomechanics* 5, 4, 350-355. [http://dx.doi.org/10.1061/\(ASCE\)1532-3641\(2005\)5:4\(350\)](http://dx.doi.org/10.1061/(ASCE)1532-3641(2005)5:4(350)).
- [18] Dolinar, B. (2006). The impact of mineral composition on compressibility of saturated soils. *Mechanics of materials* 38, 7, 599-607. <http://dx.doi.org/10.1016/j.mechmat.2005.11.003>.
- [19] Dolinar, B. (2010). Predicting the normalized, undrained shear strength of saturated fine-grained soils using plasticity-value correlations. *Applied clay science* 47, 3/4, 428-432, doi: 10.1016/j.clay.2009.12.013.
- [20] Dolinar, B. (2009). Predicting the hydraulic conductivity of saturated clays using plasticity-value correlations. *Applied clay science* 45, 1/2, 90-94. doi: 10.1016/j.clay.2009.04.001.
- [21] Carrier, W.D., Beckman, J.F. (1984). Some recent observations on the fundamental properties of remoulded clays. *Geotechnique* 34, 2, 211-228.
- [22] Krizek, R.J., Somogyi, F. (1984). Perspectives on modelling consolidation of dredged materials. *Proc. ASCE Symp. On Sedimentation Consolidation Models*, San Francisco.
- [23] Al-Tabba, A., Wood, D.M. (1987). Some measurements of the permeability of kaolin. *Geotechnique* 37, 4, 499-503.
- [24] Pane, V., Schiffman, R.L. (1997). The permeability of clay suspensions. *Geotechnique* 47, 2, 273-288.
- [25] Mesri, G., Olson, R.E. (1971). Mechanisms controlling the permeability of clays. *Clays and Clay minerals*, 19, 151-158.
- [26] Fink, D.H., Nakayama, F.S. (1972). Equation for describing the free swelling of montmorillonite in water. *Soil Science* 114 (5), 355-358.
- [27] Brindley GW, Brown G. (1980). *Crystal structures of clay minerals and their X-ray identification*. Mineralogical Society, London, pp. 495.
- [28] British Standards Institution, 1990. *Methods of test for soils for civil engineering purposes*, BS 1377.

---

# UPORABA MEŠANE METODE KONČNIH ELEMENTOV PRI INTERAKCIJI NOSILEC-TLA

---

VEDRAN JAGODNIK, GORDAN JELENIĆ IŃ ŹELJKO ARBANAS

---

## o avtorjih

Vedran Jagodnik  
University of Rijeka,  
Faculty of Civil Engineering  
R. Matejčić 3, 51 000 Reka, Hrvaška

Gordan Jelenić  
University of Rijeka,  
Faculty of Civil Engineering  
R. Matejčić 3, 51 000 Reka, Hrvaška

Željko Arbanas  
University of Rijeka,  
Faculty of Civil Engineering  
R. Matejčić 3, 51 000 Reka, Hrvaška

---

## izvleček

Članek daje pregled deformacij Bernoullijevega nosilca na Winklerjevi zemljini z uporabo mešane metode končnih elementov. Togostno matriko Bernoullijevega nosilca lahko dobimo z uporabo standardnega pristopa, ki temelji na pomikih in pri katerem je interpolirano zgolj polje pomikov, pa tudi z mešanim pristopom, ki se uporablja pri Timoshenkovem nosilcu drugega reda s popolno strižno togostjo (pri katerem sta dodatno interpolirana rotacijsko polje in iz tega izhajajoče polje strižnih napetosti), vendar pa oba pristopa privedeta do različnih rezultatov togosti zemljine Winklerjevega tipa. Poleg tega se togost zemljine razlikuje tudi v primeru, ko mešano metodo razširimo na oba elementa z dodatnim interpoliranjem porazdeljenega polja reakcije zemljine. Na ta način dobimo štiri različne elemente z enim, dvema, tremi ali štirimi neodvisno interpoliranimi polji, v katerih je togostna matrika nosilca enaka, togostne matrike zemljine pa so različne. Članek pokaže, da je najmanj konvergenten element z enim poljem, ki temelji na pomikih, medtem ko je element mešanega tipa s štirimi interpoliranimi polji najbolj konvergenten.

---

## ključne besede

Bernoullijev nosilec, Winklerjeva zemljina, mešana metoda končnih elementov



---

# ON THE APPLICATION OF A MIXED FINITE-ELEMENT APPROACH TO BEAM-SOIL INTERACTION

---

VEDRAN JAGODNIK, GORDAN JELENIĆ and ŽELJKO ARBANAS

---

## about the authors

Vedran Jagodnik  
University of Rijeka,  
Faculty of Civil Engineering  
R. Matejčić 3, 51 000 Rijeka, Republic of Croatia

Gordan Jelenić  
University of Rijeka,  
Faculty of Civil Engineering  
R. Matejčić 3, 51 000 Rijeka, Republic of Croatia

Željko Arbanas  
University of Rijeka,  
Faculty of Civil Engineering  
R. Matejčić 3, 51 000 Rijeka, Republic of Croatia

---

## abstract

*In this paper the deformation of a Bernoulli beam resting on Winkler's soil is reviewed in terms of the mixed finite-element methodology. While the stiffness matrix of the Bernoulli beam problem utilizing the standard displacement-based approach, in which only the displacement field is interpolated, may be alternatively obtained using a mixed-type approach to the absolutely shear-stiff second-order Timoshenko beam (in which the rotation and shear-stress resultant fields are additionally interpolated), the two approaches lead to different Winkler-type soil-stiffness contributions. Furthermore, extending the mixed-type formalism to both of these elements by additionally interpolating the distributed soil-reaction field, the soil-stiffness contributions also differ. In this way four different elements are obtained, with one, two, three or four independently interpolated fields, in which the beam-stiffness matrix is equal, but the soil-stiffness matrices are different. It is demonstrated that the displacement-based one-field element is the least convergent, while the mixed-type element with four interpolated fields is the most convergent.*

---

## keywords

Bernoulli beam, Winkler soil, mixed finite-element method

---

## 1 INTRODUCTION

Among many other engineering fields, the well-known Bernoulli beam theory [1, 2] finds widespread application in the numerical analyses of slender engineering structures resting on deformable soil. In contrast to beam structures that are subject to known point or distributed external loading, in this case the actual deformation of the structure results in a soil-induced reaction that depends on the actual constitution of the soil. To avoid the very complex (nonlinear, anisotropic, heterogeneous and stress-dependent) behavior of the soil, the subsoil is often modelled by a simpler system called a subgrade reaction model [3].

In [3] Winkler proposed a model that assumes a constant ratio between the contact pressure and the associated deflection of the soil (settlement) defined by the modulus of subgrade reaction  $k_s$ . Many researchers [4-11] have investigated the modulus of subgrade reaction, and it was found that the geometry, the foundation dimensions and the soil layering below the foundation structure are the most important parameters needed to define this modulus. Terzaghi made recommendations for how to obtain the modulus of the subgrade reaction from a 1 ft x 1 ft rigid plate test placed on different soil layers [5]. Biot solved the problem with an infinite beam model on a 3D elastic soil continuum loaded with a concentrated force [4].

The modulus of the subgrade reaction can be measured using different experiments such as the plate-load test, the oedometer test, the triaxial compression test and the California Bearing Ratio (CBR) test. The ranges of values for the modulus of the subgrade reaction for typical soil types are given in Table 1.

The desired value of the modulus of the subgrade reaction to be used in the present uniaxial beam model, of course, is measured in force-per-length-squared, rather than force-per-length-cubed. To distinguish between the two, the former modulus will be denoted simply as  $k$ , and is related to  $k_s$  via  $k = Bk_s$  with  $B$  as the foundation-strip width.

**Table 1.** Range of values for the modulus of the subgrade reaction  $k_s$  [12].

Soil	$k_s$ [kN/m <sup>3</sup> ]
Loose sand	4800 – 16000
Medium dense sand	9600 – 80000
Dense sand	64000 – 128000
Clayey medium dense sand	32000 – 80000
Silty medium dense sand	24000 – 48000
Clayey soil:	
$q_u \leq 200$ kPa	12000 – 24000
$200 < q_u \leq 400$ kPa	24000 – 48000
$q_u > 400$ kPa	> 48000

( $q_u$  = uniaxial compressive strength)

In [6] Vesić gave an expression for  $k$  as a direct function of the material properties of the soil (Young's modulus  $E_s$ , Poisson's ratio  $\nu$ ) as well as the material and geometric properties of the foundation strip (Young's modulus  $E$ , foundation width  $B$ , and its second moment of area  $I$ ) as:

$$k = 0.65 \sqrt[3]{\frac{E_s \cdot B^4}{E \cdot I} \cdot \frac{E_s}{1 - \nu^2}} \quad (1)$$

The solution to the problem of a beam resting on Winkler's soil changes considerably with respect to the problem of a beam with no such soil contribution and standard, point-wise, supporting conditions. The resulting deformation ceases to be polynomial and becomes a combination of trigonometric and hyperbolic functions [13].

Using the finite-element method for the problems of beam-soil interaction is as popular as elsewhere in structural analyses, and standard beam finite elements [1, 2] are regularly used in academic and commercial software. In addition, a number of special-type finite elements using a non-polynomial interpolation of the deformation field have been proposed and successfully tested against the exact results, which they are required to reproduce by design [14, 15].

Even though such 'exact' beam-soil finite elements exist, they by no means obviate the need to assess the performance of the standard finite elements based on a polynomial interpolation. For one reason, the former elements are designed for a situation of limited applicability (e.g., Bernoulli beam on Winkler's soil) and there is no guarantee that they will perform better than the standard beam elements when applied to a different problem, e.g., a non-linear beam or soil model. Additionally, the shape functions used in these elements are

non-standard and sometimes contain singularities [15] for extreme values of beam-to-soil stiffness.

With this motivation in mind, after defining the model problem in Section 2, in Section 3 we recall that the solution to the Bernoulli beam problem utilizing the standard displacement-based approach may be completely recovered using a mixed-type approach to the second-order Timoshenko beam, leading to results with a well-defined shear-rigid limit [16]. In Section 4, we investigate the application of the two approaches to the Bernoulli beam resting on Winkler's soil and show that the resulting soil-stiffness contributions become different, even though the beam-stiffness contribution is the same. Additionally, if the distributed soil-reaction field is interpolated independently from the interpolation of the displacement of the beam reference line using a mixed-type technique, we show that both of the above soil-stiffness contributions experience further changes, effectively leading to four different solutions for the soil-stiffness contribution associated with the same beam stiffness. In Section 5 we numerically analyze the results and assess their performance on two simple test examples.

## 2 THEORETICAL PROBLEM SET-UP

Let us consider a straight beam of length  $L$  and uniform cross-sectional bending stiffness  $EI$ , loaded by a distributed static loading  $q$  and an arbitrary point loading resting on a reacting soil with a distributed soil-reaction field  $f(x)$ , which is proportional to the amount of displacement, i.e.,  $f(x) = kw(x)$ , with  $k$  as the modulus of the subgrade reaction.

As a result, the beam deflects by an amount  $w(x)$  and its cross-sections rotate by an amount  $\theta(x)$  (here assumed as positive in the counter-clockwise direction), from where the stress-couple resultant may be obtained as  $M(x) = EI\theta'(x)$ , while the shear-stress resultant follows from  $T(x) = M'(x)$ , where the dash (') indicates a differentiation with respect to the longitudinal coordinate  $x$ .

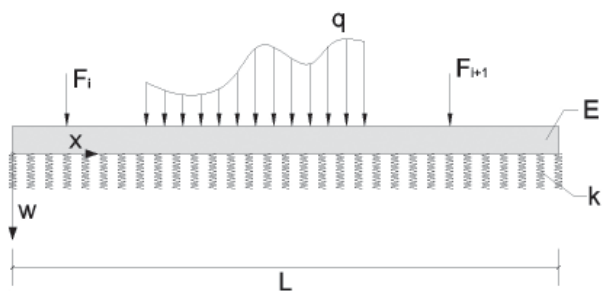


**Figure 1.** Straight beam on elastic soil.

### 3 SUMMARY OF THE BERNOULLI BEAM THEORY

#### 3.1 DISPLACEMENT-BASED APPROACH TO THE BERNOULLI BEAM PROBLEM

In the Bernoulli beam theory (see, e.g., [17]) the cross-sectional rotations are the same as the rotations of the beam centroidal line ( $\theta(x) = -w'(x)$ ) giving the stress-couple resultant in a cross-section as  $M(x) = -EIw''(x)$ . Equilibrium is achieved when the total potential energy of the problem  $V = V_{def} - U$  is stationary, where  $V_{def} = \frac{1}{2} \int_0^L EIw''^2 dx$  is the strain energy and  $U = \int_0^L q dx + U_{0,L}$  is the work of the applied loading with  $U_{0,L} = w(0)F_0 + w'(0)M_0 + w(L)F_L + w'(L)M_L$  as the work of the boundary point forces  $F_0, F_L$  and moments  $M_0, M_L$ . By dividing the beam length into  $N_{el}$  finite elements of length  $l_i = x_{i+1} - x_i > 0$  each, and assuming a distribution of the displacement field within each element using the standard Hermitean polynomials, the above becomes

$$\sum_{i=1}^{N_{el}} \delta \mathbf{p}_i^t (\mathbf{K}_{b,i} \mathbf{p}_i - \mathbf{R}_i) = 0 \quad (2)$$

with  $\mathbf{p}_i$  as the vector of the standard nodal degrees of freedom (vertical displacement and rotation at both ends),  $\delta \mathbf{p}_i$  as its variation,

$$\mathbf{K}_{b,i} = \frac{EI}{l_i^3} \begin{bmatrix} 12 & -6l_i & -12 & -6l_i \\ -6l_i & 4l_i^2 & 6l_i & 2l_i^2 \\ -12 & 6l_i & 12 & 6l_i \\ -6l_i & 2l_i^2 & 6l_i & 4l_i^2 \end{bmatrix} \quad (3)$$

as the element stiffness matrix and  $\mathbf{R}_i$  as the corresponding element load vector.

#### 3.2 BERNOULLI BEAM AS A SHEAR-RIGID SECOND-ORDER TIMOSHENKO BEAM

The above result may be reproduced using the Timoshenko beam theory (see, e.g., [17]) with an infinite shear stiffness. In the Timoshenko beam theory, the cross-sectional rotation is in general assumed to differ from the amount of rotation of the beam centroidal line by a shear angle  $\gamma(x) = \theta(x) + w'(x)$ , resulting in a shear-stress resultant  $T(x) = GA\gamma(x)$  where  $G$  is the shear modulus of the beam material and  $A$  is the shear area of the cross-section. We consider the shear-stress resultant  $T$  as an independent field and, instead of  $V = V_{def} - U$ , we start from the condition of stationarity of a mixed func-

$$\text{tional } V^* = V_d + V_{dT} - V_T - U \text{ with } V_d = \frac{1}{2} \int_0^L EI\theta'^2 dx, \\ V_{dT} = \int_0^L (w' + \theta)T dx \text{ and } V_T = \frac{1}{2} \int_0^L \frac{T^2}{GA} dx.$$

Assuming a quadratic Lagrangian interpolation for the displacements and the rotations

$$(I^1(\xi) = -\xi \frac{1-\xi}{2}, I^2(\xi) = 1 - \xi^2 \text{ and } I^3(\xi) = \xi \frac{1+\xi}{2}) \text{ and} \\ \text{a linear shear-stress resultant field } (T = \mathbf{N}_T^t \mathbf{T}_i \text{ with } \mathbf{N}_T = (1 \quad \xi)) \text{ thus leads to}$$

$$\sum_{i=1}^{N_{el}} \left[ \delta \mathbf{p}_i^t (\mathbf{K}_{d,i} \mathbf{p}_i + \mathbf{K}_{dT,i} \mathbf{T}_i - \mathbf{R}_i) + \delta \mathbf{T}_i^t (\mathbf{K}_{dT,i}^t \mathbf{p}_i + \mathbf{K}_{T,i} \mathbf{T}_i) \right] = 0 \quad (4)$$

with

$$\mathbf{K}_{d,i} = \frac{2}{l_i} \int_{-1}^1 \frac{d\mathbf{N}^t}{d\xi} \begin{bmatrix} 0 & 0 \\ 0 & EI \end{bmatrix} \frac{d\mathbf{N}}{d\xi} d\xi \quad (5)$$

$$\mathbf{K}_{dT,i} = \int_{-1}^1 \left( \frac{d}{d\xi} \frac{l_i}{2} \mathbf{N} \right)^t \mathbf{N}_T d\xi \quad (6)$$

$$\mathbf{K}_{T,i} = -\frac{l_i}{2GA} \int_{-1}^1 \mathbf{N}_T^t \mathbf{N}_T d\xi \quad (7)$$

where

$$\mathbf{N}(\xi) = \begin{bmatrix} I^1(\xi) & 0 & I^2(\xi) & 0 & I^3(\xi) & 0 \\ 0 & I^1(\xi) & 0 & I^2(\xi) & 0 & I^3(\xi) \end{bmatrix}.$$

Since (4) must hold true for any variations  $\delta \mathbf{p}_i$  and  $\delta \mathbf{T}_i$  it turns out that for any discontinuous interpolation for the shear stress resultant field (which is admissible owing to the fact that no derivatives of  $T$  with respect to  $x$  appear in  $V^*$ ) the term within the second parentheses must vanish. This results in

$$\sum_{i=1}^{N_{el}} \delta \mathbf{p}_i^t \left( \underbrace{\mathbf{K}_{d,i} - \mathbf{K}_{dT,i} \mathbf{K}_{T,i}^{-1} \mathbf{K}_{dT,i}^t}_{\mathbf{K}_{b,i}} \mathbf{p}_i - \mathbf{R}_i \right) = 0 \quad (8)$$

with  $\mathbf{K}_{b,i}$  as the stiffness matrix of a three-node element in which the displacement and the rotation at the internal node may be condensed out to eventually give

$$\mathbf{K}_{b,i} = \frac{EI}{(1+\phi)l_i^3} \begin{bmatrix} 12 & -6l_i & -12 & -6l_i \\ -6l_i & (4+\phi)l_i^2 & 6l_i & (2-\phi)l_i^2 \\ -12 & 6l_i & 12 & 6l_i \\ -6l_i & (2-\phi)l_i^2 & 6l_i & (4+\phi)l_i^2 \end{bmatrix}, \quad (9)$$

with  $\phi = \frac{12EI}{GA l_i^2}$ , which coincides with the result obtained in [16] using the stiffness-based approach. This result can also be obtained by consistently deriving the appropriate shape functions needed to obtain the exact solution, as shown by Reddy [18]. This stiffness matrix has a well-defined shear-rigid limit that coincides with (3).

## 4 BERNOULLI BEAM ON WINKLER'S SOIL

The differential equation for a Bernoulli beam resting on Winkler's soil (see, e.g., [19]) is given as

$$EIw^{IV}(x) + kw(x) = q(x) \quad (10)$$

defined over a domain  $0 < x < L$  with known values for  $w$  or its derivatives at  $x = 0, L$  as the boundary conditions. For known boundary conditions, the above differential equation is easily solved [13].

### 4.1 DISPLACEMENT-BASED APPROACH TO THE ORIGINAL BERNOULLI-WINKLER PROBLEM (ONE-FIELD INTERPOLATION)

The problem may be variationally approached in a manner completely analogous to that presented in Section 3.1 with the only difference being that the strain energy of the problem is now

$$V_{def} = \frac{1}{2} \int_0^L (EIw''^2 + kw^2) dx \text{ rather than } \frac{1}{2} \int_0^L EIw''^2 dx.$$

From  $\delta V = 0$ , therefore, it now follows

$$\sum_{i=1}^{N_{el}} \delta \mathbf{p}_i^t (\mathbf{K}_i \mathbf{p}_i - \mathbf{R}_i) = 0 \quad (11)$$

with  $\mathbf{K}_i = \mathbf{K}_{b,i} + \mathbf{K}_{s,i}$  and

$$\mathbf{K}_{s,i} = \int_{-1}^1 \frac{kl_i}{2} \mathbf{N}_i^t \mathbf{N}_i d\xi, \quad (12)$$

where  $\mathbf{K}_{s,i}$  denotes the soil part of the stiffness matrix. Using the standard Hermitean polynomials

$$\mathbf{N}_i = \left\langle \frac{2(1-\xi) - \xi(1-\xi^2)}{4} \quad \frac{l_i(1-\xi^2)(1-\xi)}{8} \right. \\ \left. \frac{(1+\xi) + \xi(1-\xi^2)}{4} \quad \frac{l_i(1-\xi^2)(1+\xi)}{8} \right\rangle$$

this matrix is computed as

$$\mathbf{K}_{s,i} = kl_i \begin{bmatrix} \frac{13}{35} & -\frac{11}{210}l_i & \frac{9}{70} & \frac{13}{420}l_i \\ -\frac{11}{210}l_i & \frac{1}{105}l_i^2 & -\frac{13}{420}l_i & -\frac{1}{140}l_i^2 \\ \frac{9}{70} & -\frac{13}{420}l_i & \frac{13}{35} & \frac{11}{210}l_i \\ \frac{13}{420}l_i & -\frac{1}{140}l_i^2 & \frac{11}{210}l_i & \frac{1}{105}l_i^2 \end{bmatrix}. \quad (13)$$

### 4.2 MIXED APPROACH TO THE ORIGINAL BERNOULLI-WINKLER PROBLEM (TWO-FIELD INTERPOLATION)

Instead of minimizing the total potential energy of the problem, it is possible to approach the task from the standpoint of the Hellinger-Reissner complementary energy principle [1]. In particular, let us introduce a new function  $f(x)$  (the distributed soil-reaction field), which, although obviously uniquely related to the unknown displacement function  $w(x)$ , serves to define a new two-field potential  $V^* = V_b + V_{bf} - V_f - U$ , where  $V_b = \frac{1}{2} \int_0^L EIw''^2 dx$ ,  $V_{bf} = \int_0^L fw dx$  and  $V_f = \frac{1}{2k} \int_0^L f^2 dx$  in which  $w(x)$  and  $f(x)$  may be treated (and interpolated) as independent fields. Furthermore, owing to the absence of any derivatives on  $f(x)$ , this function only requires  $C^1$  continuity, i.e., it does not have to be continuous between the elements. From  $\delta V^* = 0$  we therefore obtain

$$\delta V_b + \int_0^L \delta w f dx + \int_0^L \delta f w dx - \int_0^L \delta f \frac{f}{k} dx - \delta U = 0. \quad (14)$$

Dividing the beam into  $N_{el}$  finite elements as before, and now additionally assuming the interpolation of the distributed soil-reaction field within each element as  $f_i(\xi) = \mathbf{N}_{f,i}(\xi) \mathbf{f}_i$  with  $\mathbf{f}_i = \langle f \quad f_M \rangle_i$  where  $M-1$  is the order of the polynomial used to describe the distributed soil-reaction field, the above equation becomes

$$\sum_{i=1}^{N_{el}} \left[ \delta \mathbf{p}_i^t (\mathbf{K}_{b,i} \mathbf{p}_i + \mathbf{K}_{bf,i} \mathbf{f}_i - \mathbf{R}_i) + \delta \mathbf{f}_i^t (\mathbf{K}_{bf,i}^t \mathbf{p}_i + \mathbf{K}_{f,i} \mathbf{f}_i) \right] = 0 \quad (15)$$

with

$$\mathbf{K}_{bf,i} = \frac{l_i}{2} \int_{-1}^1 \mathbf{N}_i^t \mathbf{N}_{f,i} d\xi \quad (16)$$

$$\mathbf{K}_{f,i} = -\frac{l_i}{2k} \int_{-1}^1 \mathbf{N}_{f,i}^t \mathbf{N}_{f,i} d\xi. \quad (17)$$

Since (15) must hold true for any variations  $\delta \mathbf{p}_i$  and  $\delta \mathbf{f}_i$  it turns out that for any discontinuous interpolation for the

distributed soil-reaction field the term within the second parentheses must vanish. As a result

$$f_i = -K_{f,i}^{-1} K_{bf,i}^t p_i \quad (18)$$

and (15) becomes

$$\sum_{i=1}^{N_{el}} \delta p_i^t \left[ (K_{b,i} - K_{bf,i} K_{f,i}^{-1} K_{bf,i}^t) p_i - R_i \right] = 0 \quad (19)$$

The soil-stiffness contribution to the element stiffness matrix from here immediately follows as

$$K_{s,i} = -K_{bf,i} K_{f,i}^{-1} K_{bf,i}^t \quad (20)$$

As already mentioned, the interpolation for  $f(\xi)$  does not have to be continuous across the elements and  $N_{f,i}(\xi) = \langle 1 \rangle$ ,  $N_{f,i}(\xi) = \langle 1 \ \xi \rangle$ ,  $N_{f,i}(\xi) = \langle 1 \ \xi \ \xi^2 \rangle$  and  $N_{f,i}(\xi) = \langle 1 \ \xi \ \xi^2 \ \xi^3 \rangle$  all make the possible choices. For a constant approximation of the distributed soil-reaction field, the soil-stiffness contribution to the element stiffness matrix thus follows as

$$K_{s,i} = \frac{kl_i}{144} \begin{bmatrix} 36 & -6l_i & 36 & 6l_i \\ -6l_i & l_i^2 & -6l_i & -l_i^2 \\ 36 & -6l_i & 36 & 6l_i \\ 6l_i & -l_i^2 & 6l_i & l_i^2 \end{bmatrix} \quad (21)$$

while for a linear approximation of the distributed soil-reaction field, it becomes

$$K_{s,i} = \frac{kl_i}{1800} \begin{bmatrix} 666 & -93l_i & 234 & 57l_i \\ -93l_i & 14l_i^2 & -57l_i & -11l_i^2 \\ 234 & -57l_i & 666 & 93l_i \\ 57l_i & -11l_i^2 & 93l_i & 14l_i^2 \end{bmatrix} \quad (22)$$

For a quadratic approximation of the distributed soil-reaction field, the soil-stiffness contribution to the element stiffness matrix becomes

$$K_{s,i} = \frac{kl_i}{1800} \begin{bmatrix} 666 & -93l_i & 234 & 57l_i \\ -93l_i & 16.5l_i^2 & -57l_i & -13.5l_i^2 \\ 234 & -57l_i & 666 & 93l_i \\ 57l_i & -13.5l_i^2 & 93l_i & 16.5l_i^2 \end{bmatrix}, \quad (23)$$

while for a cubic and all further higher-order approximations of the distributed soil-reaction field, the soil-stiffness contribution to the element stiffness matrix is, as expected, identical to the one obtained

using the displacement-based approach (13), in which the displacement field, from which the distributed soil-reaction is computed, is cubic.

### 4.3 BERNOULLI-WINKLER BEAM AS A SECOND-ORDER SHEAR-RIGID TIMOSHENKO BEAM ON WINKLER'S SOIL [THREE-FIELD INTERPOLATION]

The problem can also be variationally approached in a manner completely analogous to that presented in Section 3.2, with the only difference being that the original three-field mixed functional  $V^*$  is now substituted with  $V^* + \frac{1}{2} \int_0^L kw^2 dx$ . From  $\delta V^* + \int_0^L \delta w k w dx = 0$ , therefore, it now follows

$$\sum_{i=1}^{N_{el}} \delta p_i^t \left[ (K_{b,i} + K_{s,i}) p_i - R_i \right] = 0 \quad (24)$$

with

$$K_{s,i} = \frac{kl_i}{2} \int_{-1}^1 N^t \begin{bmatrix} 1 & 0 \\ 0 & 0 \end{bmatrix} N d\xi \quad (25)$$

The soil contribution to the element's stiffness matrix for a shear-rigid element ( $GA \rightarrow \infty$ ) upon condensation of the mid-node degrees of freedom reads

$$K_{s,i} = \frac{kl_i}{6} \begin{bmatrix} 2 & -\frac{l_i}{4} & 1 & \frac{l_i}{4} \\ -\frac{l_i}{4} & \frac{l_i^2}{20} & -\frac{l_i}{4} & -\frac{l_i^2}{20} \\ 1 & -\frac{l_i}{4} & 2 & \frac{l_i}{4} \\ \frac{l_i}{4} & -\frac{l_i^2}{20} & \frac{l_i}{4} & -\frac{l_i^2}{20} \end{bmatrix} \quad (26)$$

It should be noted by comparing (13) and (26) that even though the shear-rigid second-order Timoshenko beam reproduces the stiffness matrix of the Bernoulli beam, the same is not true for the ensuing soil part.

### 4.4 DUAL MIXED APPROACH TO THE SHEAR-RIGID TIMOSHENKO-WINKLER PROBLEM [FOUR-FIELD INTERPOLATION]

Obviously, the mixed approaches described in Sections 3.2 (where displacement, rotation and shear-stress resultant have been interpolated as independent fields) and 4.2 (where displacement and distributed soil-reaction field have been interpolated as independent fields) can be easily

combined to form a four-field functional  $V^{**} = V_d + V_{dT} - V_T + V_{bf} - V_f - U$ . From  $\delta V^{**} = 0$  we now obtain

$$\sum_{i=1}^{N_d} \left[ \delta \mathbf{p}_i^t (\mathbf{K}_{d,i} \mathbf{p}_i + \mathbf{K}_{dT,i} \mathbf{T}_i + \mathbf{K}_{bf,i} \mathbf{f}_i - \mathbf{R}_i) + \delta \mathbf{T}_i^t (\mathbf{K}_{dT,i}^t \mathbf{p}_i + \mathbf{K}_{T,i} \mathbf{T}_i) + \delta \mathbf{f}_i^t (\mathbf{K}_{bf,i}^t \mathbf{p}_i + \mathbf{K}_{f,i} \mathbf{f}_i) \right] = 0 \quad (27)$$

which, after condensing out the shear-stress resultant and distributed soil-reaction parameters, turns into  $\sum_{i=1}^{N_d} \delta \mathbf{p}_i^t [(\mathbf{K}_{b,i} + \mathbf{K}_{s,i}) \mathbf{p}_i - \mathbf{R}_i] = 0$  with

$$\mathbf{K}_{s,i} = -\mathbf{K}_{bf,i} \mathbf{K}_{f,i}^{-1} \mathbf{K}_{bf,i}^t \quad (28)$$

It should be noted that the soil part of the stiffness matrix (28) is not necessarily the same as in (20) for the corresponding choice of interpolation for the distributed soil-reaction field, since the interpolation for the displacement field is different.

For a three-node shear-rigid beam element with a constant and a linear approximation of the distributed soil-reaction field, the soil part of the stiffness matrix upon condensation of the mid-node degrees of freedom becomes, respectively,

$$\mathbf{K}_{s,i} = \frac{kl_i}{144} \begin{bmatrix} 36 & -9l_i & 36 & 9l_i \\ -9l_i & \frac{9}{4}l_i^2 & -9l_i & -\frac{9}{4}l_i^2 \\ 36 & -9l_i & 36 & 9l_i \\ 9l_i & -\frac{9}{4}l_i^2 & 9l_i & \frac{9}{4}l_i^2 \end{bmatrix} \quad (29)$$

and

$$\frac{kl_i}{144} \begin{bmatrix} 48 & -6l_i & 24 & 6l_i \\ -6l_i & l_i^2 & -6l_i & -l_i^2 \\ 24 & -6l_i & 48 & 6l_i \\ 6l_i & -l_i^2 & 6l_i & l_i^2 \end{bmatrix},$$

while for the quadratic and higher-order approximation of the distributed soil-reaction field we obtain the same result as in (26).

## 5 NUMERICAL EXAMPLES

In this section, two problems will be analyzed: a rectangular beam on an elastic foundation with the concentrated load in the middle of the span and a beam on an elastic foundation with the concentrated force at a boundary, thus simulating a laterally loaded pile. For each example a displacement convergence analysis

is undertaken for different values of the relative soil-stiffness parameter  $\beta = \frac{kL^4}{4EI}$ .

Six values of the relative soil-stiffness parameter  $\beta$  have been considered: 1, 5, 10, 50, 100 and 500. Using the expression for  $\beta$  and back-calculating the desired value for the modulus of the subgrade reaction  $k$ , and then plugging it into the equation for the modulus of the subgrade reaction proposed by Vesić [6] (1), approximate values of the Young's modulus can be obtained, which makes it possible to classify the soils in a range between soft and hard. Which soil the particular value of the relative soil-stiffness parameter  $\beta$  is describing is given in Table 2.

**Table 2.** Soil description based on the relative soil-stiffness parameter  $\beta$ .

$\beta$	Soil Description
1	Very loose sand
5	Stiff clay
10	Medium dense sand
50	Very dense gravel
100	Weak rock mass
500	Hard rock mass

### 5.1 THIN BEAM ON WINKLER'S FOUNDATION SUBJECT TO A CONCENTRATED FORCE IN THE MIDDLE

The problem is sketched in Figure 2. The material and geometric properties of the beam and loading are summarized in Table 3.

**Table 3.** Beam parameters.

Length	3.0 m
Width	0.3 m
Young's modulus	$3.15 \cdot 10^7$ kPa
Second moment of area	$0.000675$ m <sup>4</sup>
Force	1.0 kN

Due to its symmetry, only one half of the problem is analyzed with the rotation at the symmetry line being set to zero. In the absence of the soil stiffness, all the approaches would return exact nodal results for the displacements and rotations, provided a suitable supporting (e.g., a simple support at the free end) were defined.

The results for the displacement in the middle of the beam will be normalized with respect to the exact solution provided by Hetenyi [13], expressed in terms of the parameter  $\beta$ :

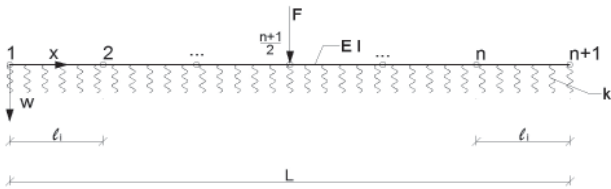


Figure 2. Mesh of  $n$  finite elements for a beam on Winkler's foundation with a point force in the middle.

$$\omega = \frac{P \cdot L^3}{8 \cdot \beta^{3/4} \cdot EI} \cdot \frac{\cos(\sqrt[4]{\beta}) + \cosh(\sqrt[4]{\beta}) + 2}{\sin(\sqrt[4]{\beta}) + \sinh(\sqrt[4]{\beta})} \quad (30)$$

### 5.1.1 Displacement convergence analysis

We first analyze the convergence properties of the different formulations and in Table 4 show the normalized displacements in the middle of the beam for meshes with two, four, eight, sixteen, thirty-two and sixty-four elements for a soft, moderately hard and hard soil ( $\beta = 5$ ,  $\beta = 50$  and  $\beta = 500$ , respectively).

It is immediately obvious that a constant approximation of the distributed soil-reaction field (equations (21) and (29)<sub>1</sub>) is inferior to the linear (equations (22) and (29)<sub>2</sub>) or quadratic interpolation (23). The use of the quadratic approximation of the distributed soil-reaction field in

Table 4. Values of normalized displacements at mid-span for  $\beta = 5, 50$  and  $500$ .

Formulation	Elements	$\beta = 5$	$\beta = 50$	$\beta = 500$
One-field (13)	2	0.998348089607226	0.987206820721338	0.919540084654748
	4	0.999897498365916	0.999168178332181	0.991938846421126
	8	0.999994057876285	0.999948078751554	0.999469328447786
	16	1.000000000000000	0.999996754921972	0.999962094889128
	32	1.000000000000000	1.000000000000000	0.999993682481521
	64	1.000000000000000	1.000000000000000	0.999993682481521
Two-field constant (21)	2	1.000506566046710	1.104105348213100	2.838429464906180
	4	1.000401093350760	1.020562977770130	1.100707562069620
	8	1.000120328005230	1.0050374422791980	1.022281887674520
	16	1.000031196149500	1.001255845196800	1.005489923558030
	32	1.000008913185570	1.000313690876030	1.001370901509890
	64	1.000002971061860	1.000077881872670	1.000341145997850
Two-field (linear) (22)	2	0.998404539782518	0.989357225761160	0.925636489986733
	4	0.999903440489631	0.999378026711319	0.993031777117948
	8	0.999994057876285	0.999962140756341	0.999583043780403
	16	1.000000000000000	0.999997836614648	0.999974729926085
	32,64	1.000000000000000	1.000000000000000	0.999993682481521
	Two-field quadratic (23)	2	0.998351060669083	0.987360421081325
4		0.999897498365916	0.999172505102885	0.992039926716786
8		0.999994057876285	0.999948078751554	0.999469328447786
16		1.000000000000000	0.999996754921972	0.999962094889128
32,64		1.000000000000000	1.000000000000000	0.999993682481521
Three-field (26)		2	0.998599144334185	0.998335274971687
	4	0.999910868144275	0.999731740216360	0.997757280940047
	8	0.999995543407214	0.999979447839157	0.999772569334765
	16	1.000000000000000	0.999998918307324	0.999981047444564
	32	1.000000000000000	1.000000000000000	0.999993682481521
	64	1.000000000000000	1.000000000000000	1.000000000000000
Four-field constant (29) <sub>1</sub>	2	0.986178620238873	0.999778253001427	2.229098490113080
	4	0.996439182363777	0.993338936501395	1.030696822288210
	8	0.999108681442747	0.998246576172258	1.004378040305770
	16	0.999777170360687	0.999561914466233	1.001029755512030
	32	0.999945035355636	0.999890749039727	1.000252700739150
	64	0.999986630221641	0.999971875990425	1.000063175184790
Four-field (linear) (29) <sub>2</sub>	2	0.998651137916691	1.000393736134050	1.013683745024950
	4	0.999915324737061	0.999937261824794	0.998742813822731
	8	0.999995543407214	0.999994591536620	0.999892602185862
	16	1.000000000000000	0.999998918307324	0.999987364963043
	32	1.000000000000000	1.000000000000000	0.999993682481521
	64	1.000000000000000	1.000000000000000	1.000000000000000

the two-field approach gives marginally less-convergent results than the use of the linear approximation of this field and in what follows only such a linear approximation of the distributed soil-reaction field will be analyzed. The corresponding formulations (22) and (29)<sub>2</sub> will be denominated as *the* two-field formulation and *the* four-field formulation, respectively.

The results from Table 4 for the one-field, two-field, three-field and four-field formulations are shown graphically in Figures 3, 4 and 5. From these figures it can be easily concluded that the three-field and four-field element formulations behave visibly better than the one-field and two-field element formulations.

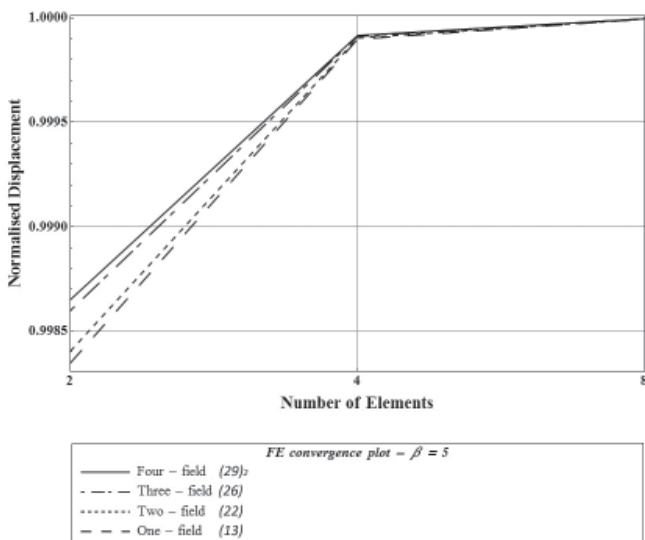


Figure 3. Normalized displacements in the middle of the beam depending on the soil stiffness for various elements ( $\beta = 5$ ).

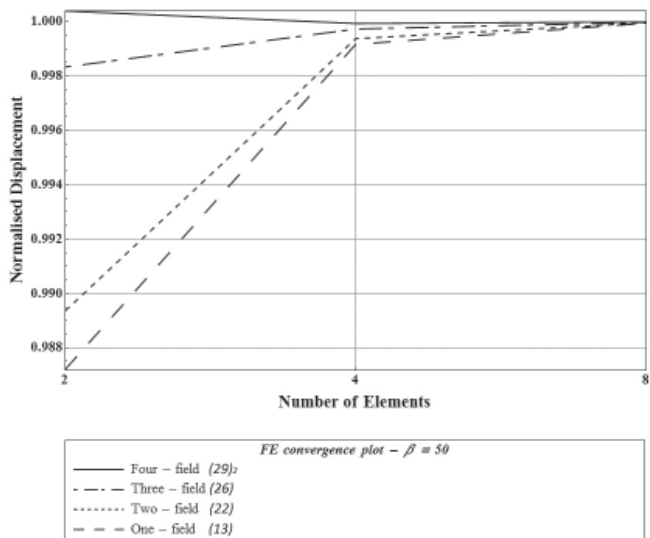


Figure 4. Normalized displacements in the middle of the beam depending on the soil stiffness for various elements ( $\beta = 50$ ).

Additionally, it can be observed that the four-field element converges better than the three-field element and, apart from the two-element case with  $\beta = 500$  (hard soil), is also the most accurate one, regardless of the mesh size. Likewise, the two-field element is more accurate than the one-field element.

It is interesting to note that the mixed character of the formulations becomes increasingly pronounced as the soil gets stiffer, whereby, for the three-field and four-field formulations, the convergence ceases to be monotonous from the stiff side. The superiority of the three-field and four-field formulations compared to the one-field and two-field formulations increases as the soil gets stiffer.

### 5.1.2 Parametric analysis for different soil-to-beam stiffness ratios

We further compare the performance of the four formulations for a fixed eight-element mesh and various soil stiffnesses, including the results for  $\beta = 1$ ,  $\beta = 10$  and  $\beta = 100$ . As an illustration, we also give the results for some other typical soils, given by the values  $\beta = 3$ ,  $\beta = 25$ ,  $\beta = 35$  and  $\beta = 60$ .

Figure 6 shows that between themselves the formulations rank in performance in direct correspondence to the number of fields interpolated, with the four-field formulation consistently the most effective and one-field formulation the least effective.

As already noted, the difference in performance between the formulations increases as the soil gets stiffer, but now it can be seen that this goes hand-in-hand with the

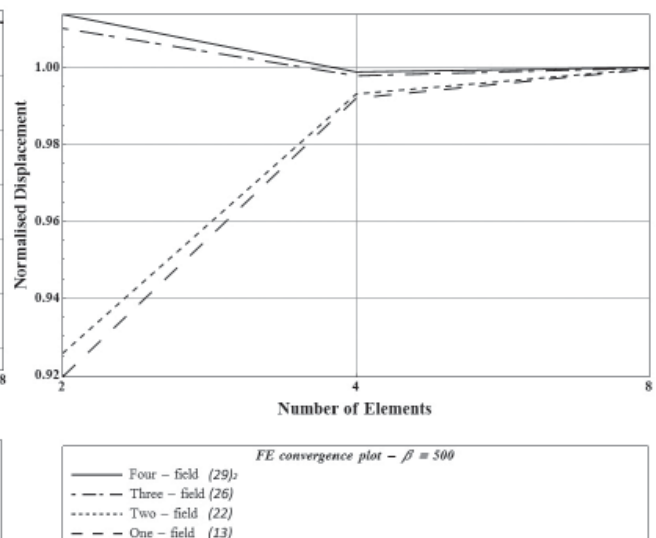


Figure 5. Normalized displacements in the middle of the beam depending on the soil stiffness for various elements ( $\beta = 500$ ).



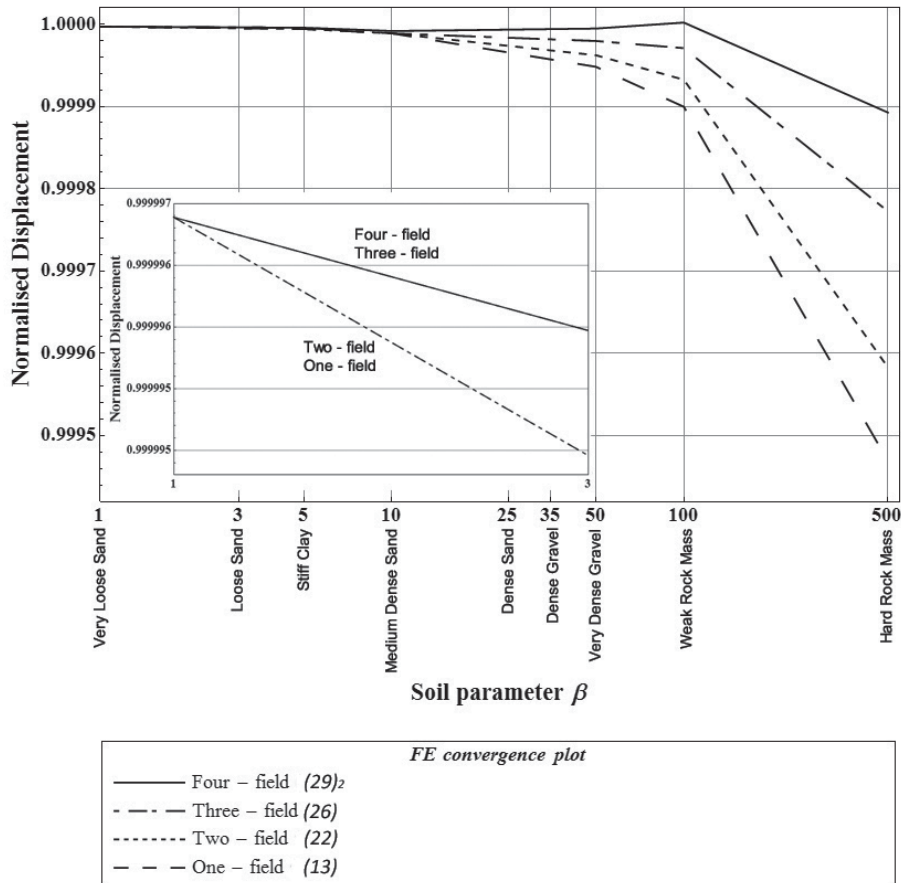


Figure 6. Normalized displacement in the middle of the beam for 8 elements varying with soil stiffness.

general deterioration of the performance. To understand why this is so, it should be noted that any finite-element formulation based on a polynomial interpolation is bound to lose the absolute accuracy as the soil gets stiffer, as in this case the exact solution is dominated by the trigonometric and hyperbolic functions.

### 5.2 THIN PILE IN WINKLER'S SOIL SUBJECT TO A HORIZONTAL FORCE AT THE HEAD

In this section, a beam will be subjected to an end force. Such a set-up can be thought of as a pile (which is essentially a beam embedded in soil) subjected to a horizontal load at the head. This is shown in Figure 7. The material and geometric properties as well as the value of the loading are the same as in the previous model problem (Table 3).

The results for the displacement at the head of the beam will be normalized with respect to the exact solution provided by Hetenyi [13], expressed in terms of the parameter  $\beta$ :

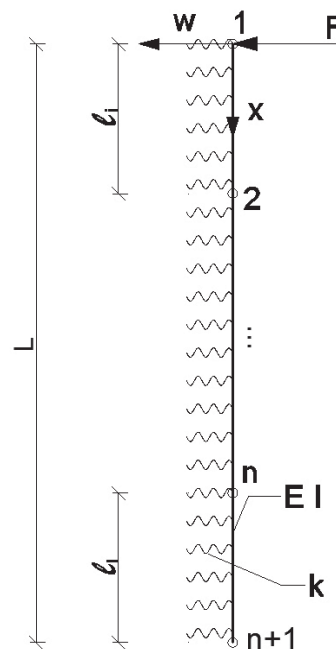


Figure 7. Horizontally loaded pile in Winkler's soil - geometric and material parameters.

$$\omega = \frac{P \cdot L^3}{2 \cdot \beta^{3/4} \cdot EI} \cdot \frac{\sinh(2\sqrt[4]{\beta}) - \sin(2\sqrt[4]{\beta})}{\cos(2\sqrt[4]{\beta}) + \cosh(2\sqrt[4]{\beta}) - 2} \quad (31)$$

### 5.2.1 Displacement convergence analysis

In this example, the constant approximation of the distributed soil-reaction field is also considerably less effective than the linear approximation, while the

quadratic interpolation of that field is marginally less effective than the linear approximation, hence these results are omitted from any further discussion.

The results for the one-field, two-field, three-field and four-field formulations (equations (13), (22), (26) and (29)<sub>2</sub>) for the finite-element meshes of two, four, eight, sixteen, thirty-two and sixty-four elements for a soft, moderately hard and hard soil ( $\beta = 5$ ,  $\beta = 50$  and  $\beta = 500$ , respectively) are given in Table 5.

**Table 5.** Values of normalized displacements at the head of pile for  $\beta = 5, 50$  and  $500$ .

Formulation	Elements	$\beta = 5$	$\beta = 50$	$\beta = 500$
One-field (13)	2	0.998641145803926	0.990463886169159	0.967540844437416
	4	0.999898368245723	0.999206289432062	0.993935963912077
	8	0.999992471721906	0.999947858429844	0.999523932385082
	16	0.999996235860953	0.999997103246102	0.999970037702558
	32	1.000000000000000	1.000000000000000	0.999998335427920
	64	1.000000000000000	1.000000000000000	1.000000000000000
Two-field (22)	2	0.998701372028683	0.993577896609060	1.010959542575590
	4	0.999902132384770	0.999409062204893	0.996364574576991
	8	0.999992471721906	0.999962342199332	0.999685395876855
	16	0.999996235860953	1.000000000000000	0.999980025135038
	32,64	1.000000000000000	1.000000000000000	1.000000000000000
	Three-field (26)	2	0.998678787194399	0.993928403830667
4		0.999905896523818	0.999594454454339	0.997574718479247
8		0.999992471721906	0.999973929214922	0.999838536508227
16		0.999996235860953	1.000000000000000	0.999990012567519
32,64		1.000000000000000	1.000000000000000	1.000000000000000
Four-field (29) <sub>2</sub>		2	0.998742777558203	0.997030827254978
	4	0.999909660662865	0.999797227227169	0.999978360562958
	8	0.999992471721906	0.999988412984410	0.999998335427920
	16	0.999996235860953	1.000000000000000	1.000000000000000
	32,64	1.000000000000000	1.000000000000000	1.000000000000000

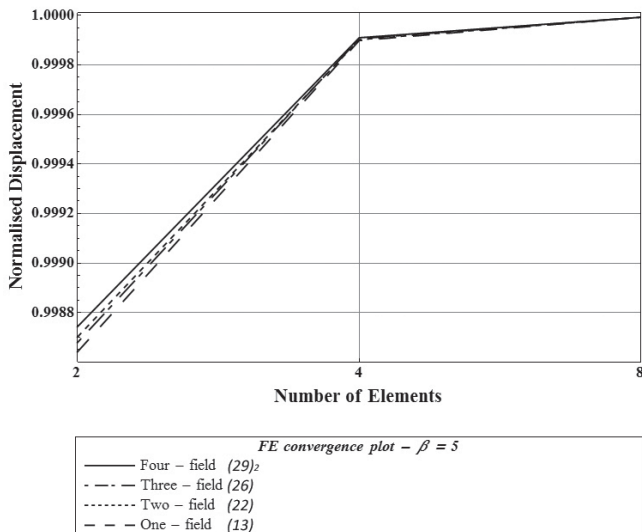


**Figure 8.** Normalized displacements at the head of the pile depending on the soil stiffness for various elements ( $\beta = 5$ ).

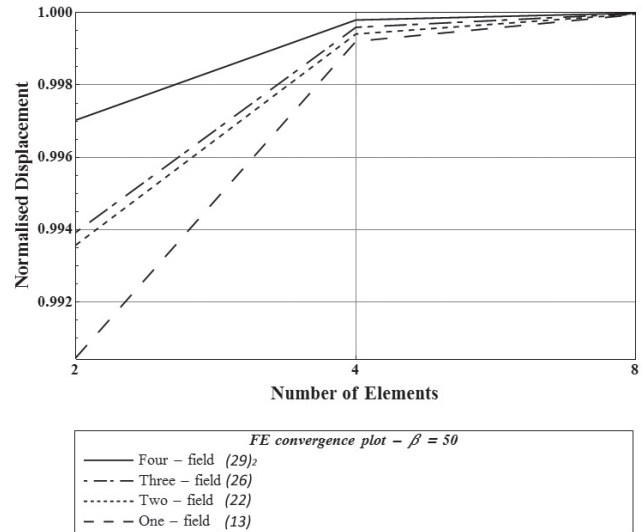


**Figure 9.** Normalized displacements at the head of the pile depending on the soil stiffness for various elements ( $\beta = 50$ ).

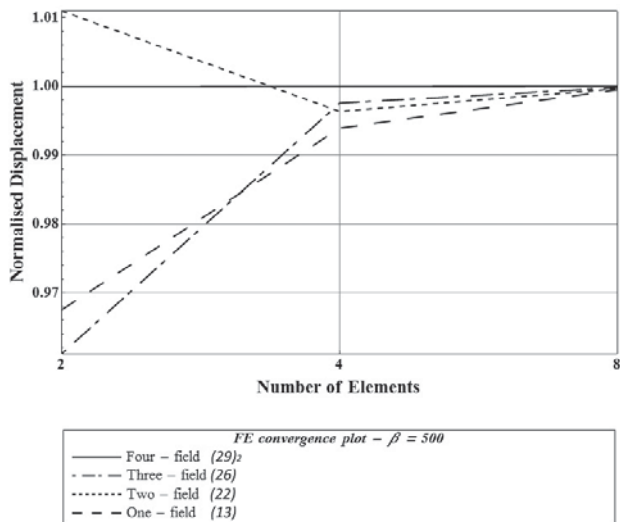


Figure 10. Normalized displacements at the head of the pile depending on the soil stiffness for various elements ( $\beta = 500$ ).

These results are shown graphically in Figures 8, 9 and 10. It can be concluded that, as in the previous example, the three-field and four-field element formulations

behave better than the one-field and two-field element formulations and this is especially true for the values of  $\beta$  of 50 and 500.

Additionally, it can be observed that the four-field element converges better than three-field element, especially for the case of  $\beta = 500$  where it gives results very close to the exact displacement. As in the previous example, the mixed character of the formulations becomes increasingly pronounced as the soil gets stiffer. As in the previous example, the superiority of the three-field and four-field formulations increases as the soil gets stiffer.

### 5.2.2 parametric analysis for different soil-to-pile stiffness ratios

Again, we also compare the performance of the four formulations for a fixed eight-element mesh and various soil stiffnesses, including the results for  $\beta = 1$ ,  $\beta = 10$  and  $\beta = 100$ . As before, we now also give the results for some other typical soils, given by the values  $\beta = 3$ ,  $\beta = 25$ ,  $\beta = 35$  and  $\beta = 60$ . Figure 11 shows that the formulations again rank in performance as in the previous example, with the four-field formulation being by far the most effective.

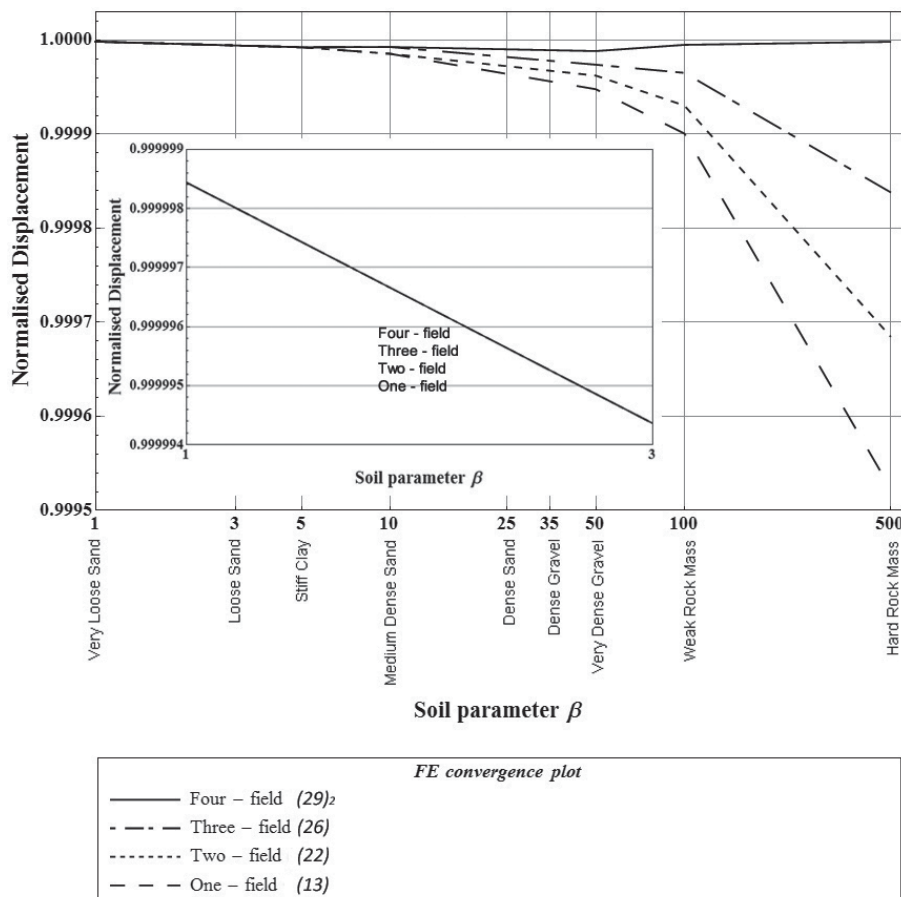


Figure 11. Normalized displacement at the head of the pile for 8 elements varying with soil stiffness.

The difference in performance between the formulations again increases as the soil gets stiffer, but now it can be seen that, in contrast to the previous example, the four-field formulation gives surprisingly good results, even for very hard soils.

## 6 CONCLUSIONS

The classic problem of a Bernoulli beam resting on Winkler's soil has been reviewed in the light of a mixed finite-element design methodology.

It has been recalled that the same standard stiffness matrix of the Bernoulli beam may be obtained either from the classic interpolation of the displacement field using Hermitean polynomials (one-field approach) or as the shear-rigid limit of the second order mixed-type Timoshenko beam in which displacements, rotations and shear-stress resultants are interpolated independently (three-field approach). Still, applying these interpolations to the Bernoulli-Winkler problem results in different respective soil-stiffness contributions. It has been shown on the two model problems analyzed (a beam on an elastic foundation loaded by a central force and a pile horizontally loaded at the head) that the three-field approach is superior to the one-field approach.

Additionally, in both of these finite-element design principles we have investigated the possibility to interpolate the distributed soil-reaction field as an independent field, thus effectively obtaining what we have named the two-field and the four-field approaches. We have analyzed the performance of the finite elements in which this field is approximated by polynomial functions of various orders (constant, linear and, in the two-field approach, quadratic) and concluded that a linear approximation gives the best results.

In both cases, interpolating the distributed soil-reaction field independently improves the results of the underlying formulation, i.e., the two-field approach turns out to be more effective than the one-field approach, while the four-field approach is more effective than the three-field approach. In both the numerical problems analyzed, the four-field approach gives the best results for the displacements regardless of the soil stiffness. The results are surprisingly accurate for the horizontally loaded pile embedded in hard soil.

## ACKNOWLEDGEMENTS

This work has been financially supported by the Ministry of Science, Education and Sports of the Republic of

Croatia through the Research Project 114-0000000-3025 (Improved accuracy in non-linear beam elements with finite 3D rotations).

## REFERENCES

- [1] Bathe K. J. (1985). *Finite Element Procedures*, Prentice-Hall, New Jersey.
- [2] Zienkiewicz O. C., Taylor R. L. (2005). *The Finite Element Method for Solid and Structural Mechanics*, Elsevier Butterworth-Heinemann, Oxford.
- [3] Winkler E. (1867). *Die Lehre Von Der Elastizitat Und Festigkeit*, Dominicus, Prague.
- [4] Biot M. A. (1937). Bending of infinite beams on an elastic foundation, *Journal of Applied Mechanics*, 57, A, pp. 1-7.
- [5] Terzaghi K. (1955). Evaluation of coefficients of subgrade reaction, *Geotechnique*, 5, pp. 297-326.
- [6] Vesić A. (1961). Beams on elastic subgrade and the Winkler's hypothesis, *Proceedings of 5<sup>th</sup> International Conference on Soil Mechanics and Foundation Engineering*, vol. 1, Michigan, pp. 845-850.
- [7] Horvath J. S. (1983). Modulus of subgrade reaction: new perspective, *Journal of Geotechnical Engineering*, 109, pp.1591-1596.
- [8] Horvath J. S. (1989). *Subgrade models for soil-structure interaction analysis*, Foundation Engineering: Current Principles and Practices, ASCE, Illinois, pp. 599-612.
- [9] Daloglu A. T., Vallabhan C. V. G. (2000). Values of k for slab on Winkler foundation, *Journal of Geotechnical and Geoenvironmental Engineering*, 126, pp.463-471.
- [10] Vallabhan C. V. G., Das Y. C. (1988). Parametric study of beams on elastic foundations, *Journal of Engineering Mechanics*, 114, pp. 2072-2082.
- [11] Vallabhan C. V. G., Das Y. C. (1991). Modified Vlasov model for beams on elastic foundations, *Journal of Geotechnical Engineering*, 117, pp. 956-966.
- [12] Bowles J. E. (2001). *Foundation Analysis and Design*, McGraw-Hill, New Jersey.
- [13] Hetenyi M. (1964). *Beams on Elastic Foundation*, University of Michigan Press: Ann Arbor, Michigan.
- [14] Ting B. Y., Mockry E. F. (1984). Beam on elastic foundation finite element, *Journal of Structural Engineering*, 110, pp. 2324-2339.
- [15] Eisenberger M., Yankelevsky D. Z. (1985). Exact stiffness matrix for beams on elastic foundation, *Computers and Structures*, 21, pp. 1355-1359.
- [16] Przemieniecki J. (1968). *Theory of Matrix Structural Analysis*, McGraw-Hill, New York.

- [17] Timoshenko S. P. (1958). *Strength of Materials, Part 1: Elementary Theory and Problems*, Van Nostrand Reinhold, New York.
- [18] Reddy J. N. (1997). On locking-free shear deformable beam finite elements, *Computer Methods in Applied Mechanics and Engineering*, 149, pp. 113-132.
- [19] Timoshenko S. P. (1958). *Strength of Materials, Part 2: Advanced Theory and Problems*, Van Nostrand Reinhold, New York.

---

# NAPOVED PARAMETROV KOMPRIMIRANJA GROBO ZRNATIH ZEMLJIN Z VSEBNOSTJO DROBNIH DELCEV Z UPORABO MLR IN GEP

---

OSMAN SIVRIKAYA, CAFER KAYADELEN İN EMRE CECEN

---

## o avtorjih

### vodilni avtor

Osman Sivrikaya  
Nigde University,  
Department of Civil Engineering  
51240 Nigde, Turčija  
E-pošta: osivrikaya@nigde.edu.tr

Cafer Kayadelen  
Kahramanmaraş Sutcuimam University,  
Department of Civil Engineering  
Kahramanmaraş, Turčija  
E-pošta: ckayadelen@ksu.edu.tr

Emre Cecen  
Fatih University,  
Department of Civil Engineering  
34500, Buyukcekmece-Istanbul, Turčija  
E-pošta: emrececen@fatih.edu.tr

---

## izvleček

Določitev parametrov komprimiranja zemljin, največje suhe prostorninske mase ( $\gamma_{dmax}$ ) in optimalne vlažnosti ( $w_{opt}$ ) pri različni energiji stiskanja ( $E$ ) je pomemben proces. Cilj te študije je razviti korelacije za ocenitev parametrov komprimacije v odvisnosti od energije stiskanja grobo zrnatih zemljin z različno vsebino drobnih delcev, o čemer obstaja v literaturi le malo študij. Za izpeljavo korelacij za napovedovanje  $\gamma_{dmax}$  in  $w_{opt}$ , ki so pridobljeni s standardnimi (SP) in modificiranimi (MP) Proctorjevimi preizkusi z indeksnimi lastnostmi grobo zrnatih zemljin z različno vsebnostjo drobnih delcev, sta uporabljeni genetsko programiranje (GEP) in multi-linearna regresivna analiza (MLR). Za razvoj modelov je uporabljenih 86 nizov podatkov, ki so dobili v univerzitetnih laboratorijih v Turčiji, in šest parametrov, kot so vsebnost gramoza ( $G$  %), vsebnosti peska ( $S$  %), vsebnost drobnih delcev ( $FC$  %), meja židkosti ( $w_L$  %) in indeks plastičnosti ( $IP$  %) finih delcev ter energijo stiskanja ( $E$  Joule). Uspešnost modelov je temeljito preučena z različnimi statističnimi orodji za preverjanje. Rezultati so pokazali, da so modeli GEP in MLR precej uporabni za napovedovanje največje suhe prostorninske mase in optimalne vlažnosti nekoherentnih zemljin z različno vsebnostjo drobnih delcev pri energiji stiskanja s SP in MP. Predlagane korelacije so dober način za ocenitev parametrov stiskanja, ko načrtujemo projekte, ki so finančno in časovno omejeni.

---

## ključne besede

grobo zrnata zemljina, komprimacija, MLR, GEP

---

# PREDICTION OF THE COMPACTION PARAMETERS FOR COARSE-GRAINED SOILS WITH FINES CONTENT BY MLR AND GEP

---

OSMAN SIVRIKAYA, CAFER KAYADELEN AND EMRE CECEN

---

## about the authors

### corresponding author

Osman Sivrikaya  
Nigde University,  
Department of Civil Engineering  
51240 Nigde, Turkey  
E-mail: osivrikaya@nigde.edu.tr

Cafer Kayadelen  
Kahramanmaraş Sutcuimam University,  
Department of Civil Engineering  
Kahramanmaraş, Turkey  
E-mail: ckayadelen@ksu.edu.tr

Emre Cecen  
Fatih University,  
Department of Civil Engineering  
34500, Buyukcekmece-Istanbul, Turkey  
E-mail: emrececen@fatih.edu.tr

---

## abstract

*The determination of the compaction parameters of soils, the maximum dry unit weight ( $\gamma_{dmax}$ ) and the optimum water content ( $w_{opt}$ ), at various compaction energy ( $E$ ) levels is an important process. The aim of this study is to develop correlations in order to estimate the compaction parameters dependent on the compaction energy for coarse-grained soils with various fines contents on which limited studies exist in the literature. Genetic Expression Programming (GEP) and Multi Linear Regression (MLR) analyses are used in the derivation of the correlations for the prediction of  $\gamma_{dmax}$  and  $w_{opt}$  obtained from Standard Proctor (SP) and Modified Proctor (MP) tests with the index properties of coarse-grained soils with various fines contents. To develop the models, a total of 86 data sets collected from university laboratories in Turkey and six parameters, such as gravel content (G %), sand content (S %), fines content (FC %), liquid limit ( $w_L$  %) and plasticity index ( $I_P$  %) of fines content and compaction energy ( $E$  Joule), are used. The performance of the models is comprehensively examined using several statistical verifi-*

*cation tools. The results revealed that the GEP and MLR models are fairly promising approaches for the prediction of the maximum dry unit weight and the optimum water content of cohesionless soils with various fines contents at SP and MP compaction energy levels. The proposed correlations are reasonable ways to estimate the compaction parameters for the preliminary design of a project where there are financial and time limitations.*

---

## keywords

coarse-grained soils, compaction, MLR, GEP

---

## 1 INTRODUCTION

The structures on fills and embankments should be constructed with caution. Unless the fill, the embankment and the foundation soil satisfy the design criteria, the structures on them both can fail due to an insufficient soil strength. Thus, it causes environmental disaster, affects lives and causes economic losses. Therefore, fills and embankments should be constructed under control using specified methods and codes. Soil improvement can be carried out by compacting the soil to enhance the soil characteristics, such as an increase in the soil modulus, a reduction in the hydraulic conductivity and an increase in the shear strength. Field compaction is required when constructing fills or embankments under required specifications. In this context, mechanical compaction is the most commonly used method in surface ground improvement. Mechanical compaction is generally considered to be more economical than the other soil-stabilization techniques.

Compaction is involved in various commonly performed earthwork projects, such as highways, railway subgrades, airfield pavements, earth dams and landfill liners, which require a degree of compaction of the soil to a desired dry unit weight and water content. In

the field, soils are usually compacted using tampers, sheepsfoot rollers, rubber-tired rollers, and various other equipment. In the laboratory, soil compaction is usually performed with the Proctor compaction apparatus. The Proctor compaction tests provide a standard method for a standard amount of compaction energy.

The most important parameters obtained from the compaction curve are two important compaction characteristics, i.e., the maximum dry unit weight ( $\gamma_{dmax}$ ) and the optimum water content ( $w_{opt}$ ), representing the compaction behavior. The behavior of the compacted soils depends on the dry unit weight, the water content, the compaction energy level, the soil type and their gradation.

Indirect correlative approaches are necessary or inevitable for estimating the engineering properties of soils, particularly for a project where there is a financial limitation, a lack of test equipment or a limited time frame. Thus, it is useful to estimate the engineering properties of soils, by using other soil parameters that can be obtained easily [1, 2]. Correlations are frequently used in the preliminary design stage of projects [3]. However, many of the correlations in the literature are not well defined or clear enough to be applied to field data. Thus, their usage results in confusions or erroneous conclusions. Some uncertainties, such as whether the correlation has a statistical meaning, which test results, are used in the correlation and what type of soil the correlation is valid for, have considerable effects on the correlation equations. Therefore, the correlation equations with compaction parameters should be used cautiously by taking these uncertainties into consideration.

Approaches such as GEP, Artificial Neural Networks (ANNs) and Adaptive Network Based Fuzzy Inference Systems (ANFISs) which allow developing a spatial model for complex systems have recently emerged as promising approaches in engineering tasks. These modelling techniques are also becoming more popular and have been used commonly as a tool in geotechnical engineering applications.

The compaction characteristics of soils are primary tools for the effective control of field compaction. The determination of compaction parameters ( $w_{opt}$  and  $\gamma_{dmax}$ ) is a time-consuming process and a considerable effort is required to obtain them. Therefore, it is useful and sometimes inevitable to employ indirect methods, such as correlative equations. The aim of the current study is to develop MLR and GEP models from the statistical point of view to estimate the maximum dry unit weight and the optimum water content using Standard Proctor (SP) and Modified Proctor (MP) compaction test data

and index the properties of coarse-grained soils with fines contents (percentage passing  $75\mu\text{m}$ ), and to present simple models to estimate  $w_{opt}$  and  $\gamma_{dmax}$  for an arbitrary compaction energy.

### 1.1 MULTIPLE LINEAR REGRESSION (MLR)

The MLR is a method for obtaining an equation to predict one variable using several other variables. The significance tests for each statistical parameter and the resulting lines are made with a 5 % confidence level. The significance of the regression coefficients (a, b, c, d, e, f and g) is examined by means of a t-test and it is found that the regression coefficients have significant dependence on the developed models.

In this study, a relationship is sought using all six independent variables ( $G$ ,  $S$ ,  $FC$ ,  $I_p$ ,  $w_L$  and  $w_p$ ) to establish the best accurate and precise equations for predicting the optimum water content and the maximum dry unit weight for the SP and MP compaction data. In order to develop the relationships of the dependent variables ( $w_{opt}$  and  $\gamma_{dmax}$ ) with each independent variable (energy  $E$ , gravel content  $G$ , sand content  $S$ , fines content  $FC$ =clay + silt content, liquid limit  $w_L$  and plasticity index  $I_p$ ), Multi Linear Regression (MLR) analyses are performed using the method of least squares, as follows:

$$f(w_{opt}, \gamma_{dmax}) = a + b \cdot G + c \cdot S + d \cdot FC + e \cdot I_p + f \cdot w_L \quad (1)$$

where  $G$ ,  $S$ ,  $FC$ ,  $w_L$  and  $I_p$  are in percent, and the unit of  $\gamma_{dmax}$  and  $w_{opt}$  is  $\text{kN/m}^3$  and %, respectively. The correlation coefficient ( $R$ ) and standard errors ( $SEs$ ) have been determined for each regression equation obtained with a statistical approach. In addition, the models were developed based on the energy level.

### 1.2 GENETIC EXPRESSION PROGRAMING (GEP)

GEP was presented by Ferreira [4] for first time. Its evaluation system is similar to the biological evaluation. It is a computer program that is encoded in linear chromosomes of fixed-length. The GEP algorithm (Fig. 1) uses five major preliminary steps for solving a problem. These are named as "the function set", where arithmetic operations, testing functions (such as IF and CASE statements) and Boolean functions are defined, "the terminal set" where independent variables of the problem are stated, "the fitness function" where the evaluation of the solving is made, "control parameters" where the qualitative numerical values that control the run are declared



and “the stop condition” where the announcement of a result and the termination criteria of the run is set. The GEP algorithm starts by the random generation of an initial chromosome (the initial population) that is represented by a mathematical function. Then these chromosomes are converted into an expression tree (ET). In the next step a comparison is made between the predicted values and the actual values. The GEP process stops when the desired results fulfil the initially stated error criteria.

If the initially stated error criteria are not fulfilled, some chromosomes are chosen by a method that is referred to as roulette-wheel sampling and they are mutated to obtain new chromosomes. The process is repeated for a certain number of generations or until a solution has been found [4]. After the desired fitness score is obtained, this process terminates and then the knowledge is coded in genes and chromosomes are decoded for the best solution to the problem [5].

GEP is composed of two main elements that are referred to as the chromosomes and the expression trees (ETs). In GEP, the chromosome consists of one or more genes in which there is some coded information about the

problem. The mathematical information is translated to the ET using a bilingual and conclusive language called Karva Language (the language of the genes) and by means of the language of ET. The genotype is accurately derived by using Karva Language. GEP genes are made up of two parts that are named as the head and the tail. The head of a gene has some functions, variables and constants. This part is used for encoding a function for the expression. The variables and constants in the tail are used as supplementary terminal symbols and they are needed for additional terminal symbols only if the variables in the head are not sufficient to encode a function. The head of a gene includes arithmetic, trigonometric or any other mathematical or user defined functions, like (+, -, ·, /,  $\sqrt{\quad}$ ,  $\sin$ ,  $\cos$ ). The terminal symbols in the tail are composed of the constants and the independent variables of the problem like (1, a, b, c).

At the beginning of the model construction the user specifies the length of the head (i.e., the number of symbols) which is the significant parameter in the GEP process. The encoding process takes place by reading the ET from left to right in the top line of the tree and from the top to the bottom and the ET is converted to Karva Language. The GEP genes include a non-coding part similar to the coding and non-coding sequences of biological genes.

The GEP operators are implemented by operator rate, which indicates a certain probability of a chromosome. Users decide the operator rate before the analysis. The mutation rate is recommended to be between 0.001 and 0.1. On the other hand, it is suggested that the transposition rate and cross-over rate are 0.1 and 0.4, respectively [5].

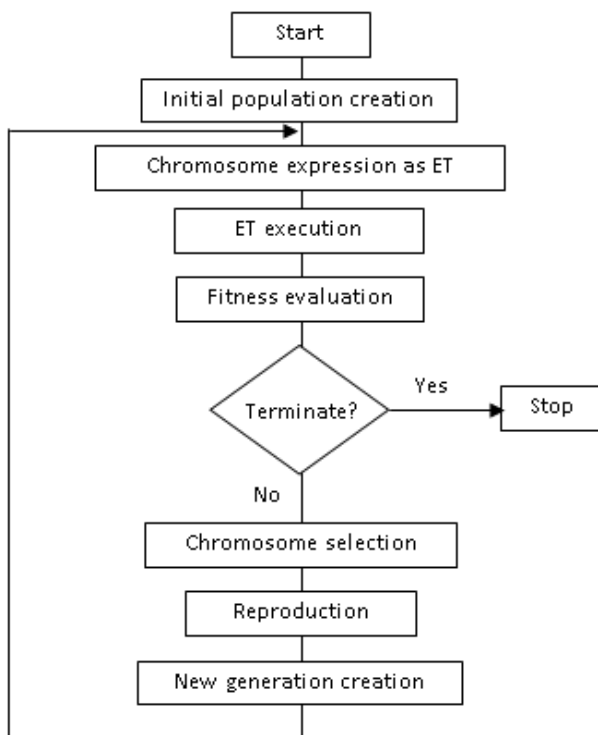


Figure 1. GEP algorithm [5].

### 1.3 PREVIOUS STUDIES ON COMPACTION PARAMETERS

Many attempts have been made to obtain the optimum water content and maximum dry unit weight of compacted fine-grained soils. The correlation equations for fine-grained soils relate the optimum water content and the maximum dry unit weight to factors using soil classification descriptors, index properties (liquid limit  $w_L$ , and plastic limit  $w_p$ ), the specific gravity of solids ( $G_s$ ), and the grain-size distribution. Sivrikaya [2] developed the correlations with the SP compaction test data for fine-grained soils used as mineral liner for solid waste, and concluded that the optimum water content has a good correlation with the plastic limit in comparison with the liquid limit and the plasticity index. For the estimation of  $w_{opt}$  in fine-grained soils, Gurtug and Sridharan [6], Sivrikaya et al. [1] and Sivrikaya and Soycan [7] also attempted to develop an empirical correlation that consists of  $w_p$  and the compaction energy ( $E$ ).

In the literature, there are fewer studies on the compaction of coarse-grained soils than the compaction parameters for fine-grained soils. Wang and Huang [8] developed correlations for estimating the optimum water content and the maximum dry unit weight for synthetic soils consisting of mixtures of bentonite clay, silt (limestone dust), sand and fine gravel. In their non-linear models, while  $w_{opt}$  is estimated from the plastic limit ( $w_p$ ), finess modulus ( $F_m$ ) and uniformity coefficient ( $U$ ) of soils,  $\gamma_{dmax}$  is estimated using the solid unit weight ( $\gamma_s$ ), effective grain size ( $D_{10}$ ),  $F_m$  and  $w_p$ . In addition, Sivrikaya and Olmez [9] improved the correlations, where the gravel content ( $G$ ), sand content ( $S$ ), fine-grained content ( $FC$ ), plasticity index ( $I_p$ ),  $w_L$  and  $w_p$  are used as independent variables for coarse-grained soils employing SP compaction parameters. In their models,  $w_{opt}$  and  $\gamma_{dmax}$  are estimated from the combination of independent parameters by performing multi-linear analyses. To the best of the authors' knowledge, there is no available study to estimate the maximum dry unit weight and the optimum water content of coarse-grained soils with various fines contents at any compactive effort from the index properties.

There are a great many studies on the determination of compaction parameters of fine-grained soils using MLR and ANN approaches in comparison with coarse-grained soil. However, studies using the MLR and GEP models on the determination of compaction parameters based on the compaction energy of coarse-grained soils with fines contents of more than 5 % do not appear to exist in the literature as far as the authors are concerned. The main purpose of this paper is to present new correlations based on GEP and MLR for the prediction of the

compaction parameters based on the compaction energy of coarse-grained soils with fines content.

## 2 MATERIALS AND METHODS

The laboratory test results used for this study were obtained from samples that were recovered from the field in different regions of Turkey. The laboratory tests include index and Standard Proctor (SP) and Modified Proctor (MP) compaction tests. The data consist of consistency parameters (liquid limit, plastic limit, and plasticity index), grain size distribution (gravel, sand and fines content %) and compaction parameters (optimum water content and maximum dry unit weight).

Sieve and hydrometer analyses were performed taking ASTM D-221 and D-422 into consideration [10, 11]. The Atterberg (consistency) limit tests were determined by considering ASTM D-4318 [12]. The compaction tests were conducted by using the SP and MP compaction method in accordance with ASTM D-698 and D-1557, respectively [13, 14]. The soils are classified as coarse-grained soils according to the Unified Soil Classification System (USCS) [15].

The input parameters used herein were selected in such a manner that the compaction is defined by these parameters in accord with the methods used practically in engineering situations. Therefore,  $E$ ,  $G$ ,  $S$ ,  $FC$ ,  $w_L$  and  $I_p$  were chosen as the inputs parameters. The number of data pairs for the SP and MP compaction was 63 and 23, respectively. The statistical parameters of the soils studied are also determined and presented in Table 1 and Table 2.

**Table 1.** Statistical parameters of the soils studied for the SP compaction tests.

	Grain size distribution			$w_L$	$w_p$	$I_p$	$w_{opt}$ (%)	$\gamma_{dmax}$ (kN/m <sup>3</sup> )
	Gravel (%)	Sand (%)	$FC^*$ (%)					
Maximum	89.00	79.00	49.00	83.00	44.00	40.00	32.00	22.60
Minimum	0.00	4.00	5.00	19.00	10.00	5.00	6.50	12.70
Range	89.00	75.00	44.00	64.00	34.00	35.00	25.50	9.90
Average	46.79	33.73	19.56	31.71	17.78	14.46	13.18	18.96
Median	50.00	30.00	17.00	29.00	16.00	14.00	11.50	19.20
St. Deviation	23.95	17.20	11.61	10.74	7.18	5.47	5.60	2.08
Variance	573.75	295.82	134.88	115.35	51.60	29.93	31.34	4.34
Skewness Coeff.	-0.36	0.65	0.88	2.30	1.91	1.81	1.93	-1.14
Kurtosis Coeff.	-0.82	-0.20	-0.02	7.74	3.93	6.74	3.83	1.49

\*FC represents fines content percentage that is passing 75  $\mu$ m diameters.

**Table 2.** Statistical parameters of the soils studied for the MP compaction tests.

	Grain size distribution			$w_L$	$w_P$	$I_P$	$w_{opt}$ (%)	$\gamma_{dmax}$ (kN/m <sup>3</sup> )
	Gravel (%)	Sand (%)	$FC^*$ (%)					
Maximum	84.00	64.00	43.00	49.00	35.00	29.00	17.00	23.30
Minimum	3.00	9.00	6.00	17.00	11.00	6.00	4.50	17.20
Range	81.00	55.00	37.00	30.00	24.00	23.00	12.50	6.10
Average	53.35	31.35	16.61	32.09	17.65	15.78	9.25	20.81
Median	61.00	26.00	12.00	29.00	16.00	15.00	7.50	21.70
St. Deviation	20.87	15.20	11.62	9.67	5.21	6.52	3.68	1.99
Variance	435.44	230.92	134.93	93.56	27.18	45.52	13.56	3.94
Skewness Coeff.	-0.75	0.71	1.09	0.15	1.57	0.15	0.63	-0.38
Kurtosis Coeff.	0.17	-0.34	0.05	-1.48	3.86	-0.91	-0.76	-1.45

\*FC represents fines content percentage that is passing 75  $\mu$ m diameters.

### 3 RESULTS AND DISCUSSION

This paper intends to investigate the potential use of GEP and MLR in predicting the compaction parameters of coarse-grained soils with fines contents that have great significance on soil compaction based on the compaction energy. For quantitative assessments of the model's predictive abilities, the results obtained from these correlations are comprehensively evaluated in terms of statistics.

In order to see the accuracy of the results obtained through the proposed MLR models, the coefficient of correlation ( $R$ ) and the standard errors ( $SE$ s) are used as statistical verification tools. The standard error ( $SE$ ) of the estimate is a measurement of the deviation around the regression line. It is well known that the correlation equation obtained from the MLR method is accurate and precise as long as its coefficient of correlation value reaches 1 or close to 1 and the standard deviation is 0 or close to 0.

In order to analyse the performance of the developed GEP models several statistical verification criteria are used such as the coefficient of correlation ( $R$ ), the root-mean-square error ( $RMSE$ ) and the standard deviation ( $\sigma$ ) of the errors. The definitions of these evaluation criteria are given below

$$R = \frac{\sum_{i=1}^n (u_i^m - \bar{u}^m) (u_i^p - \bar{u}^p)}{\sqrt{\sum_{i=1}^n (u_i^m - \bar{u}^m)^2} \sqrt{\sum_{i=1}^n (u_i^p - \bar{u}^p)^2}} \quad (2)$$

$$RMSE = \sqrt{\frac{\sum_{i=1}^n (u_i^m - u_i^p)^2}{n}} \quad (3)$$

$$\sigma = \sqrt{\frac{\sum_{i=1}^n (e - \bar{e})^2}{(n-1)}} \quad (4)$$

where  $u_i^m$  and  $u_i^p$  are the measured and predicted values, respectively,  $\bar{u}^m$  and  $\bar{u}^p$  are the mean of the measured and predicted values,  $e$  is the absolute error ( $|u_i^m - u_i^p|$ ),  $\bar{e}$  is the mean of the absolute error,  $n$  is the number of the sample.

Of the 86 data sets in this study, 69 are used for training the models and 17, which are not used in the training stage, are presented for testing of the GEP models. In the MLR analyses all the data are used.

#### 3.1 DEVELOPED MLR MODELS

In this study, the correlations have been improved between the optimum water content and maximum dry unit weight obtained from the SP and MP compaction tests and the index properties of coarse-grained soils with fines contents of more than 5 % by attempting different combinations of soil index parameters ( $G$  %,  $S$  %,  $FC$  %,  $w_L$ ,  $w_P$ ,  $I_P$ ) as independent parameters. The

**Table 3.** Correlation equations obtained from the MLR analyses according to the SP compaction data.

Model number	Correlation equation	R	SE
SP-1	$w_{opt} = -0.032G - 0.009S + 0.046FC + 0.659w_L - 0.473I_p$	0.987	± 2.37 %
SP-2	$w_{opt} = 0.420w_L$	0.982	± 2.71 %
SP-3	$\gamma_{dmax} = 0.253G + 0.236S + 0.218FC - 0.234w_L + 0.161I_p$	0.999	± 0.89 kN/m <sup>3</sup>
SP-4	$\gamma_{dmax} = 23.673 - 0.357w_{opt}$	0.960	± 0.59 kN/m <sup>3</sup>

**Table 4.** Correlation equations obtained from the MLR analyses according to the MP compaction data.

Model number	Correlation equation	R	SE
MP-1	$w_{opt} = -0.005G - 0.007S + 0.141FC + 0.267w_L - 0.073I_p$	0.992	± 1.40 %
MP-2	$w_{opt} = 0.292w_L$	0.983	± 1.88 %
MP-3	$\gamma_{dmax} = 0.265G + 0.278S + 0.127FC - 0.213w_L + 0.166I_p$	0.998	± 1.65 kN/m <sup>3</sup>
MP-4	$\gamma_{dmax} = 25.702 - 0.528w_{opt}$	0.980	± 0.41 kN/m <sup>3</sup>

obtained best accurate and precise equations with the correlation coefficients and standard errors of estimate from the MLR analyses for SP and MP compaction data are presented in Tables 3 and 4, respectively.

**MODELS ON SP COMPACTION PARAMETERS**

The correlations have been improved between the optimum water content and the maximum dry unit weight obtained from SP compaction tests and index properties by using 63 data sets for the regression analyses (Table 3).

The analyses results have shown that the SP-1 model including the input data of all the index properties without a plastic limit are observed to give the best  $w_{opt}$  results with  $R = 0.987$  and  $SE = \pm 2.37\%$  (Table 3 and Fig. 2). In addition, it is found that the correlation ( $w_{opt} = 0.41w_L$  with  $R = 0.982$  and  $SE = \pm 2.71\%$ ) of the optimum water content with liquid limit (SP-2 model) gives the best results among the consistency index parameters (Table 3 and Fig. 3). However, it is stated in the previous studies that the correlation of the optimum water content with plastic limit gives better results than the correlation of the optimum water content with the liquid limit for fine-grained soils [2, 6].

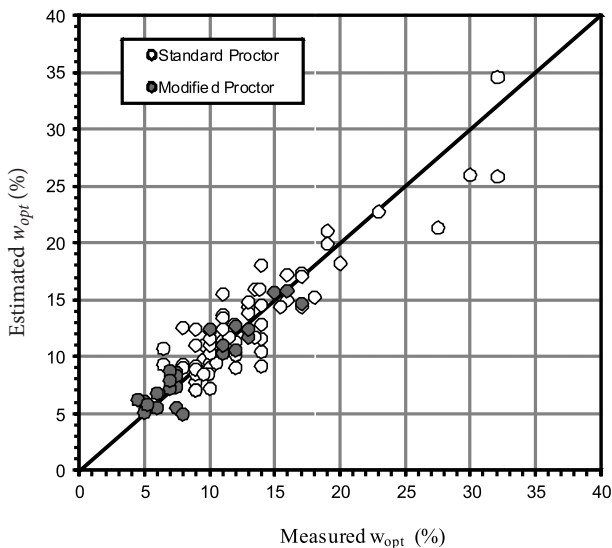


**Figure 2.** Comparison of optimum water contents obtained from the SP and MP compaction tests with values estimated from Model SP-1 and MP-1.

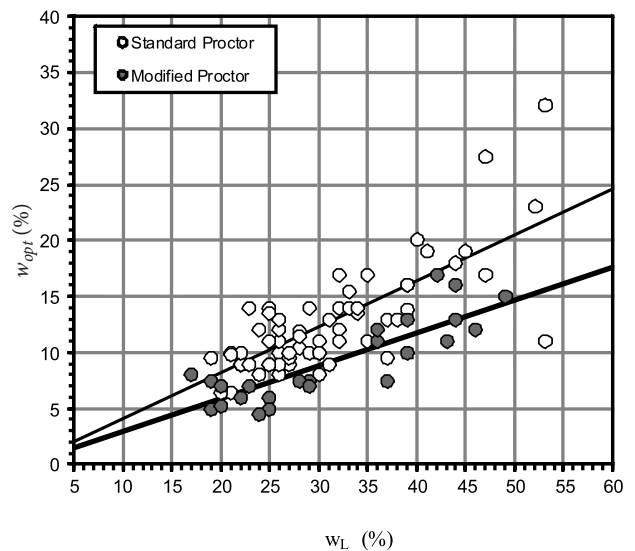


**Figure 3.** Relationships between the optimum water content obtained from the SP and MP compaction tests and the liquid limit.

For the correlations between the maximum dry unit weight obtained from the SP compaction tests and the index properties, it was found that the SP-3 model with  $R = 0.999$  and  $SE = \pm 0.89 \text{ kN/m}^3$  gave the best results for all the parameters (Table 3 and Fig. 4). The correlations were also attempted only for the consistency parameters. The results of the regression analyses have shown that it is not likely to estimate the maximum dry unit weight only from the consistency indices, as expected. Furthermore, the results reveal that  $\gamma_{dmax}$  can be estimated very precisely from  $w_{opt}$  using the SP-4 model with  $R = 0.960$  and  $SE = \pm 0.59 \text{ kN/m}^3$  instead of the index properties of the soils (Table 3 and Fig. 5)

**MODELS ON MP COMPACTION PARAMETERS**

Twenty-three data sets were used for the regression analyses on  $w_{opt}$  and  $\gamma_{dmax}$  obtained from the MP compaction tests with the index properties of coarse-grained soils. A large number of models were attempted, but the only MLR models with  $w_{opt}$  estimating best results are given in Table 4. The MP-1 model including input data of all the index properties without the plasticity index were observed to give the best results with  $R = 0.992$  and  $SE = \pm 1.40 \%$  due to the minimum SE and the maximum R value (Table 4 and Fig. 2). The correlation of the optimum water content with the liquid limit gives better results than the plastic limit and the plasticity index. As far as the regression analyses are concerned, the dominant input parameter affecting the optimum water content appears to be the liquid limit for coarse-grained soils with fines contents of more than 5 % instead of the plastic limit in fine-grained

soils [1, 2, 6]. Fig. 2 shows a plot of the optimum water content versus the liquid limit. The optimum water content increases with the increasing liquid limit. It was found that the correlation of  $w_{opt}$  with  $w_L$  (MP-2 model) has R of 0.983 and SE of  $\pm 1.88 \%$  (Table 4 and Fig. 3).

As can be seen in Table 4, the MP-3 model including the input data of G, S, FC,  $w_L$  and  $I_p$  were found to give the best result. Fig. 4 shows a plot of MP-3 with  $R = 0.998$  and  $SE = \pm 1.65 \text{ kN/m}^3$ . It is observed from the regression analyses that while the correlation of  $\gamma_{dmax}$  with the consistency index parameters is not accurate, the correlation of  $\gamma_{dmax}$  with the grain distribution ratios gives better results.  $\gamma_{dmax}$  can be estimated easily and precisely from  $w_{opt}$  instead of the index properties of the soils using MP-4 model with  $R = 0.980$  and  $SE = \pm 0.41 \text{ kN/m}^3$  (Table 4 and Fig. 5).

**CORRELATIONS ON  $w_{opt}$  AND  $\gamma_{dmax}$  WITH  $\epsilon$**

Correlations based on the compaction energy on the compaction parameters were also developed and given in Table 5. Even though the correlations appear to be satisfactory in terms of R, they are good at SE except for the SMP-3 model. Therefore, a new approach for estimating the compaction parameters of coarse-grained soils with fines contents of more than 5 % are introduced for the SP and MP compaction energy levels.

Considering the correlations between  $w_{opt}$  and the consistency parameters of soils for both SP and MP compaction data, it is found that the most appropriate

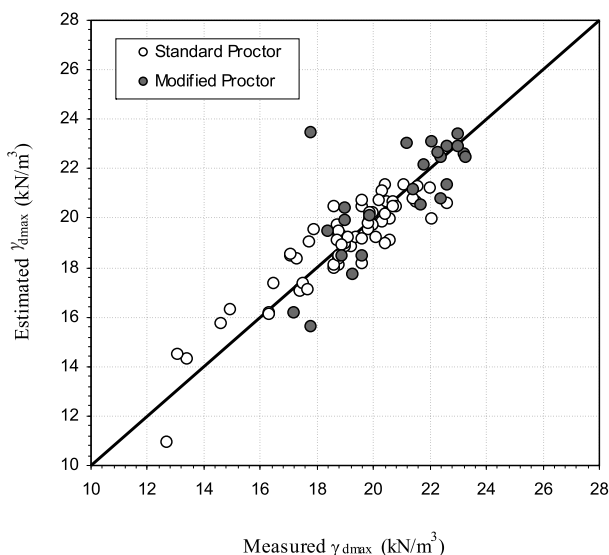


**Figure 4.** Comparison of maximum dry densities obtained from the SP and MP compaction tests with the values estimated from Model SP-3 and MP-3.

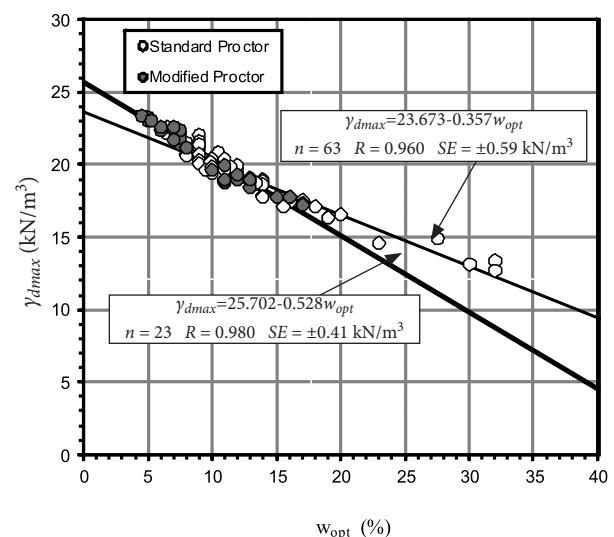


**Figure 5.** Linear relationships between the optimum water content and the maximum dry unit weight obtained from the SP and MP compaction tests.

**Table 5.** Correlation equations obtained from the MLR analyses based on the SP and MP compaction data.

Model number	Correlation equation	R	SE
SMP-1	$w_{opt} = 0.447w_L - 0.002E$	0.982	± 2.55 %
SMP-2	$w_{opt} = -0.002E - 0.011G - 0.001S + 0.072FC + 0.61w_L - 0.421I_p$	0.986	± 2.26 %
SMP-3	$\gamma_{dmax} = 0.006E + 0.875w_{opt}$	0.924	± 7.58 kN/m <sup>3</sup>
SMP-4	$\gamma_{dmax} = 0.001E + 0.251G + 0.241S + 0.194FC - 0.228w_L + 0.146I_p$	0.998	± 1.15 kN/m <sup>3</sup>

correlation is between the optimum water content and the liquid limit, as proved and mentioned before (Table 3, Table 4 and Fig. 3). Fig. 3 shows the variation of the optimum water content with the liquid limit for the Standard and Modified Proctor compaction energy level. From Fig. 3 it is clear that:

$$w_{opt} = Kw_L \quad (5)$$

where  $w_{opt}$  is the optimum water content,  $w_L$  is the liquid limit and K is a coefficient depending on E. K decreases from 0.420 for Standard Proctor to 0.292 for Modified Proctor (Fig. 6a). On the other hand, the K values for the fine-grained soils were found to be 0.94 and 0.28 for the SP and MP compaction energy levels, respectively [1]. The variation in K shows that the optimum water content is significantly affected by the change in the compaction energy level. As seen in Fig. 6a, the variation of K with  $\ln E$  is linear, as expected [1, 6, 16]. The developed empirical equations are as follows:

$$K = 0.90 - 0.077\ln E \quad (6)$$

$$w_{opt} = (0.90 - 0.077\ln E)w_L \quad (7)$$

where the unit of  $w_{opt}$  and E is in percent (%) and in kilojoules per cubic meter (kJ/m<sup>3</sup>), respectively.

There is a possibility that  $\gamma_{dmax}$  can be estimated using either  $w_{opt}$  or other index parameters. However, it has been observed in this study and stated in previous studies that the estimation of  $\gamma_{dmax}$  using  $w_{opt}$  is more reliable than using consistency parameters in the light of statistical parameters (n, R, SE) [2, 6, 16, 17, 18].

Fig. 5 shows the correlation of  $\gamma_{dmax}$  with  $w_{opt}$  for the Standard and Modified Proctor compaction energy levels. As seen from Fig. 5, the correlations are found to be satisfying. Therefore,  $\gamma_{dmax}$  is described as a function of E and  $w_{opt}$  instead of other index properties due to the high R and low SE values in this study. The model is developed in order to estimate the maximum dry unit weight in terms of the optimum water content based on the SP and MP compaction energy levels. The model is in the form of

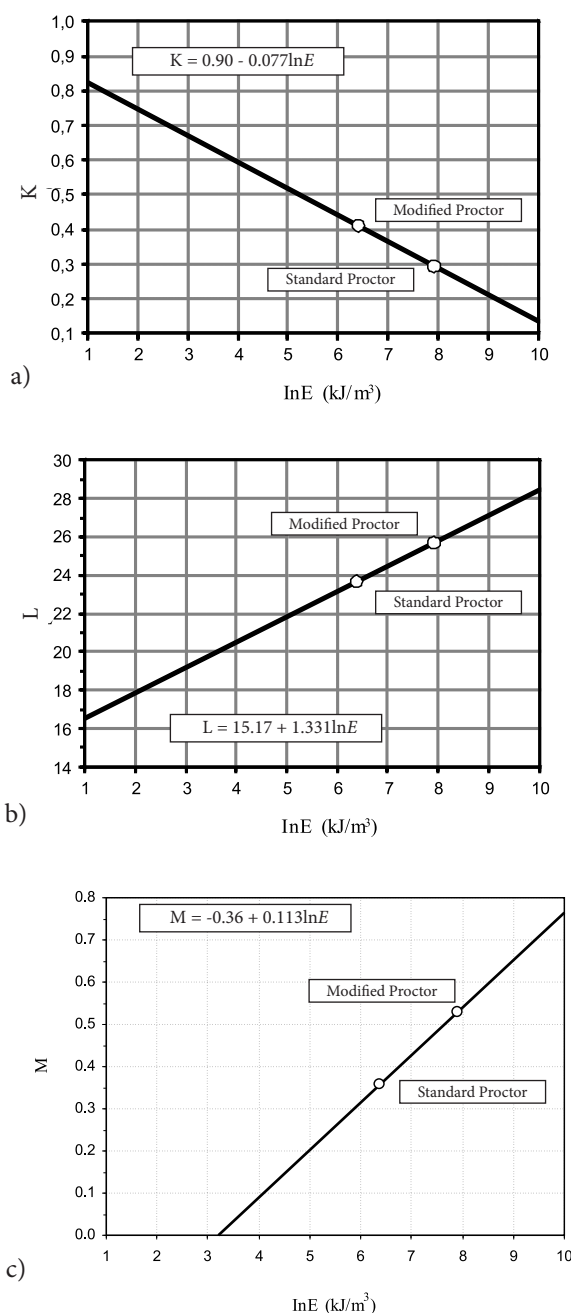


**Figure 6.** Variations of K, L and M coefficients with compaction energy.

$$\gamma_{dmax} = L \cdot M w_{opt} \quad (8)$$

Both coefficients L and M are described as a function of  $E$  in this model. Figs. 6b and 6c show the variation of the L and M coefficients with  $\ln E$ , respectively. The L and M coefficients vary with  $\ln E$  linearly as found before [1, 16]. The L and M values are obtained as 23.673 and 0.357, respectively, for the SP compaction energy level and 25.702 and 0.528, respectively, for the MP compaction energy level, respectively (Figs. 6a,b). However, the L and M values for fine-grained soils were found to be 21.97 and 0.27, respectively, for the SP compaction energy level and 23.78 and 0.38, respectively, for the MP compaction energy level [1]. While the K coefficient increases with increasing  $\ln E$ , the L and M coefficients increase with decreasing of  $\ln E$ , which was also shown and proved for fine-grained soils by Blotz et al. [16], Gurtug and Sridharan [6] and Sivrikaya et al. [1]. The developed empirical equations are presented as

$$L = 15.17 + 1.331 \ln E \quad (9)$$

$$M = -0.36 + 0.113 \ln E \quad (10)$$

$$\gamma_{dmax} = (15.17 + 1.331 \ln E) \cdot (-0.36 + 0.113 \ln E) w_{opt} \quad (11)$$

where the unit of  $\gamma_{dmax}$  and  $E$  is in kilonewtons per cubic meter ( $\text{kN/m}^3$ ) and in kilojoules per cubic meter ( $\text{kJ/m}^3$ ), respectively.

Even though some scattering in the data distribution may exist (Figs. 3 and 5), the methods proposed to estimate the optimum water content and the maximum dry unit weight at any compaction energy can have some errors, which are insignificant and within the acceptable range (in  $w_{opt}$  for SP and MP compaction  $SE = \pm 2.71$  and  $\pm 1.88$  %, respectively; in  $\gamma_{dmax}$  for SP and MP compaction  $SE = \pm 0.59$  and  $\pm 0.41$   $\text{kN/m}^3$ , respectively). Therefore, the developed methods could be very useful during the preliminary design stage in practice. They could be used to predict the optimum water content of soil samples for a comparison with the natural moisture content in a preliminary assessment of earthwork materials.

### 3.2 DEVELOPED GEP MODELS

The GEP models developed here are mainly aimed to generate the mathematical functions for the prediction of the compaction parameters based on the compaction energy of coarse-grained soils with fine grains. In this study, four GEP models (GEP-1, GEP-2, GEP-3 and GEP-4) are developed. To predict  $w_{opt}$  GEP 1 and 2, in which two and six input parameters such as  $E$ ,  $w_L$  and  $E$ ,  $G$ ,  $S$ ,  $FC$ ,  $w_L$ ,  $I_p$  are employed, respectively, are developed. In the GEP-3 and GEP-4 models, different two ( $E$ ,

$w_{opt}$ ) and six ( $E$ ,  $G$ ,  $S$ ,  $FC$ ,  $w_L$ ,  $I_p$ ) input parameters are used respectively. Thus, four mathematical functions are generated in the form of  $w_{opt} = f(E, w_L)$ ,  $w_{opt} = f(E, G, S, FC, w_L, I_p)$ ,  $\gamma_{dmax} = f(E, w_{opt})$  and  $\gamma_{dmax} = f(E, G, S, FC, w_L, I_p)$  for the prediction of compaction parameters based on the compaction energy in coarse-grained soils with fine grains. Table 6 presents the model parameters used for both models. DTREG software is used for the GEP algorithm [19]. The functions for the compaction parameters in coarse-grained soils with fine grains based on the compaction energy are generated as below:

GEP-1

$$w_{opt} = \sin(\sqrt{w_L}) - \cos(w_L) - \cos((w_L)^2) \cdot \left[ \frac{w_L}{E} (\sqrt[3]{w_L})(w_L + E)w_L \right]^{1/3} + \left[ \frac{(w_L - E)}{E} \right]^3 \frac{1}{[\cos(E) + 1]} \quad (12)$$

GEP-2

$$w_{opt} = \cos \left[ \cos(\sqrt{w_L}) - G + I_p \right] + \sin(E) + 0.12 \left[ w_L - \sqrt{G^{1/3} I_p} \right] + \sin(E) - \cos \left[ I_p - FC + w_L + E + S \right] \quad (13)$$

GEP-3

$$\gamma_{dmax} = \left[ \frac{\log(E)}{w_{opt}} + \log(E) \right] \sin[\log(w_{opt})] + \sqrt{a \tan(w_{opt}) + \sin(E)} + \log(E + w_{opt}) + a \tan(w_{opt})^2 + \sin(E) + \log \sqrt{E} \quad (14)$$

GEP-4

$$\gamma_{dmax} = \frac{(FC + 2G + S - 7.8)}{w_L} + 8.09 + \sin \left[ \frac{w_L}{\left( -7.1 - a \tan \left( \frac{\log(S)}{-8.39} \right) \right)} \right] + \log \left[ E - 4.78 w_L - \sqrt[3]{I_p * G} \right] \quad (15)$$

**Table 6.** GEP parameters of the models developed.

	GEP-1	GEP-2	GEP-3	GEP-4
Generation	118333	150552	7854	8702
Program size	37	34	32	35
Number of the genes	3	3	3	4
Length of the gene head	7	8	7	8
Max. fitness	1000			
Linking function	+			
Function set	+, -, *, /, √, exp, log, sin, cos, arctan			
Mutation rate	0.044			
One-point recombination rate	0.3			
Two-point recombination rate	0.3			
Inversion rate	0.1			
Transposition rate	0.1			

The compaction parameters estimated from all the GEP models are graphically compared with the measured values in Fig. 7 and Fig. 8. It clearly appears that the results from the GEP are in good agreement with the measured values. This also shows that all the models are found to be able to learn a complex relationship between the input parameters relating to the soils and the compaction parameters.

In addition, the values of the compaction parameters estimated from the GEP models are graphically compared with those from the MLR models in Fig. 9 and Fig. 10. Table 7 presents the statistical performances of the MLR

and GEP models. As far as this table is concerned, all the models for the compaction parameters, except for MLR-SMP-3, give satisfactory agreement in terms of the statistical evaluation criteria. The best results in terms of the  $R$ ,  $RMSE$  and  $\sigma$  values are obtained for MLR-SMP-2 ( $R=0.94$ ,  $RMSE=2.69$ ,  $\sigma=1.84$ ) among the MLR models and GEP-2 ( $R=0.95$ ,  $RMSE=3.11$ ,  $\sigma=2.29$ ) among the GEP models to estimate  $w_{opt}$ , and for MLR-Eq. 11 ( $R=0.97$ ,  $RMSE=0.57$ ,  $\sigma=0.42$ ) among the MLR models and GEP-3 ( $R=0.98$ ,  $RMSE=0.42$ ,  $\sigma=0.20$ ) among the GEP models to estimate  $\gamma_{dmax}$ . These models have fairly high  $R$  values and low  $RMSE$  values, which are a measurement of the deviation around the regression line.

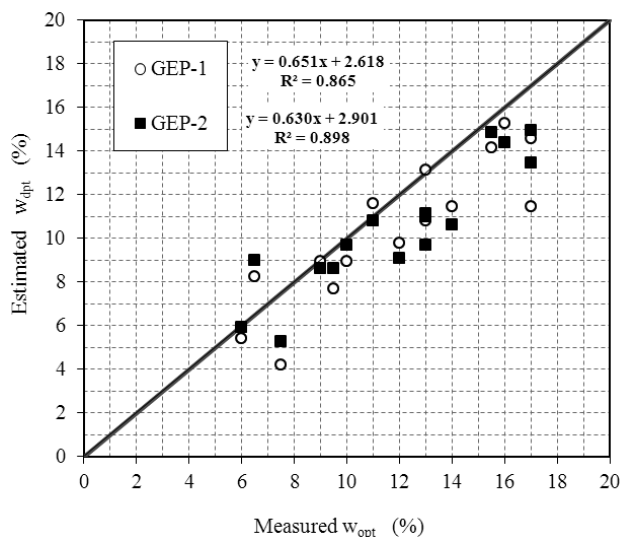


**Figure 7.** Comparison of measured and estimated  $w_{opt}$  based on  $E$  from the GEP-1 and GEP-2 models.

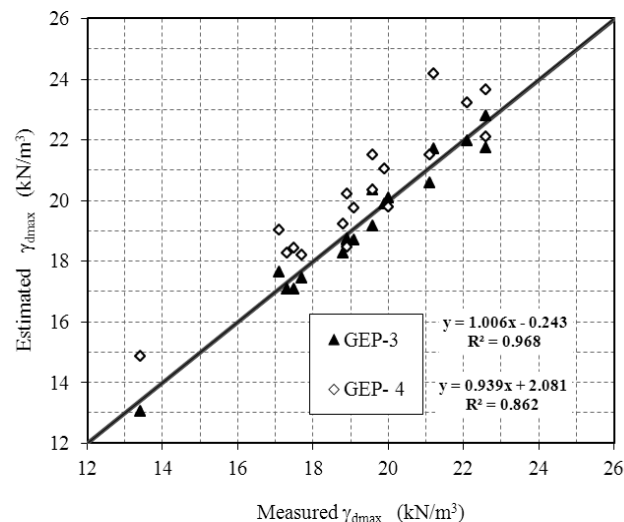


**Figure 8.** Comparison of measured and estimated  $\gamma_{dmax}$  based on  $E$  from the GEP-3 and GEP-4 models.



The overall error performances of the relationship between the two groups (predicted and actual values) can be interpreted from the  $R$  values. If the  $R$  value of a relationship between two groups is as high as 0.8, it is accepted from the statistical point of view that this correlation is satisfactory [20]. The  $RMSE$  value also has great significance for the statistics as well as the  $R$  value, because although a relationship provides high  $R$  value, it may give a high  $RMSE$  value.

When the models are compared in terms of the types of analyses (MLR and GEP) it can be seen that the MLR model (MLR-SMP-2) gives better results to estimate  $w_{opt}$  and the GEP model (GEP-3) gives better results to estimate  $\gamma_{dmax}$ . However, MLR-Eq. 11 can be used for esti-

**Table 7.** Performance statistics of the models.

	$R$	$RMSE$	$\sigma$
MLR-SMP-1	0.92	3.09	2.23
MLR-SMP-2	0.94	2.69	1.84
MLR-Eq. 7	0.94	3.05	2.43
GEP-1	0.93	3.18	2.33
GEP-2	0.95	3.11	2.29
MLR-SMP-3	-0.44	7.30	5.06
MLR-SMP-4	0.94	1.09	0.53
MLR-Eq. 11	0.97	0.57	0.42
GEP-3	0.98	0.42	0.23
GEP-4	0.95	1.05	0.51

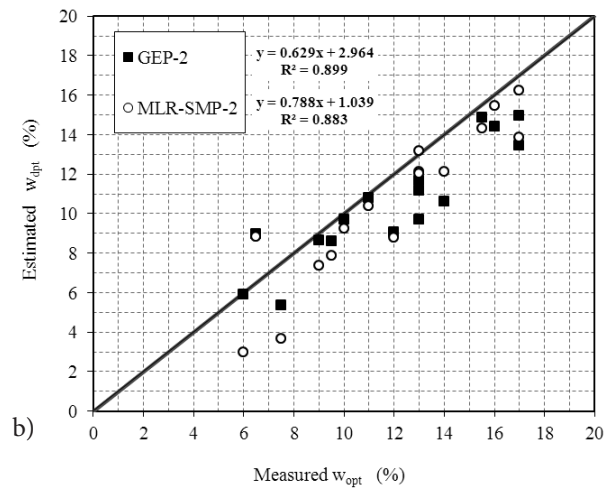
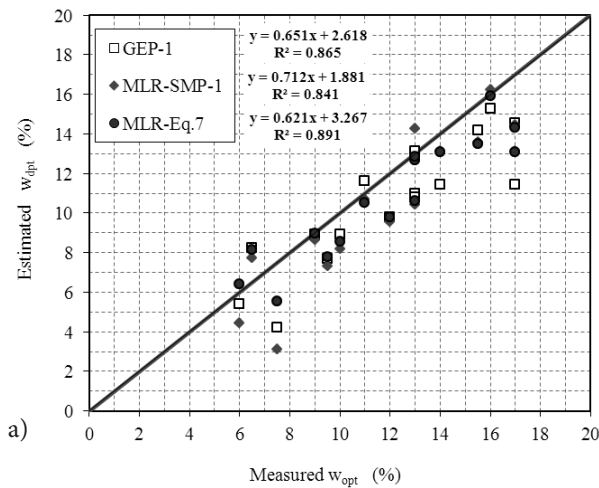


**Figure 9.** Comparison of estimated  $w_{opt}$  from the MLR and GEP models.

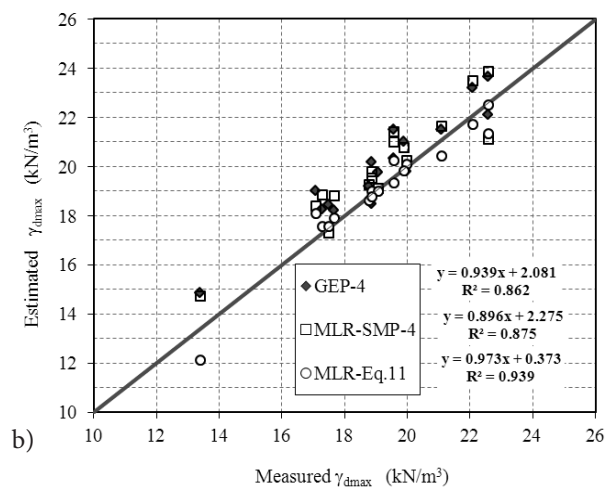
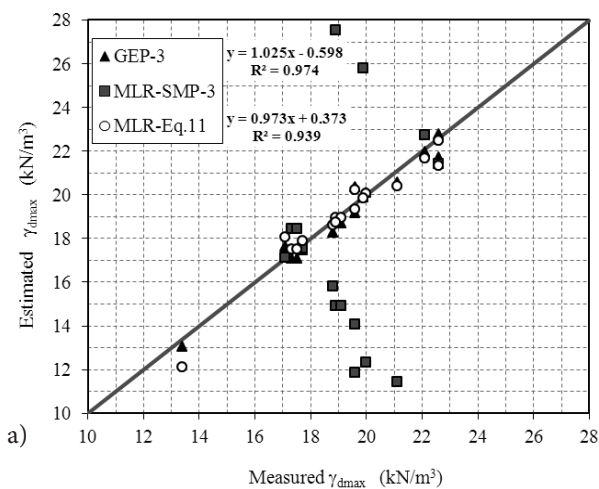


**Figure 10.** Comparison of estimated  $\gamma_{dmax}$  from the MLR and GEP models.

imating  $\gamma_{dmax}$  due to its simplicity and ease in practice. The evaluations given above reveal that the MLR-SMP-2, MLR-Eq. 11, GEP-3 and MLR-Eq. 11 generated by the GEP and MLR models provide a good prediction ability. The prediction accuracy of the models appears to be sufficient from statistical point of view in the prediction of the compaction parameters.

## 4 CONCLUSIONS

The optimum water content,  $w_{opt}$  and the maximum dry unit weight,  $\gamma_{dmax}$  are the principle parameters to control field compaction in which the applied compaction energies may vary depending on the field requirements and the soil type. A determination of these properties plays an important role in the design of compaction projects. In this study, the correlations between the compaction and index properties of coarse-grained soils with fines contents of more than 5 % are developed by performing MLR analyses using 63 SP compaction data and 23 MP compaction data. The MLR and GEP models that include compaction energy have also been described for estimating  $w_{opt}$  and  $\gamma_{dmax}$  for SP and MP compaction energy levels. The MLR and GEP models are found to give very reliable results for predicting both  $w_{opt}$  and  $\gamma_{dmax}$  for the SP and MP compaction test data.

It is concluded from this study that  $w_{opt}$  has a much better correlation with  $w_L$  than  $w_p$ , and  $\gamma_{dmax}$  can be estimated more precisely from  $w_{opt}$  instead of the index properties of soils. Thus, two mathematical equations (Eq. 7 and Eq. 11) are generated and proposed for estimating  $w_{opt}$  using  $w_L$  and  $E$ , and  $\gamma_{dmax}$  using  $w_{opt}$  and  $E$  from the MLR models. The correlations are formed as  $w_{opt} = Kw_p$  and  $\gamma_{dmax} = L-Mw_{opt}$  where the coefficients of  $K$ ,  $L$  and  $M$  are introduced as a function of  $E$ . As  $w_L$  and  $E$  are known, at first  $w_{opt}$  could be obtained from Eq. 7 then  $\gamma_{dmax}$  could be obtained by substituting  $w_{opt}$  into Eq. 11 for any compaction energy levels.

In addition, four GEP models are developed. A satisfactory agreement is obtained as a result of the testing procedures of the GEP-2 and GEP-3 models. This is evidenced by some statistical performance criteria used for evaluating the models. The overall evaluation of the results obtained throughout the paper revealed that the MLR and GEP computing techniques used here are very encouraging for the data used. The author recommends that the models developed for estimating the compaction parameters for any compaction energy level could be used in a preliminary design stage due to laborious, time-consuming and costly tests. Additional important parameters in the compaction are the roughness of

the surface of the grains, the shape of grains, and the composition of minerals, etc. Though a great effort was made to use unbiased and heterogeneous media the conclusions introduced in this study are significant for the coarse-grained soil samples taken from particular sites with the same geological history. Future studies are needed to expand these results in order to be internationally valid.

## REFERENCES

- [1] Sivrikaya, O., Togrol, E., Kayadelen C. (2008). Estimating compaction behaviour of fine-grained soils based on compaction energy. *Can. Geotech. J.*, Vol. 45, No. 6, pp. 877-887.
- [2] Sivrikaya, O. (2008). Models of compacted fine-grained soils used as mineral liner for solid waste. *Envir. Geolog.*, Vol. 53, No. 7, pp.1585-1595.
- [3] Sivrikaya, O., Togrol, E. (2006). Determination of undrained strength of fine-grained soils by means of SPT and its application in Turkey. *Engin. Geolog.*, Vol. 86, No. 1, pp. 52-69.
- [4] Ferreira, C. (2001). Gene Expression Programming: A New Adaptive Algorithm for Solving Problems. *Complex Systems*, Vol. 13, No. 2, pp. 87-129.
- [5] Teodorescu, L., Sherwood, D. (2008). High Energy Physics event selection with Gene Expression Programming. *Computer Physics Communications*, Vol. 178, No. 6, pp. 409-419.
- [6] Gurtug, Y., Sridharan, A. (2004). Compaction behaviour and prediction of its characteristics of fine grained soils with particular reference to compaction energy. *Soils and Found.*, Vol. 44, No. 5, pp. 27-36.
- [7] Sivrikaya, O., Soykan, Y.T. (2011). Estimation of compaction parameters of fine-grained soils in terms of compaction energy using artificial neural networks. *Int. J. for Numer. and Anal. Methods in Geomech.*, Vol. 35, No. 17, pp. 1830-1841.
- [8] Wang, M., Huang, C. (1984). Soil compaction and permeability prediction models. *ASCE J. of Environ. Eng.*, Vol. 110, No. 6, pp. 1063-1083.
- [9] Sivrikaya, O., Olmez, A. (2007). Correlations between compaction parameters and index properties of Soils. *Proc. of the 2<sup>nd</sup> Geotech. Symp., Adana, Turkey, pp 47-60 (in Turkish)*.
- [10] ASTM D-221 (2003). Standard practice for dry preparation of soil Samples for particle-size analysis and determination of soil constants. ASTM International, West Conshohocken.
- [11] ASTM D-422 (2003). Standard test method for particle-size analysis of soils. *ASTM International*, West Conshohocken.

- [12] ASTM D-4318 (2000). Standard test methods for liquid limit, plastic limit, and plasticity index of soils. *ASTM International*, West Conshohocken.
- [13] ASTM D-698 (2000). Standard test methods for laboratory compaction characteristics of soil using standard effort. *ASTM International*, West Conshohocken.
- [14] ASTM D-1557 (2003). Standard test methods for laboratory compaction characteristics of soil using modified effort. *ASTM International*, West Conshohocken.
- [15] ASTM D-2487 (2000). Standard practice for classification of soils for engineering purposes (Unified Soil Classification System). *ASTM International*, West Conshohocken.
- [16] Blotz, R.L., Benson, H., Boutwell, P. (1998). Estimating optimum water content and maximum dry unit weight for compacted clays. *ASCE J. of Geotech. and Geoenviron. Engin.*, Vol. 124, No. 9, pp. 907-912.
- [17] Gurtug, Y., Sridharan, A. (2002). Prediction of compaction characteristics of fine grained soils. *Geotechnique*, Vol. 52, No. 10, pp. 761-763.
- [18] Nagaraj HB (2000) Prediction of engineering properties of fine-grained soils from their index properties. *PhD thesis*, Indian Institute of Science, Bangalore, India.
- [19] Sherrod, P.H. (2008). DTREG Predictive Modeling Software. <http://www.dtreg.com>.
- [20] Smith, G.N. (1986) Probability and statistics in civil engineering: An Introduction. Collins, London.

---

# EVOLUCIJSKA-OSNOVNA NAPOVED $\epsilon_{50}$ PRI POMIKIH PILOTOV V GLINI ZARADI BOČNE OBREMENITVE

---

BABAK EBRAHIMIAN IN AIDA NAZARI

---

## o avtorjih

### vodilni avtor

Babak Ebrahimiyan  
University of Tehran,  
School of Civil Engineering  
Tehran, Iran  
E-mail: bebrahimian@ut.ac.ir

The Highest Prestigious Scientific and Professional National Foundation,  
Iran's National Elites Foundation (INEF),  
Teheran, Iran

Aida Nazari  
Iran University of Science and Technology  
School of Civil Engineering  
Tehran, Iran

---

## izvleček

Analiziranje pilotov, ki so izpostavljeni bočnim obremenitvam, razkriva, da je njihovo obnašanje odvisno od odpornosti tal na poljubni točki vzdolž pilota, kot funkcija odklona pilota oziroma krivulje  $p$ - $y$ . Po drugi strani pa imajo deformacijske lastnosti zemljin, ki so opredeljene kot "deformacija zemljin pri 50 % maksimalnem deviatornem pritisku ( $\epsilon_{50}$ )", precejšen vpliv na nastalo krivuljo  $p$ - $y$ . V tej raziskavi je predlaganih več modelov za napovedovanje  $\epsilon_{50}$ , predvsem za načrtovanje zelo dolgih pilotov na morskih naftnih in plinskih ploščadih na področju South Pars v Perzijskem zalivu v Iranu. V članku so ocenjene  $\epsilon_{50}$  z uporabo obsežnih podatkov o tleh, vključno z rezultati terenskih in laboratorijskih preizkusov z uporabo evolucijske polinomske regresije (EPR). Preučevani so učinki nedrenirane strižne trdnosti, normalizirane odpornosti zemljine pri penetracijskem preizusu, pre-obremenjenega pritiska, indeksa plastičnosti in prekonsolidacijskega razmerja  $\epsilon_{50}$  v morskih glinah. Nazorno je prikazano, da privede normalizirana odpornost zemljine pod konico pilota, ki je pokazatelj nedrenirane strižne trdnosti tal, do realnejših vrednosti  $\epsilon_{50}$ , v primerjavi z laboratorijsko dobljenim parametrom nedrenirane strižne trdnosti. Kakovost ocenjevanja modelov je izboljšana z uporabo indeksnih kazalnikov lastnosti tal in pre-obremenilnega pritiska. Za preverjanje učinkovitosti predlaganih modelov so za napovedovanje obnašanja pilotov uporabljeni tudi rezultati obsežnih preizkusov bočne obremenitve pilotov na različnih lokacijah.

---

## ključne besede

bočno obremenjen pilot, konusni penetracijski preizkus, morska glina, evolucijsko polinomska regresija (EPR), področje South Pars

---

# EVOLUTIONARY-BASED PREDICTION OF $\epsilon_{50}$ FOR THE LATERAL LOAD-DISPLACEMENT BEHAVIOR OF PILES IN CLAY

---

BABAK EBRAHIMIAN and AIDA NAZARI

---

## about the authors

### corresponding author

Babak Ebrahimiyan  
University of Tehran,  
School of Civil Engineering  
Tehran, Iran  
E-mail: bebrahimiyan@ut.ac.ir

The Highest Prestigious Scientific and Professional National Foundation,  
Iran's National Elites Foundation (INEF),  
Tehran, Iran

Aida Nazari  
Iran University of Science and Technology  
School of Civil Engineering  
Tehran, Iran

---

## abstract

Analyzing piles that are subjected to lateral loads reveals that their behavior depends on the soil's resistance at any point along the pile as a function of the pile's deflection, known as the p-y curve. On the other hand, the deformation characteristics of soil defined as "the soil strain at 50% of maximum deviatoric stress ( $\epsilon_{50}$ )" have a considerable effect on the generated p-y curve. In this research, several models are proposed to predict  $\epsilon_{50}$  specifically for designing the very long pile foundations of offshore oil and gas platforms in the South Pars field, Persian Gulf, Iran. Herein,  $\epsilon_{50}$  is evaluated using extensive soil data, including in-situ and laboratory test results using evolutionary polynomial regression (EPR). The effects of the undrained shear strength, the normalized tip resistance of the cone penetration test, the over-burden pressure, the plasticity index and the over-consolidation ratio on  $\epsilon_{50}$  are investigated in marine clays. It is demonstrated that the normalized cone tip resistance, which is an indication of the soil's undrained shear strength, leads to more realistic  $\epsilon_{50}$  values compared with the laboratory-derived undrained shear strength parameter. In addition, the application of the soil-index properties and the over-burden pressure in the models, improves their estimation quality. Furthermore, the results of full-scale lateral pile load tests at different sites are used in order to validate the performance of the proposed models when it comes to predicting the behavior of the lateral piles.

---

## keywords

p-y curve; laterally loaded pile; piezocone penetration test (PCPT); marine clay; evolutionary polynomial regression (EPR); South Pars field

---

## 1 INTRODUCTION

Pile foundations are often required to be designed against significant lateral, in addition to vertical, loads. These lateral loads can be imposed by wind, earth pressure, wave, tide, current and ship impact, mooring rope, earthquake, vehicle traction, etc. The performance of pile foundations is usually governed by either deflection or bearing capacity. Exceeding the maximum allowable lateral load may cause the failure of the soil around the pile, or structural failure of the pile itself. In order to design a pile foundation safely and economically, an accurate assessment of its behavior should be made using pile load test data and/or the well-known analytical or numerical methods. As full-scale load tests are very expensive and time consuming, analytical and numerical approaches are normally used to evaluate the lateral behavior of pile-soil systems.

The lateral pile-soil interaction behavior is commonly characterized by a series of uncoupled, nonlinear springs applied along the pile, known as p-y curves. Various formulations have been proposed to predict these p-y curves in different site conditions [1-7]. The American Petroleum Institute (API) method [7] is a widely used method based on Matlock's field research [1].

The pile geometry and the soil properties are the key parameters for developing p-y curves. These curves mostly depend on the ultimate horizontal soil reaction ( $P_u$ ) and the critical lateral displacement ( $y_c$ ) corresponding to 50% mobilized  $P_u$ .  $y_c$  is defined as

$$y_c = 2.5\epsilon_{50}D \quad (1)$$

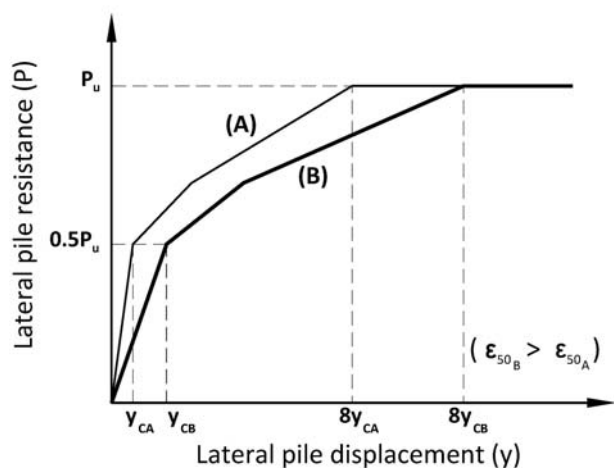


Figure 1. Typical p-y curves for pile in cohesive soil under static loading.

where  $D$  is the pile diameter, and  $\epsilon_{50}$  is the strain at one-half of the maximum stress in laboratory undrained compression tests on undisturbed cohesive soil samples. Typical p-y curves for cohesive soils, shown in Fig.1, illustrate the role of the above-mentioned parameters on developing such curves. The curves A and B in this figure are schematic p-y curves for soils with different  $\epsilon_{50}$  values. As  $\epsilon_{50B} > \epsilon_{50A}$ , with the same pile geometry we have  $y_{CB} > y_{CA}$ . As shown in this figure,  $\epsilon_{50}$  is an effective factor in generating the p-y curves for clays. It is clear that higher  $\epsilon_{50}$  values lead to softer pile behavior and higher lateral displacements for constant lateral load ratios ( $P/P_u$ ). Furthermore, the ultimate lateral load is obtained at higher levels of pile lateral displacements as the  $\epsilon_{50}$  increases. Hence, the lateral stiffness and the resistance of the pile-soil system are affected by  $\epsilon_{50}$ .

Sullivan et al. [8] recommended  $\epsilon_{50}$  values for different clayey soils based on their undrained shear strength. However, such proposed  $\epsilon_{50}$  values are not consistent with those obtained from experimental measurements conducted at different sites and do not result in accurate p-y curves in most soil conditions [9,10].

Hamilton et al. [10] performed some triaxial compression tests under isotropically consolidated undrained (CIU) and unconsolidated undrained (UU) conditions on Tilbrook Grange clays and measured the  $\epsilon_{50}$  values. They realized that the  $\epsilon_{50}$  values obtained from the CIU tests show less scatter than those of the UU tests and found a trend line for  $\epsilon_{50}$ . It was demonstrated that the  $\epsilon_{50}$  values obtained from laboratory tests were nearly five times greater than the values recommended by Sullivan for sites having similar undrained shear strengths.

Afterwards, they compared different p-y curves derived from laboratory  $\epsilon_{50}$  values and those recommended by Sullivan. It was demonstrated that the uncertainty of the predicted p-y curves decreases from 65% to 35% if the laboratory  $\epsilon_{50}$  values are used instead of those recommended by Sullivan. Additionally, they noted that the use of p-y curves based on the Matlock method with  $\epsilon_{50}$  values from CIU tests leads to a more reliable prediction of the lateral load-displacement response.

Hamilton et al. [10] discussed different methods to develop p-y curves for piles in stiff, over-consolidated clays. They compared the measured values of  $\epsilon_{50}$  derived from UU tests with those typically assumed from the Sullivan recommendations and indicated that a slightly better prediction of the load-displacement curves is achieved using measured  $\epsilon_{50}$  values instead of those recommended by Sullivan.

Dunnivant [11] performed experimental and analytical investigations to predict the influences of the pile and soil characteristics as well as the loading conditions on the lateral pile-soil interaction in saturated over-consolidated clays. It was shown that the over-consolidation ratio (OCR) of the soil can affect the reference critical displacement ( $y_c$ ) in the p-y curves. In other words, for over-consolidated clays, the value of  $y_c$  would be smaller than those available in the literature. The degradation of p-y curves in over-consolidated clays begins at much smaller deflections than in soft clays. Also, it was recognized that the pile stiffness and the pile diameter could affect  $y_c$ .

Davies [12] and Robertson et al. [6] presented a preliminary semi-empirical method to evaluate p-y curves based on flat dilatometer test (DMT) data. They employed the DMT-based p-y curves to model the behavior of three full-scale lateral pile load tests. They showed that  $\epsilon_{50}$  has an increasing trend versus depth in both clays and sands in the considered sites. It was found that the predicted deflections using the DMT results agree well with those obtained from the pile load tests. In all the studied cases the calculated bending moments from the DMT-derived p-y curves were larger than those calculated from the measured pile deflection profiles.

Soil properties such as  $\epsilon_{50}$  are very sensitive to soil disturbance due to the coring procedure, and using  $\epsilon_{50}$  values based on the tests on core samples may finally lead to a considerable deviation in predicting the real pile behavior. On the other hand, in-situ testing methods, such as the flat dilatometer (DMT), the pressuremeter (PMT) and the cone penetration test (CPT) offer excellent means by which representative soil properties can be obtained [6,12,13]. Therefore, such in-situ tests,

with a minimum soil disturbance, can be used for evaluating  $\varepsilon_{50}$  and developing p-y curves.

The cone penetration test (CPT) is a reliable in-situ test for its continuous sounding capability and good repeatability. It provides valuable geotechnical information in the soil. Furthermore, the similarity between the CPT penetration process and the pile installation has led to its popularity in deep foundation analysis and design. The total cone tip resistance obtained from the CPT has a strong correlation with the soil's shear strength [14]; on the other hand, due to the direct dependence of  $\varepsilon_{50}$  on the shear strength, the total tip resistance of the CPT can be employed in evaluating  $\varepsilon_{50}$ .

Despite the significant influence of  $\varepsilon_{50}$  on determining the p-y curves, prediction methods used to evaluate this parameter are very rare in the literature. Therefore, this study investigates the use of CPT data to predict  $\varepsilon_{50}$  in clayey soils and examines the capability of predicted  $\varepsilon_{50}$  values to generate realistic p-y curves for laterally loaded piles at different sites. The present calculations of  $\varepsilon_{50}$  are based on a comprehensive databank from laboratory and field tests, performed in the South Pars field, Persian Gulf, southwest of Iran. The field is an extremely strategic offshore area which contains the world's largest gas resources. Many gas-extraction facilities supported

on long pile foundations have been constructed in this important region and a large number of such facilities are still under development. Hence, this research mainly focuses on an accurate evaluation of  $\varepsilon_{50}$  as an influential parameter in the analysis and design of piles against lateral loads in this region. In this regard, several statistical models based on the evolutionary polynomial regression (EPR) method are proposed to evaluate the  $\varepsilon_{50}$  values for clayey soils. The effects of the cone tip resistance, the undrained shear strength, the over-burden pressure as well as different index properties of the soils, such as the over-consolidation ratio and the plasticity index on  $\varepsilon_{50}$  are evaluated and discussed. In particular, the effect of the undrained shear strength of the cohesive soils obtained from field tests on  $\varepsilon_{50}$  is investigated and compared with the recommended values available in the literature. Finally, the validation of the proposed models is performed for full-scale piles tested at two different sites with different soil conditions.

## 2 SITE DESCRIPTION

The survey area, approximately  $50 \times 45 \text{ km}^2$ , is located in the Persian Gulf, Iran, between  $27^\circ 27'$  to  $27^\circ 28'$  Northing and  $52^\circ 27'$  to  $52^\circ 44'$  Easting (Fig. 2). The

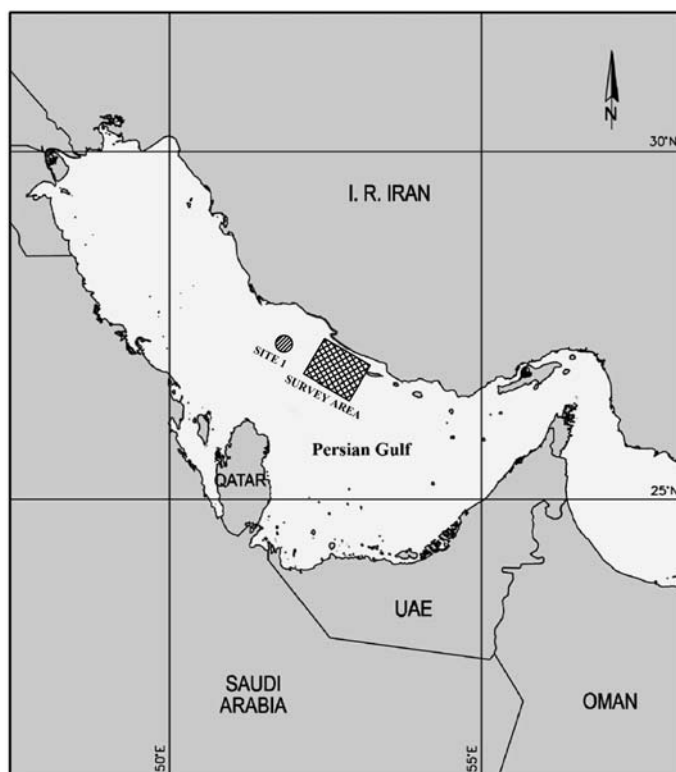


Figure 2. Location of survey area in South Pars Field, south-west of Iran.

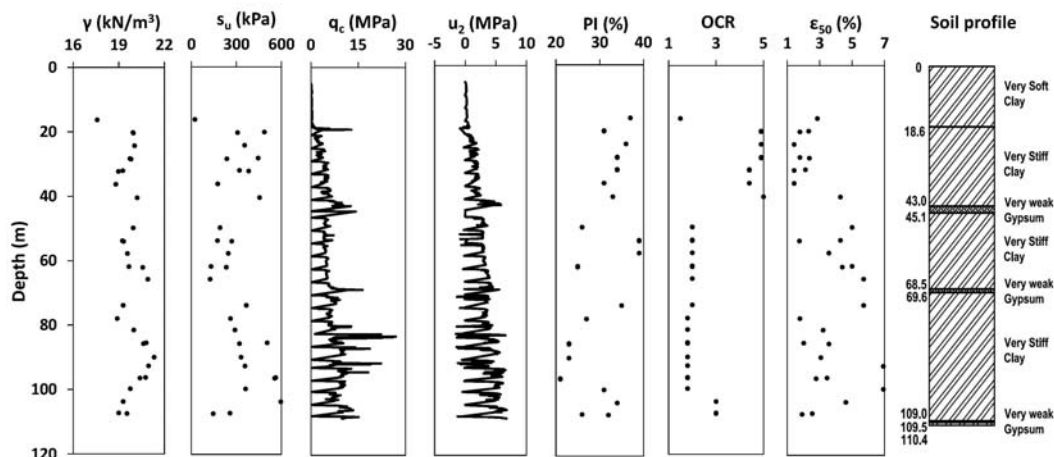


Figure 3. Soil profile and the field and laboratory results for a typical 110 m borehole within survey area.

soil investigation activities were comprised of sixteen boreholes: eight boreholes with a depth of 110 m and the rest with a depth of 80 m below the seabed. In-situ and laboratory tests were carried out to determine the geotechnical properties of the sub-seabed soils. The in-situ tests included piezocone penetration and torvane. Laboratory tests such as unconsolidated undrained (UU) triaxial compression were performed, which resulted in the undrained shear strength of the soil. The strain at 50% of the maximum deviatoric stress ( $\epsilon_{50}$ ) and the strain at failure were also obtained from stress-strain curves in the UU tests. Atterberg limits and sieve tests were performed as well. Typical profiles of the soil properties are shown in Fig. 3 for a 110 m borehole within the considered survey area. The sub-seabed soils are generally clay, including very soft clay at the top, up to approximately 20 m, which become stiffer with depth. In addition, lenses of sandy silt and gypsum are found at several depths.

### 3 EVOLUTIONARY POLYNOMIAL REGRESSION

Evolutionary polynomial regression (EPR) is a useful toolbox developed on a modeling methodology based on the hybrid regression method by Giustolisi et al. [15] and Giustolisi and Savic [16]. It is a symbolic data-driven method that is used to create polynomial models to evolutionary compute based on input data and belongs to the family of Genetic Programming [17]. The constitutive modeling of soil [18] and an assessment of earthquake-induced soil liquefaction and lateral displacement [19] are some successful examples of the use of EPR in the field of geotechnical engineering.

The EPR method includes two general stages: searching the model structures based on an integer Genetic Algorithm (GA) and evaluating each of the model parameters, such as the numerical constant coefficients considering linear optimization [16]. The general symbolic expression derived from EPR is as follows:

$$\hat{Y} = \sum_{j=1}^m F(X, f(X), a_j) + a_0 \quad (2)$$

where  $\hat{Y}$  is the estimated outputs of the system derived from EPR,  $F$  is the function constructed by the program,  $X$  is the input variables matrix,  $f$  is a user-defined function,  $a_j$  is an adjustable parameter determined by the program, and  $m$  is the number of terms of the expression defined by the user, excluding the bias  $a_0$ , if any. The general process can be rewritten based on vector form as

$$Y_{N \times 1}(\theta, Z) = [I_{N \times 1} \ Z_{N \times n}^j] \times [a_0 \ a_1 \ \dots \ a_n]^T = Z_{N \times d} \times \theta_{d \times 1}^T \quad (3)$$

where  $Y_{N \times 1}(\theta, Z)$  is the least-squares estimate vector of the  $N$  target values,  $\theta_{d \times 1}$  is the vector of  $d = m + 1$  parameters  $a_j$  and  $a_0$  ( $\theta^T$  is the transposed vector),  $Z_{N \times d}$  is a matrix formed by  $I$ , unitary vector for bias  $a_0$ , and  $m$  vectors of variables  $Z^j$  that for a fixed  $j$  are a product of the independent predictor vectors of inputs,  $X = \langle X_1 X_2 \dots X_k \rangle$ .

The EPR performs an evolutionary search of the model space using an analogy with stepwise regression [20], rather than by means of the traditional symbolic regression search based on parse tree structures. In this way, the EPR performs a global search of the input exponents and a combination of input variables according to the user-defined cost function.



The program search is based on pseudo-polynomial and true structures using a single and multi-objective genetic algorithm, with different general expression forms. The expression form considered in this research is defined as below:

$$Y = a_0 + \sum_{j=1}^m a_j \cdot (X_1)^{ES(j,1)} \cdot \dots \cdot (X_k)^{ES(j,k)} \cdot f\left((X_1)^{ES(j,k+1)}\right) \cdot \dots \cdot f\left((X_k)^{ES(j,2k)}\right) \quad (4)$$

In the above expression,  $X_i$  are the  $k$  candidate inputs vectors,  $a_j$  are constant values,  $ES$  is the matrix of unknown exponents that can be edited by the user within the defined range of values, and  $m$  is the length of the expressions defined by the user, which represents the number of maximum terms in each set of results. Each monomial of the polynomial models can contain user-defined functions. For this purpose,  $f()$  is the function that can be selected by the user based on available functions in the program. These functions may be logarithmic, exponential, tangent hyperbolic, etc.

In order to determine all the models corresponding to the optimal trade-off between the fitness and the brevity of the model, the EPR performs a multi-objective search exhibiting various mathematical models representing the best fitness for possible models. For a particular purpose, one can choose the best models based on short gap reconstruction, gaining a physical insight or forecasting the phenomenon. The fitness model defined in the EPR is the Coefficient of Determination ( $CoD$ ), which refers to how closely the regression expression fits the data points:

$$CoD = 1 - \frac{\sum_n (p - m)^2}{\sum_n (m - \bar{m})^2} \quad (5)$$

where  $p$  is the predicted values by model derived from the EPR,  $m$  is the measured value,  $\bar{m}$  is the average of the measured values, and  $n$  is the number of data points. More details about the EPR architecture for model representation as well as the method employed for the parameter estimation can be found in Giustolisi and Savic [16].

## 4 RESULTS AND DISCUSSION

The field and laboratory test results, including 274 data series, are considered as the databank for the numerical regression. In the present study, five variables are identified as the primary input data of cohesive soils for evaluating  $\varepsilon_{50}$  as an output. The input data includes the undrained shear strength ( $s_u$ ), the normalized cone tip resistance ( $q_c$ ), the total over-burden pressure ( $\sigma_0$ ), the plasticity index ( $PI$ ) and the over-consolidation ratio ( $OCR$ ).

In pattern recognition procedures it is common practice to divide the available data into two subsets: training and testing. The model is firstly developed using the former and then tested using the latter one to ensure that the final obtained model has the ability to properly estimate  $\varepsilon_{50}$  for unseen or untrained cases. Here, the entire databank is divided into several random combinations of training and testing sets until a robust representation of the whole population, in terms of statistical properties, is achieved for both training and testing sets. The statistical properties of the parameters considered in this study, including the values of maximum, minimum, mean, and the standard deviation, are presented in Table 1 for the training, testing and all datasets. The training dataset includes 80% of all the data (219), and the rest (55) are used as the testing dataset. The statistical values of the training, testing and all datasets, shown in Table 1, are close to each other.

Table 1. Statistical characteristics of databank.

Subsets	Statistical characteristics	$\sigma_0$ (kPa)	$s_u$ (kPa)	$q_c$ (kPa)	$PI$ (%)	$OCR$	Measured $\varepsilon_{50}$ (%)
Testing data (55 data)	Minimum	216	19	162	14	0.9	0.9
	Maximum	1933	504	8767	40	4	9.2
	Mean	1081	241	4155	29	2.2	3.9
	Standard deviation	462	112	2190	6.8	0.74	2.1
Training data (219 data)	Minimum	217	19	139	12	0.9	0.7
	Maximum	2207	634	8943	47	5.3	9.3
	Mean	1077	274	4184	30	2.4	3.5
	Standard deviation	515	129	1996	7.4	1.1	2.0
All data (274 data)	Minimum	216	19	139	12	0.9	0.7
	Maximum	2207	634	8943	47	5.3	9.3
	Mean	1078	268	4178	30	2.4	3.6
	Standard deviation	505	126	2037	7.3	1.0	2.1

**Table 2.** Proposed models for estimating  $\varepsilon_{50}$ .

No.	Equation	Involved parameters	$R^2$ (%)	RMSE	MAE
Model 1	$\varepsilon_{50} = -0.79 + 1.5s_u^{0.2}$	$s_u$	6.6	1.99	1.65
Model 2	$\varepsilon_{50} = 1.48 + 1.2 \times 10^{-3} q_c^{0.9}$	$q_c$	20.8	1.84	1.52
Model 3	$\varepsilon_{50} = 4.84 - 8.76 \times 10^{-2} q_c^{0.3} PI^{0.5} OCR^{-0.1} - 1.24 \times 10^{-12} q_c^{3.3} OCR^{-0.3} + 5.43 \times 10^{-6} q_c^{1.4} PI^{0.7} OCR^{-0.1} - 2.1 \times 10^{-3} q_c^{0.5} PI^{0.8} OCR^{0.7}$	$q_c, PI, OCR$	36.7	1.64	1.34
Model 4	$\varepsilon_{50} = 1.55 - 2.7 \times 10^{-13} \sigma^{1.5} q_c^{2.6} PI^{-1.3} OCR^{-0.2} - 1.8 \times 10^{-10} \sigma^{0.6} q_c^{1.3} PI^{1.6} OCR^2 + 1.5 \times 10^{-6} \sigma^{1.5} q_c^{0.4} PI^{0.1} OCR^{0.6}$	$\sigma_0, q_c, PI, OCR$	64.8	1.22	1.02

After several analyses in the EPR framework, four relationships are developed for evaluating  $\varepsilon_{50}$ , which are presented in Table 2. To examine the robustness and assess the performance of the EPR models, the following three statistical criteria were used:

- Coefficient of determination ( $R^2$ ), is a measure used to determine the relative correlation between two sets of variables, and defined as:

$$R^2 = 1 - \frac{\sum_{i=1}^n (m_i - p_i)^2}{\sum_{i=1}^n (m_i - \bar{m})^2} \quad (6)$$

- Root mean square error (RMSE), is a measure of the error, defined as:

$$RMSE = \sqrt{\frac{\sum_{i=1}^n (m_i - p_i)^2}{n}} \quad (7)$$

The advantage of this criterion is that large errors receive greater attention than smaller ones.

- Mean absolute error (MAE) is another measure of the error which eliminates the emphasis given to large errors, presented as:

$$MAE = \frac{\sum_{i=1}^n |m_i - p_i|}{n} \quad (8)$$

In the above relations,  $m_i$  and  $p_i$  are the  $i^{th}$  measured and predicted values of the output parameter ( $\varepsilon_{50}$ ), respectively,  $n$  is the number of data points, and  $\bar{m}$  indicates the average of the measured output.

The suggested models to evaluate  $\varepsilon_{50}$  as well as the values of the statistical criteria are presented in Table 2. It is clear that the performance of the models improves from model 1 to 4, since the  $R^2$  value increases while the RMSE and MAE values decrease. Based on the results summarized in Table 2, the EPR model 4 was chosen as the most appropriate one, which is developed using four input parameters:  $q_c, \sigma_0, PI, OCR$ .

The first relationship is developed between the undrained shear strength of the soil and  $\varepsilon_{50}$ , and the second one uses the normalized cone tip resistance ( $q_c$ ) to predict  $\varepsilon_{50}$ , as shown in Table 2. By comparing the statistical characteristics of models 1 and 2, it can be seen that the  $\varepsilon_{50}$  values predicted from the field-based resistance property ( $q_c$ ) are more accurate than those predicted from the laboratory-based resistance ( $s_u$ ). By using  $q_c$  instead of  $s_u$ ,  $R^2$  increases from 6.6 for model 1 to 20.8 for model 2. However, the  $R^2$  value is not yet acceptable, and it seems that other influential parameters should be included in the model development process. Therefore, after several trial-and-error procedures it was found that the index properties of the soil, e.g., OCR and PI, have strong effects on the predicted  $\varepsilon_{50}$  values. According to Table 1, it is realized that model 3, which includes the above-mentioned factors, predicts  $\varepsilon_{50}$  more accurately than model 2. Furthermore, model 4 shows that the over-burden pressure also has a significant positive influence on the prediction accuracy.

Fig. 4 illustrates the predicting capability of the models by plotting the  $\varepsilon_{50}$  values against their corresponding measured values in training and testing datasets and their statistical characteristics are shown for a quantitative comparison. Considering the data scatter in the graphs of Fig. 4, the results of the models for the testing dataset are generally consistent with those for the

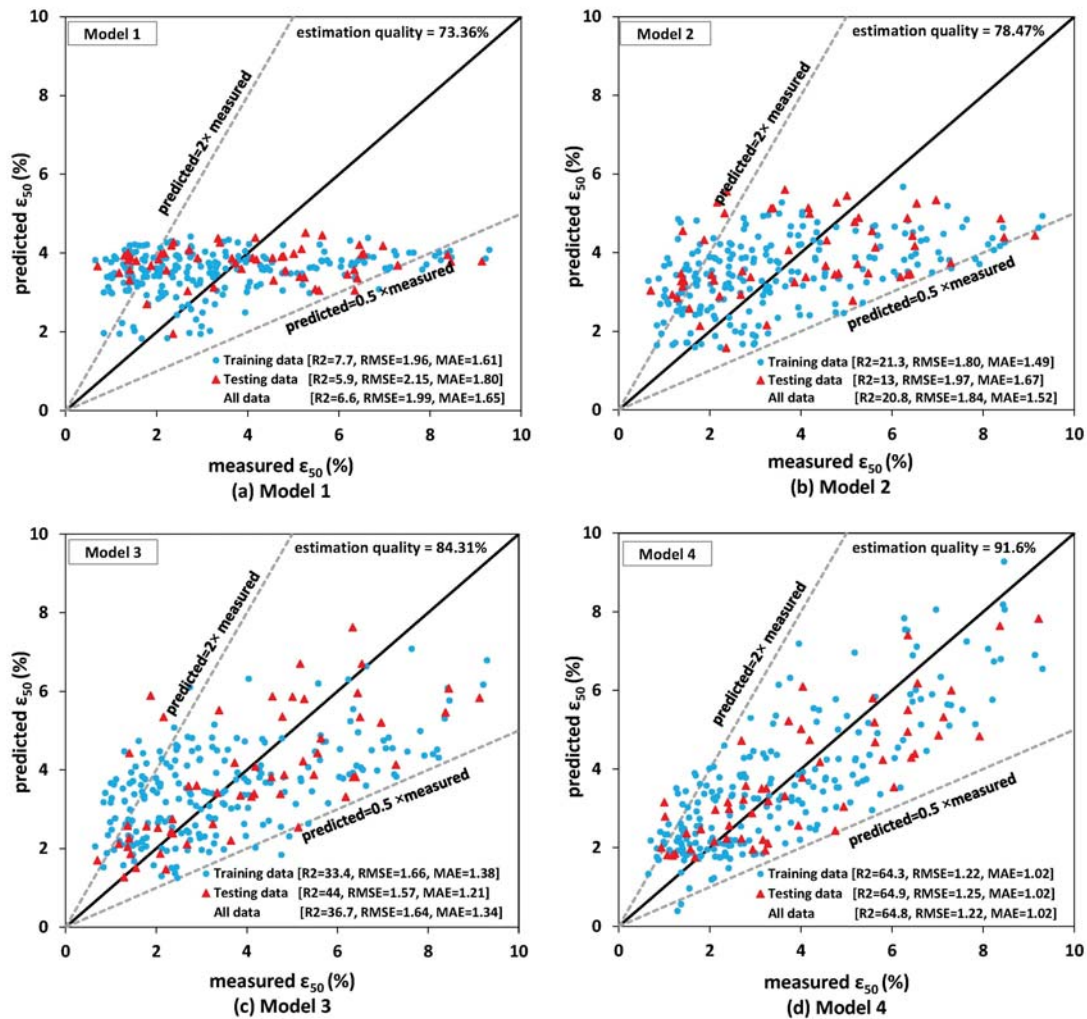


Figure 4. Predicted versus measured  $\varepsilon_{50}$  values for the proposed EPR-based models.

training dataset. The more the points are distributed uniformly around the ideal 45° line, and the less scatter around this line, the better the capability of the model at predicting  $\varepsilon_{50}$ . In this regard, it is clear that model 4 behaves better than the others. The upper and lower lines in Fig. 4 show the boundaries for a zone that is characterized by the ratios of the predicted-to-measured  $\varepsilon_{50}$  between 0.5 and 2.0. The estimation quality of each model, defined as the number of points that fall inside these two boundaries as a percentage of the total points, is shown in the figure. As the performance of the models improves, the data show more concentration in the mentioned zone. While all the models show acceptable estimation qualities, the estimation quality for model 4 has the highest value (91.6%) among the proposed models.

It is clear from Fig 4 that the predicted  $\varepsilon_{50}$  values from model 1, which was developed merely from the undrained shear strength ( $S_u$ ), are not well distributed along the diagonal line and are concentrated in a narrow horizontal band. However, implementing the normalized cone tip resistance ( $q_c$ ), instead of  $S_u$ , in model 2 smoothed the above-mentioned shortcoming.

The log-normal distribution, used by Briaud and Tucker [21], is an appropriate statistical criterion to further evaluate the performance of the proposed models. In this regard, the natural logarithm of the ratio of the predicted-to-measured  $\varepsilon_{50}$  i.e.,  $\ln(\varepsilon_{50p} / \varepsilon_{50m})$ , is calculated for each data point and then the mean and standard deviation of these values are determined as follows:

$$\mu_{\ln(\epsilon_{50p}/\epsilon_{50m})} = \frac{1}{n} \sum_{i=1}^n \ln(\epsilon_{50p}/\epsilon_{50m})_i \quad (9)$$

$$\sigma_{\ln(\epsilon_{50p}/\epsilon_{50m})} = \sqrt{\frac{1}{n-1} \sum_{i=1}^n \left( \ln(\epsilon_{50p}/\epsilon_{50m})_i - \mu_{\ln(\epsilon_{50p}/\epsilon_{50m})} \right)^2} \quad (10)$$

$$f(\epsilon_{50p}/\epsilon_{50m}) = \frac{1}{\sqrt{2\pi}\sigma_{\ln(\epsilon_{50p}/\epsilon_{50m})}} \exp \left[ -\frac{1}{2} \left( \frac{\ln(\epsilon_{50p}/\epsilon_{50m}) - \mu_{\ln(\epsilon_{50p}/\epsilon_{50m})}}{\sigma_{\ln(\epsilon_{50p}/\epsilon_{50m})}} \right)^2 \right] \quad (11)$$

where the subscripts  $p$  and  $m$  denote the “predicted” and “measured”, respectively,  $n$  is the number of data considered in the analysis,  $\mu_{\ln}$  and  $\sigma_{\ln}$  are indicators for the accuracy and precision of the models, respectively, which are used to identify the log-normal distribution of the density function as:

A better distribution is achieved when  $\mu_{\ln(\epsilon_{50p}/\epsilon_{50m})}$  and  $\sigma_{\ln(\epsilon_{50p}/\epsilon_{50m})}$  approach unity and zero, respectively. The log-normal distribution of  $\epsilon_{50p}/\epsilon_{50m}$  for the proposed models are presented in Fig. 5.

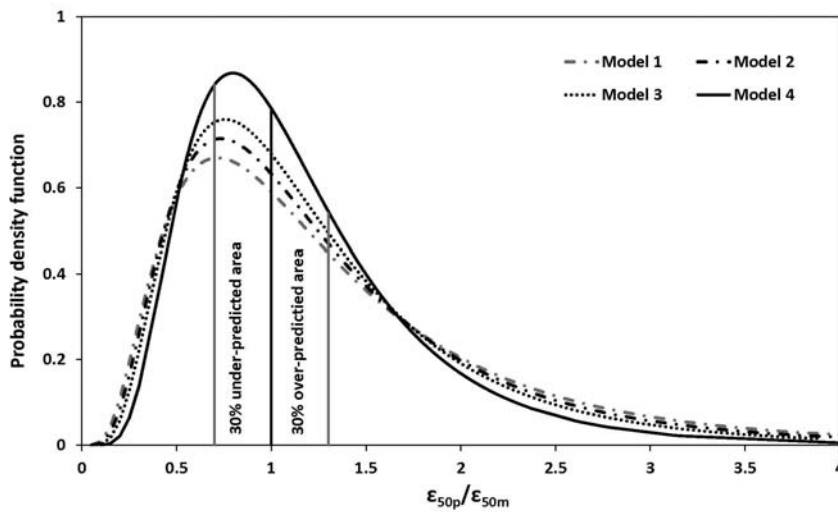


Figure 5. Log-normal distribution of  $\epsilon_{50p}/\epsilon_{50m}$  for the proposed models.

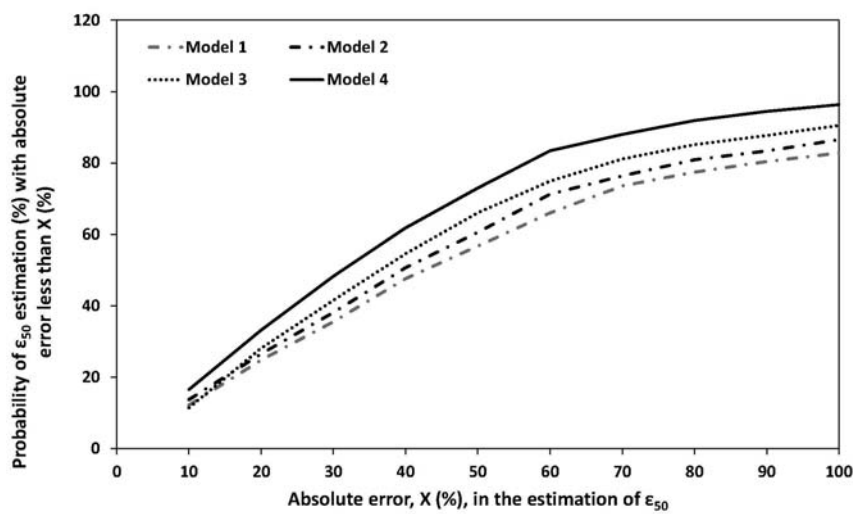


Figure 6. Probability of  $\epsilon_{50}$  estimation with absolute error less than a given error,  $x$  (%).

The probability of predicting  $\varepsilon_{50}$  with a 0 to 90% accuracy (10-100% absolute error) is calculated from Fig. 5 and shown in Fig. 6. The total area below each curve in Fig. 5 is equal to one. Therefore, at a specified absolute error level, the probability of predicting  $\varepsilon_{50}$  is derived by calculating the total area below the log-normal distribution curve within the accuracy limits. At a constant absolute error, a higher probability indicates the better ability of the model at predicting  $\varepsilon_{50}$ . Based on this definition, the performance of the models improves from model 1 to 4 at all levels of absolute error.

The ability of the different models to predict  $\varepsilon_{50}$  can be evaluated using cumulative probability, as used by Long and Wysocky [22]. They used the concept of cumulative probability as a criterion to evaluate the bias of their model. The cumulative probability for each  $\varepsilon_{50p}/\varepsilon_{50m}$  can be obtained with the following definition:

$$CP_i = \frac{i}{n+1} \quad (12)$$

where  $i$  is the data number arranged in an ascending order. The cumulative probability versus the ratio  $\varepsilon_{50p}/\varepsilon_{50m}$  for the proposed models is depicted in Fig. 7. In order to assess the ability of each model at estimating  $\varepsilon_{50}$ , the 50% and 90% cumulative probabilities (CP50% and CP90%) are calculated. The difference between CP90 and CP50 (CP90%–CP50%) represents the discrepancy from an accurate estimation. Ideally, if all the data are predicted with no bias, the distribution of the estimated-to-measured  $\varepsilon_{50}$  against CP will be a straight line with a value of unity, indicating an exact

estimation. In reality, the better performance of the model is achieved when  $\varepsilon_{50p}/\varepsilon_{50m}$  is closer to unity at CP50%. Lower (CP90%–CP50%) for each model indicates the better prediction accuracy of the proposed model. According to this criterion, it is observed in Fig. 7 that model 4 leads to an optimum value of CP50% equal to unity and a lower value of (CP90%–CP50%) compared with the other models.

In a statistical analysis a model would behave better if the residual values, i.e., the difference between the measured and predicted values of  $\varepsilon_{50}$ , are concentrated more uniformly around the mean value of the residuals. The mean value of the residuals is calculated by:

$$MR = \frac{1}{n} \sum_{i=1}^n (\varepsilon_{50m} - \varepsilon_{50p})_i \quad (13)$$

Fig. 8 (see next page) depicts the residuals of the training and testing sets for all the presented models versus the data number. In this figure, the residuals are scattered along a line indicating the mean ( $MR$ ). In addition, the upper and lower bounds of the residual scatter ( $MR \pm \sigma$ ;  $\sigma$  is the standard deviation of residuals) are shown in the figure. The ideal performance of each model is achieved by  $MR$  and  $\sigma$  equal to zero. In general, the lower absolute values of these two parameters represent the better performance of the model. A comparison between the proposed models in Fig. 8, with respect to the above parameters, shows an improvement of the models from 1 to 4 by decreasing the absolute  $MR$  and  $\sigma$  values.

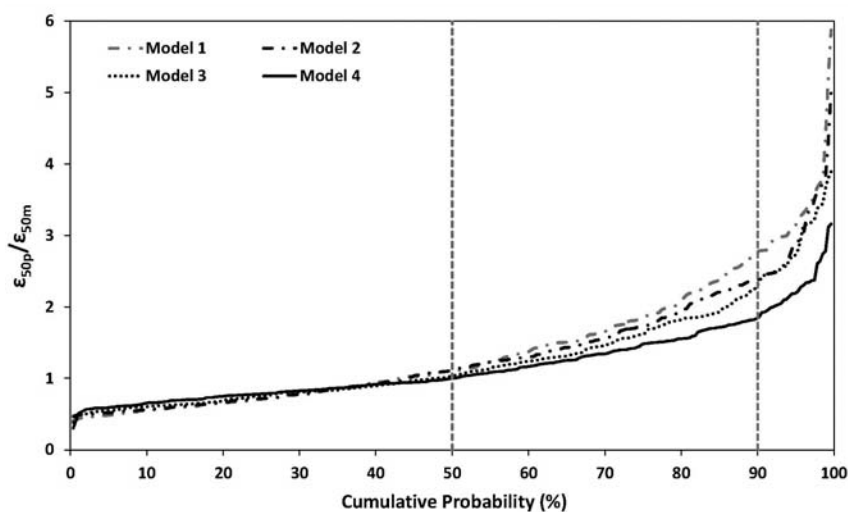


Figure 7. Cumulative probability plot of  $\varepsilon_{50p}/\varepsilon_{50m}$  for the proposed models.

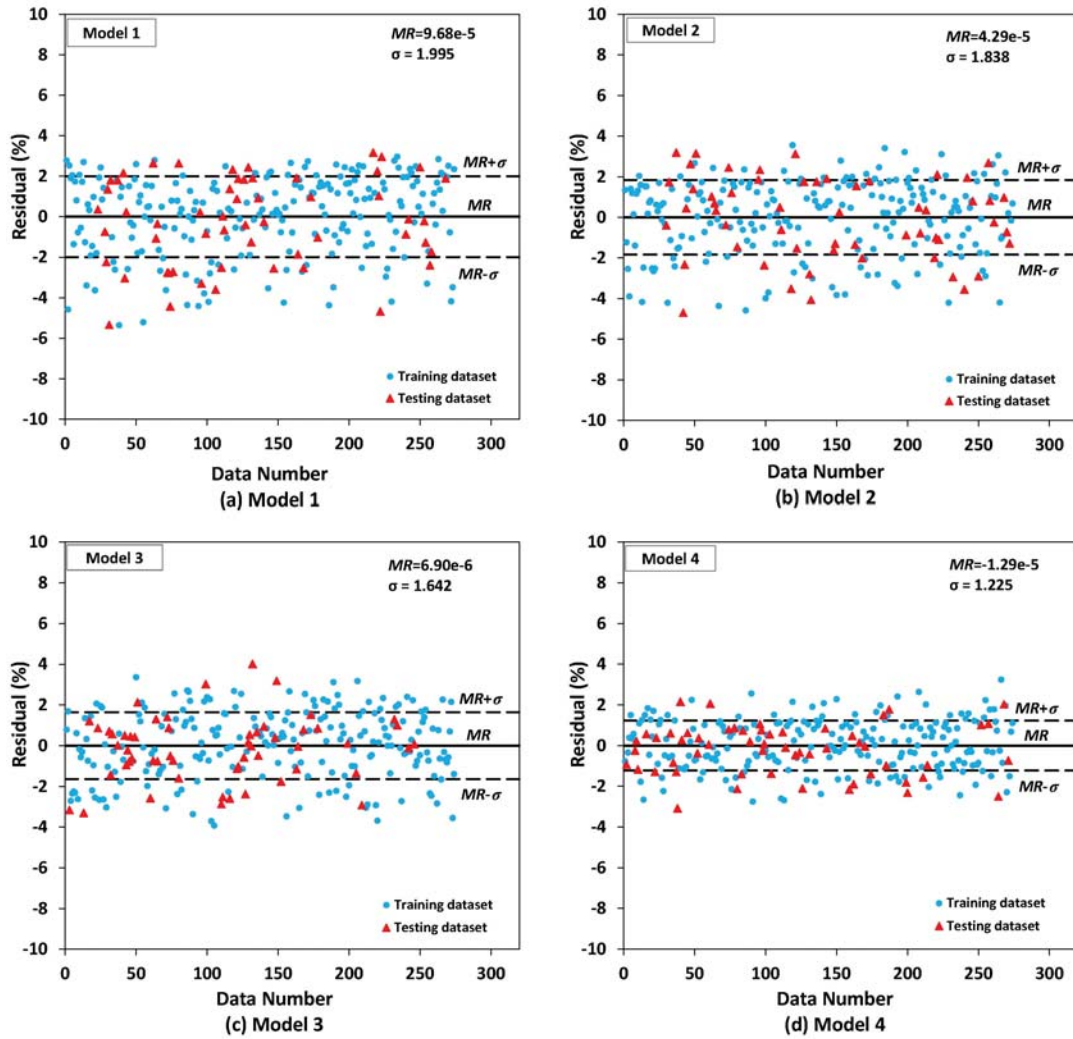


Figure 8. Distribution of residual for the EPR-based models.

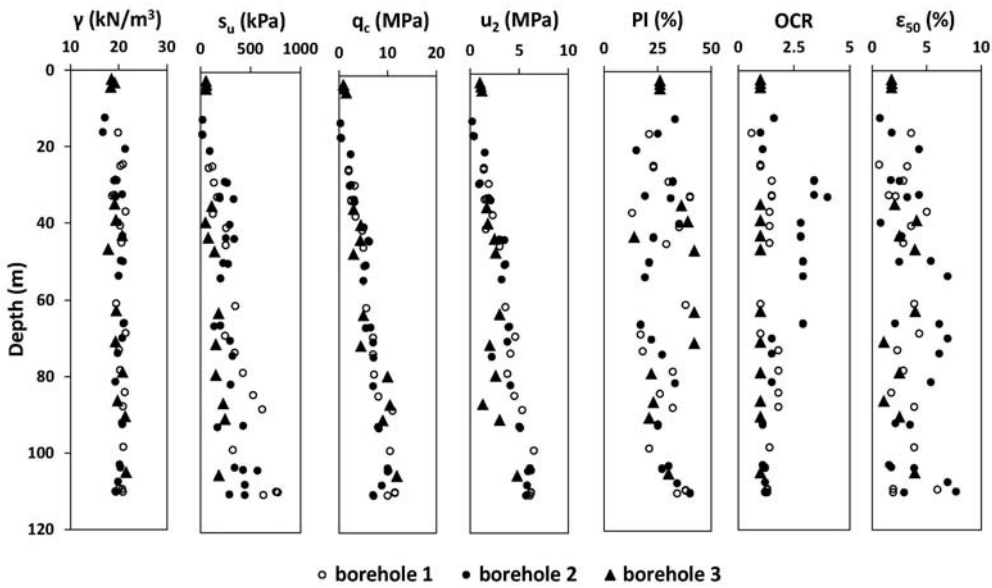


Figure 9. Geotechnical characteristics of soil in the boreholes of Site 1.

## 5 VALIDATION OF THE PROPOSED MODELS

In order to validate the proposed models, the test results at three different sites are considered. The first site is located at South Pars field, Persian Gulf, Iran, outside the survey area, shown as Site 1 in Fig. 2. The soil is a very soft clay overlying a sandy silt or silty sand layer at shallow depths. Stiff to very stiff clay dominates at deeper parts. The profiles of the soil properties in three boreholes within this site are presented in Fig. 9. Fig. 10 shows the  $\epsilon_{50}$  values predicted by different models as well as the measured values obtained from UU tests in borehole depths. In all the figures the recommended  $\epsilon_{50}$  values by Sullivan et al. [8] are significantly lower than the measured ones. However, the  $\epsilon_{50}$  values predicted by models 1 and 4 compare relatively well with the measured ones in the full range of values along the borehole depths, as shown in Fig. 10. Generally, the  $\epsilon_{50}$  values show an increasing trend with depth from both laboratory measurements and the predictions of the currently proposed models. This result is in contradiction with the values of  $\epsilon_{50}$  recommended by Sullivan.

Herein, it is attempted to validate the current models using the p-y curve results obtained from the pile load tests conducted at two different sites (Sites 2 and 3). General information about the considered sites is given in Table 3.

Figs. 11(a) and (b) show the p-y curves generated based on the  $\epsilon_{50}$  values from different models as well as Sullivan's recommendations for two different depths at Sites 2 and 3, respectively. The figures also include the p-y curves obtained from full-scale tests. It is noted that the procedure for generating p-y curves is based on API [27]. The figures show that the calculated p-y curves from the EPR-based models agree relatively well with the measured p-y curves. However, the p-y curves calculated from the Sullivan's recommendations show lower values of the lateral displacement at all the lateral load levels. This implies that using the  $\epsilon_{50}$  parameter from the Sullivan recommendations in generating the p-y curve leads to a stiffer behavior of the pile-soil system against lateral loads in comparison with the real behavior. It is observed that the predicted lateral displacements at 50% of the maximum lateral load from the proposed models are 1.5–3.5 and 2–4 times as large as those obtained from the Sullivan recommendations for Sites 2 and 3, respectively.

In addition, the ratio of the predicted-to-measured lateral pile displacements at the maximum lateral load levels for the generated p-y curves at both sites is summarized in Table 6. It is clear from Table 6 that the generated p-y curves based on the  $\epsilon_{50}$  values from the proposed models yield lateral pile displacements very close to the measured ones, with a maximum error of 6%. However, using the  $\epsilon_{50}$  values from Sullivan's recommendation in generating the p-y curves leads to very non-conservative lateral pile displacements at both sites.

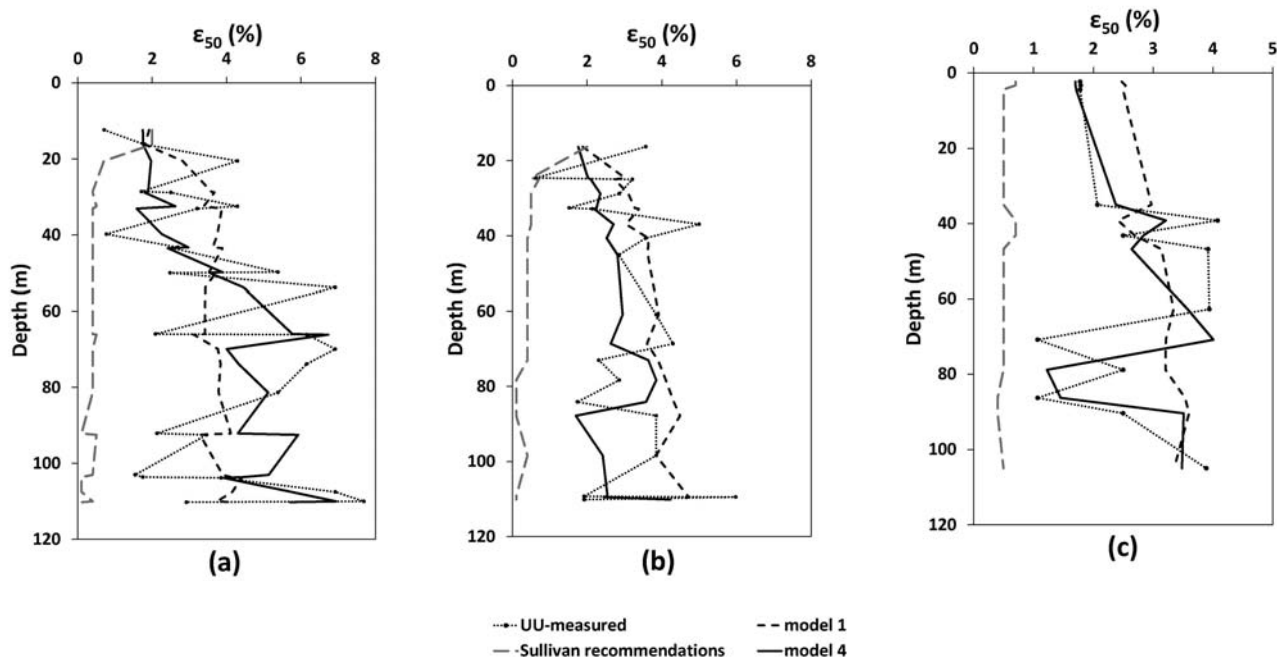
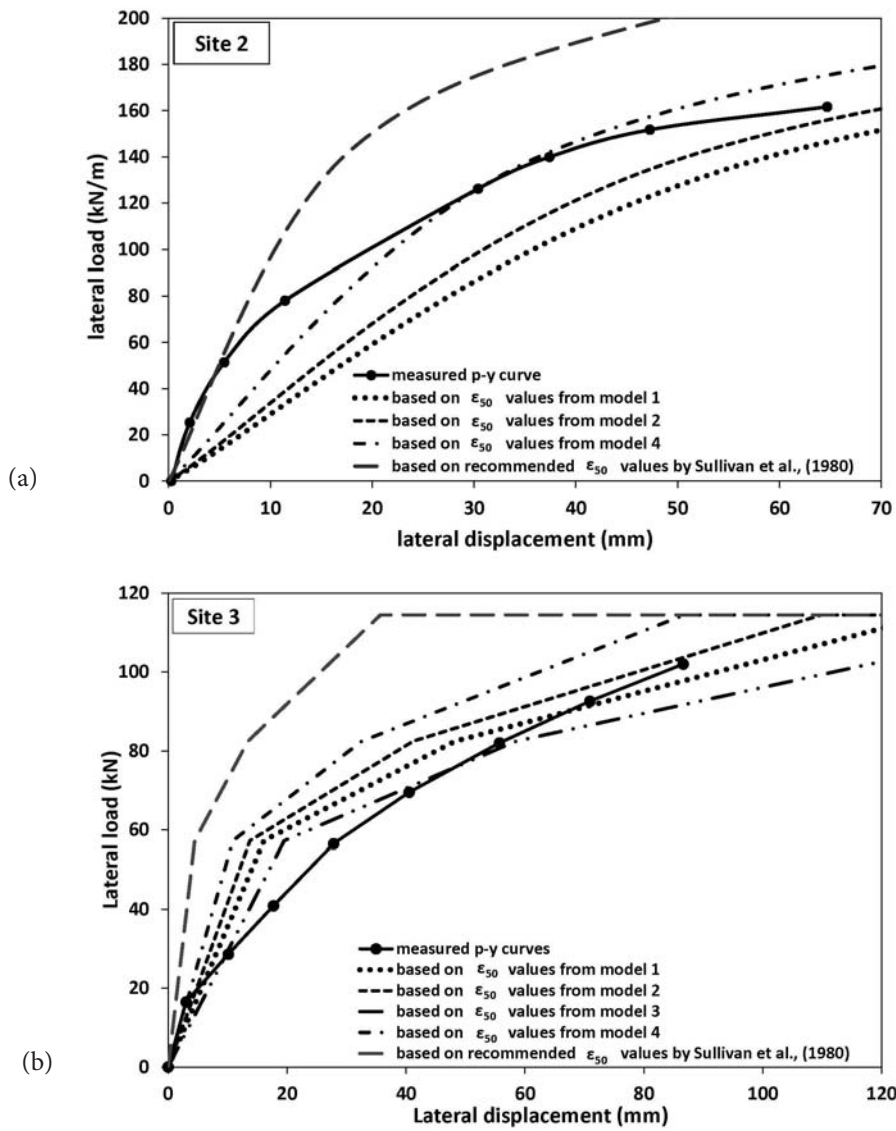


Figure 10. Profiles of predicted and measured  $\epsilon_{50}$  values in Site 1 from (a) borehole 1, (b) borehole 2, and (c) borehole 3.

**Table 3.** General information about Sites 2 and 3.

Site No.	Location	Source of p-y curve data	Pile section	Pile section dimension (m)	Depth of measurement (m)	Pile length (m)	Relevant geotechnical properties	Reference
2	Incheon Bridge, Korea	Full-scale field load tests on piles	Circular	Diameter = 1.016 Thickness = 0.016	4D from ground surface (D= pile diameter)	26.6	Table 4	[23-25]
3	Bridge construction site near Oskaloosa, Iowa	Lateral load tests on steel and concrete piles	UHPC <sup>1</sup> H-shaped	0.254×0.254	5D from ground surface (D=equivalent diameter, 0.287)	10.7	Table 4	[26]

<sup>1</sup> Ultra-high-performance concrete



**Figure 11.** Measured and calculated p-y curves: (a) Site 2 at depth = 4D; and (b) Site 3 at depth = 5D, (D = pile diameter).



**Table 4.** Soil properties of Site 2 [23-25].

Type	Depth (m)	Unit weight (kN/m <sup>3</sup> )	Moisture content (%)	$s_u$ (kPa)	Friction angle ( $\varphi$ ) (°)	Recommended $\epsilon_{50}$ in the literature
Upper clay	0-6.3	17.5	21.2	15-30	-	0.02
Lower clay	6.3-16.5	17.5	7.6	30-50	-	0.01
Silty clay	16.5-22.0	17.8	12.7	70	-	0.005
Residual soil	22.0-24.0	18.0	4.33	-	34	-

**Table 5.** Soil properties of Site 3 [26].

Depth (m)	classification	Unit weight (kN/m <sup>3</sup> )	Moisture content (%)	LL (%)	PI (%)	$s_u$ (kPa)	Friction angle ( $\varphi$ ) (°)	Recommended $\epsilon_{50}$ in the literature
0-1.5	ML	18.8	21.2	42.1	10.4	60	-	0.007
1.5-2.8	CL	18.5	7.6	44.4	17.9	60	-	0.007
2.8-4.9	CL	18.5	12.7	27.9	7.4	136	-	0.005
4.9-5.8	SC	20.5	4.33	32.5	17.7	-	41	-
5.8-7.7	CL	20.4	4.83	36.7	19.2	-	35	-
7.7-9.2	SW	20.6	20.6	-	-	-	42	-
9.2-10.5	CL	20.4	-	-	-	800	-	0.004
10.5-12.0	SW	20.4	-	-	-	-	-	-

**Table 6.** Ratio of predicted-to-measured lateral pile displacement.

Site No.	At maximum lateral load level		
	Depth	Average of proposed models	Sullivan et al. [8]
2	4D	1.05	0.36
3	5D	1.06	0.31

## 6 SUMMARY AND CONCLUSIONS

In this research, the results of the field and laboratory test data of the South Pars field, Persian Gulf, Iran, are used to develop models for evaluating  $\epsilon_{50}$  using the EPR. In this regard the cone tip resistance of the CPT and several parameters of cohesive soils ( $S_u$ ,  $\sigma_0$ ,  $OCR$  and  $PI$ ) are considered when developing the models. The conclusions are as follows:

- According to the statistical analyses, the models developed using the cone tip resistance ( $q_c$ ) yield more accurate  $\epsilon_{50}$  values than those developed using the undrained shear strength of the soils ( $S_u$ )

obtained from the UU tests. In general  $\epsilon_{50}$  is more realistically predicted using the field-based, instead of the laboratory-based, resistance of the soil.

- The index properties of the soil, e.g.,  $OCR$  and  $PI$ , significantly improve the performance of the proposed models in predicting  $\epsilon_{50}$ .
- According to the statistical criteria, the models that are developed considering the effect of the overburden pressure ( $\sigma_0$ ) lead to better predicted  $\epsilon_{50}$  values.
- The models are validated with the field data of Site 1, located outside the main survey area, as shown in Fig. 2. The predicted  $\epsilon_{50}$  values are in relatively good agreement with the measured ones for the full range of values along all the borehole depths in this site. It was found that the predicted  $\epsilon_{50}$  values from the proposed models increase with soil depth, which agrees with the laboratory measurements.
- Further model validation with the full-scale lateral pile load test data at two different sites demonstrate the models' capability in providing the  $\epsilon_{50}$  parameter to generate p-y curves consistent with the real behavior of a pile-soil system measured in the field. In particular, the results indicate that the p-y curves generated based on the  $\epsilon_{50}$  values from the proposed models are in better agreement with the field data

rather than the p-y curves obtained from previously recommended  $\varepsilon_{50}$  values in the literature.

## ACKNOWLEDGEMENT

The first author wants to express his sincere gratitude to the Iran's National Elites Foundation (INEF) for the moral support and encouragement.

## REFERENCES

- [1] Matlock, H. (1970). Correlations for design of laterally loaded piles in soft clay. *Proc. Offshore Technology Conf.*, H.M. Coyle and R.E. Bartoske-witz, eds., Houston, Texas, pp. 577-594.
- [2] Reese, L.C. and Welch, R.C. (1975). Lateral loading of deep foundations in stiff clay. *J. Geotech. Geoenv. Eng.*, Vol. 101, No. 7, pp. 633-49.
- [3] Reese, L.C., Cox, W.R. and Koop, F.D. (1975). Field testing and analysis of laterally loaded piles in stiff clay. *Proc. Offshore Technology Conf.*, Houston, Texas, pp. 671-690.
- [4] O'Neill, M.W. and Gazigoglu, S.M. (1984). Evaluation of p-y relationships in cohesive soils. *Proc. Symp. Analysis and Design of Pile Foundations*, ASCE, 1-5 October, pp. 192-213.
- [5] Gabr, M.A. and Borden, R. (1988). Analysis of load deflection response of laterally loaded piers using DMT. *Proc. 1<sup>st</sup> Int. Symp. Penetration Test-ing*, Balkema, Rotterdam, The Netherlands, pp. 513-520.
- [6] Robertson, P.K., Davies., M.P. and Campanella, R.G. (1989). Design of laterally loaded driven piles using the flat dilatometer. *Geotech. Test. J.*, Vol. 12, No. 1, pp. 30-38.
- [7] American Petroleum Institute. (1993). Recommended practice for planning, designing and constructing fixed offshore platforms. API recommended practice RP-2A, Washington, D.C.
- [8] Sullivan, W.R., Reese, L.C. and Fenske, C.W. (1980). Unified method for analysis of laterally loaded piles in clay. *Numerical Methods in Offshore Piling*. ICE, London, pp. 135-146.
- [9] Hamilton, J.M. and Dunnavant, T.W. (1993). Analysis of behavior of the Tilbrook Grange lateral test pile. Large-scale pile tests in clay. Edited by J. Clarke, Thomas Telford, London, U.K., pp. 448-461.
- [10] Hamilton, J.M., Long, M.M., Clarck, J. and Lambson, M.D. (1993). Cyclic lateral loading of an instrumented pile in overconsolidated clay at Tilbrook Grange. Large-scale pile tests in clay. Edited by J. Clarke, Thomas Telford, London, U.K., pp. 381-403.
- [11] Dunnavant, T.W. (1986). Experimental and analytical investigation of the behavior of single piles in overconsolidated clay subjected to cyclic lateral loads. Ph.D. Dissertation, University of Houston, Houston, Texas.
- [12] Davies, M.P. (1987). Predicting axially and laterally loaded pile behavior using in-situ testing methods. M.Sc. Thesis, Department of Civil Engineering, The University of British Columbia, Vancouver, B.C. .
- [13] Schmertmann, J. (1978). Guidelines for cone penetration test, performance and design. Federal highway administration, Report No. FHWA-TS-78-209, U.S. Department of Transportation, Washington, D.C.
- [14] Lunne, T., Robertson, P.K. and Powell, J.J.M. (1997). Cone penetration testing in geotechnical practice. Blackie Academic, EF Spon/Routledge Publication, New York.
- [15] Giustolisi, O., Savic, D.A. and Doglioni, A. (2004). Data reconstruction and forecasting by evolutionary polynomial regression. *Proc. 6<sup>th</sup> Int. Conf. Hydroinformatics*, Singapore, pp. 1245-1252.
- [16] Giustolisi, O. and Savic, D.A. (2006). A symbolic data-driven technique based on evolutionary polynomial regression. *J. Hydroinf.*, Vol. 8, No. 3, pp. 207-222.
- [17] Koza, J.R. (1992). Genetic programming: on the programming of computers by natural selection. MIT Press, Cambridge, MA. ISBN 0-262-11170-5.
- [18] Javadi, A.A. and Rezaia, M. (2009). Intelligent finite element method: an evolutionary approach to constitutive modeling. *Adv. Eng. Inf.*, Vol. 23, pp. 442-451.
- [19] Rezaia, M., Faramarzi, A. and Javadi, A.A. (2011). An evolutionary based approach for assessment of earthquake-induced soil liquefaction and lateral displacement. *Eng. Appl. Artif. Intell.*, Vol. 24, pp. 142-153.
- [20] Draper, N.R. and Smith, H. (1998). Applied regression analysis. Third Edition, John Wiley and Sons, NewYork.
- [21] Briaud, J.L. and Tucker, L.M. (1988). Measured and predicted axial response of 98 piles. *J. Geotech. Eng.*, Vol. 114, No. 9, pp. 984-1001.
- [22] Long, J.H. and Wysockey, M.H. (1999). Accuracy of methods for predicting axial capacity of deep foundations. *Proc. OTRC 99 Conf.*, Analysis, Design, Construction, and Testing of Deep Foundation, ASCE, Geotechnical Special Publication 88, pp. 190-195.

- [23] Jeong, S.S., Kim, Y.H., Kim J.H. and Shin, S.H. (2007). Cyclic lateral load tests of offshore large diameter piles of Incheon Bridge in marine clay. *Proc. 17<sup>th</sup> Int. Offshore and Polar Engineering Conf.*, Lisbon, Portugal, 1-6 July, pp. 1353–1361.
- [24] Kim, Y.H., Jeong, S.S. and Won, J.O. (2009). Effect of lateral rigidity of offshore piles using proposed p–y curves in marine clay. *Mar. Georesour. Geotechnol.*, Vol. 27, No. 1, pp. 53–77.
- [25] Kim, Y. and Jeong, S. (2011). Analysis of soil resistance on laterally loaded piles based on 3D pile-soil interaction. *Comput. Geotech.*, Vol. 38, pp. 248-257.
- [26] Suleiman, M., Vande Voort, Th. and Sritharan, S. (2010). Behavior of driven ultrahigh-performance concrete H-piles subjected to vertical and lateral loadings. *J. Geotech. Geoenv. Eng.*, ASCE, Vol. 136, No. 10, pp. 1403-1413.
- [27] American Petroleum Institute. (2000). Recommended practice for planning, designing and constructing fixed offshore platforms-working stress design. API recommended practice RP-2A, 21<sup>st</sup> edition, Washington, D.C.

---

# PREISKAVE VPLIVA TOPLOTNO ENERGETSKIH POLJ NA LASTNOSTI ZEMLJIN

---

SRINIVAS KADALI, SUSHA LEKSHMI S.U., SUSMITA SHARMA and D.N. SINGH

---

## o avtorjih

Srinivas Kadali  
Indian Institute of Technology Bombay,  
Department of Civil Engineering,  
Powai, Mumbai-400076, Indija  
E-pošta: srinivasciv@gmail.com

Susha Lekshmi  
Indian Institute of Technology Bombay,  
Department of Civil Engineering,  
Powai, Mumbai-400076, Indija  
E-pošta: sushalekshmi.su@gmail.com

Susmita Sharma  
Indian Institute of Technology Bombay,  
Department of Civil Engineering,  
Powai, Mumbai-400076, Indija  
E-pošta: susmita.sharma4@gmail.com

## vodilni avtor

D.N. Singh  
Indian Institute of Technology Bombay,  
Department of Civil Engineering,  
Powai, Mumbai-400076, Indija  
E-pošta: dns@civil.iitb.ac.in

---

## izvleček

Članek opisuje podrobnosti študije o preiskavah zemljin in njihovih spremembah pri povišanih temperaturah. Do takšnih situacij pride običajno pri načrtovanju temeljev za peči, kotle, naprave za kovanje, opekarne, izstrelitvene ploščadi, pri polaganju podzemnih napajalnih kablov in klimatizacijskih vodov, pri podzemnih eksplozijah, odlaganju visoko radioaktivnih in strupenih industrijskih odpadkov, modifikaciji in stabilizaciji zemljin itd. V takih primerih je pomembno opraviti preiskave za določitev sprememb, ki so jim podvržene zemljine pri izpostavljanju povišanim temperaturam. V preiskavi so bili posamezni vzorci šestih zemljin s popolnoma različnimi lastnostmi izpostavili temperaturi do 300°C (v zaporednih stopnjah po 50°C), po vsaki končani stopnji termične obdelave pa so bile določene njihove fizikalne, kemične in mineraloške lastnosti. Na osnovi kritične sinteze rezultatov je pojasnjeno, da povišane temperature povzročijo (i) spremembo barve, (ii) povečanje specifične teže, velikosti delcev in izgubo teže, (iii) zmanjšanje specifične površine, sposobnosti kationske izmenjave in zeta potenciala in (iv) strukturne spremembe zemljin. Čeprav bi te spremembe močno vplivale na inženirske lastnosti zemljin, je obseg tega članka omejen zgolj na prikaz fizikalnih, kemičnih in mineraloških sprememb zemljin, ki se pojavijo pri izpostavljanju zemljin povišanim temperaturam.

---

## ključne besede

povišane temperature, zemljine, določanje lastnosti, fizikalne lastnosti, kemične lastnosti, mineraloške lastnosti

---

# INVESTIGATIONS TO ESTABLISH THE INFLUENCE OF THE THERMAL ENERGY FIELD ON SOIL PROPERTIES

---

SRINIVAS KADALI, SUSHA LEKSHMI S.U., SUSMITA SHARMA and D.N. SINGH

## about the authors

Srinivas Kadali  
Indian Institute of Technology Bombay,  
Department of Civil Engineering,  
Powai, Mumbai-400076, India  
E-mail: srinivasciv@gmail.com

Susha Lekshmi S.U.  
Indian Institute of Technology Bombay,  
Department of Civil Engineering,  
Powai, Mumbai-400076, India  
E-mail: sushalekshmi.su@gmail.com

Susmita Sharma  
Indian Institute of Technology Bombay,  
Department of Civil Engineering,  
Powai, Mumbai-400076, India  
E-mail: susmita.sharma4@gmail.com

## corresponding author

D.N. Singh  
Indian Institute of Technology Bombay,  
Department of Civil Engineering,  
Powai, Mumbai-400076, India  
E-mail: dns@civil.iitb.ac.in

## abstract

*This paper describes details of a study to investigate and demonstrate the changes undergone by soil when it is exposed to elevated temperatures. Such situations are commonly encountered while designing the foundations for the furnaces, boiler units, forging units, brick kilns, rocket launching pads, buried power-supply cables, air-conditioning ducts, underground explosions, disposal of high-level radioactive and industrial toxic wastes, ground modifications or soil-stabilization techniques, etc. As such, investigations to establish changes undergone by the soil when it is exposed to elevated temperatures assume some importance. With this in view, individual samples of six soils, with entirely different characteristics, were subjected to temperatures up to 300°C (sequentially in steps of 50°C) and after each step of thermal treatment, these samples were characterized for their physical, chemical and mineralogical properties. Based on a critical synthesis of the*

*results, it has been demonstrated that elevated temperatures cause (i) a change in the color, (ii) an increase in the specific gravity, particle size and weight loss, (iii) a reduction in the specific surface area, cation-exchange capacity and zeta-potential, and (iv) a structural transformation of the soil. Though these changes would affect the engineering properties of the soil to a large extent, the scope of this paper is limited to demonstrating the alterations in physical, chemical and mineralogical changes, only, occurring in the soil when it is exposed to elevated temperatures.*

## keywords

elevated temperatures, soil, characterization, physical characteristics, chemical characteristics, mineralogical characteristics

## NOMENCLATURE

CEC = cation-exchange capacity  
DTA = differential thermal analysis  
EC = electrical conductivity  
EGME = ethylene glycol monoethyl ether  
FTIR = Fourier transform infrared  
FWHM = full wave half maximum  
LSD = laser scanning diffraction  
L/S = liquid-to-solid ratio  
LL = liquid limit  
OM = organic matter  
PI = plasticity index  
PL = plastic limit  
PLE = percentage linear expansion  
SL = shrinkage limit  
SSA = specific surface area  
TCD = thermal conductivity detector  
TDS = total dissolved solids  
TGA = thermo gravimetric analysis  
USCS = unified soil-classification system  
XRD = X-ray diffraction

$XRF$	= X-ray fluorescence
$d$	= lattice spacing
$G$	= specific gravity
$U$	= electrophoretic mobility
$V$	= average linear velocity
$W_a$	= weight of <i>EGME</i> absorbed on the soil
$W_s$	= weight of the dry soil
$\lambda$	= wavelength
$\xi$	= zeta-potential
$\eta$	= viscosity
$\phi$	= angle of incidence of the X-rays
$\theta$	= exposure temperature
$\theta_c$	= deviation in temperature with respect to the reference material (i.e., alumina)

---

## INTRODUCTION

The scenario where soil comes into contact with elevated temperatures (i.e., the thermal energy field) is frequently encountered in various civil-engineering activities.

Some of these situations are the design and execution of the foundations for furnaces [1], boiler units, forging units, brick kilns, rocket launching pads, buried power-supply cables and air-conditioning ducts [2], events like volcanic eruptions and activities such as underground explosions, disposal of high-level radioactive [3] and industrial toxic wastes [4], and ground modification or stabilization techniques with the application of chemicals and thermal energy [5-10]. Hence, understanding the influence of elevated temperatures on soil properties becomes necessary. In this context, a brief account of the studies related to this concept, conducted by earlier researchers, is reported in the following.

Farag [4] has reported the use of incineration as a method to treat soil contaminated with the leakage from waste-disposal facilities. Varlakov et al. [3] introduced a heat treatment (between 800 and 1000°C) as an effective solution to decontaminate soils from radioactive and toxic substances. Alcocer and Chowdhury [6] also employed a thermal treatment as a remedy for soils contaminated with crude oil. Earlier researchers [5, 7-9] studied the effect of a heat treatment (300 to 700°C) on clayey bricks. Based on these studies it is clear that the heat treatment of clayey soils (up to 700°C) leads to physical, chemical and microstructural changes, and hence a reduction in their cation-exchange capacity and compressibility. Furthermore, Litvinov [11] and Mitchell [12] have reported that the heat treatment of clayey soils changes their angle of internal friction, cohesion and hence their strength is altered. Also, it has been demon-

strated that when soils are exposed to high temperatures, they tend to degrade due to the removal of a significant amount of organic matter [13-16], changes in their specific gravity [17], a reduction in the specific surface area, *SSA*, due to changes in the particle size [18], changes in the consistency limits, an optimum water content and the dry density of the soil [19, 20], volume change characteristics, i.e., shrinkage [21], a variation in the chemical characteristics (viz., cation-exchange capacity, *CEC*, pH and electrical conductivity, *EC*) [22], a deterioration of the structure and porosity, and a considerable loss of nutrients through the volatilization and alteration of soil minerals [23-25]. Though these studies demonstrate that the exposure of soil to elevated temperatures influences its engineering properties (viz., shear strength, compressibility and hydraulic conductivity etc.) to a great extent [26-28], they are (mostly) soil specific and lack a proper explanation regarding the basic mechanism responsible for the alteration of the soil properties when exposed to elevated temperatures.

As such, with an intention to investigate the changes undergone by soils under these circumstances, individual samples of six soils, of entirely different characteristics, were subjected to temperatures up to 300°C, (this being the maximum temperature associated with nuclear wastes [29-30]), sequentially in steps of 50°C. After each step of thermal treatment, these samples were characterized for their physical (viz., appearance, *SSA*, particle size and specific gravity, *G*); chemical (viz., *CEC*, zeta-potential,  $\xi$ ) and mineralogical properties, as described in this paper. Based on a critical synthesis of the results, it has been clearly demonstrated that these properties of the soils are altered when they are exposed to elevated temperatures. Incidentally, as mentioned above, these properties in turn are responsible for controlling the engineering behavior of the soil (viz., shear strength, compressibility, hydraulic conductivity, thermal and chemical stabilization, etc.), to a large extent. However, the scope of this paper is limited to establishing the changes occurring in the soil properties due to their exposure to elevated temperatures, only.

---

## 2 EXPERIMENTAL INVESTIGATIONS

Two commercially available soils: bentonite and white clay, designated as BT and WC, respectively, from the mines of Gujarat, Western India, were used in this study. In addition, four naturally occurring soils, sampled from a depth of 1 m, from (a) Surat, Gujarat, India, (b) and (c) marine clay from the coast of Mumbai, India, and (d) desert sand from Rajasthan, India, designated as S1, S2, S3 and S4, respectively, were selected for this study. These

six soils in their natural state, and after exposing them to elevated temperatures, were characterized to establish their physical, chemical, mineralogical and thermal properties, details of which are presented in the following.

### 3 PHYSICAL CHARACTERIZATION

#### 3.1 SPECIFIC GRAVITY

The specific gravity,  $G$ , of the soil sample was determined with the help of an ULTRA-PYCNOMETER (Quanta-chrome, USA), available in the Environmental Geotechnology Laboratory, Department of Civil Engineering, IIT Bombay, India, which employs helium gas as the displacing fluid, as per the guidelines provided by the ASTM [31]. The average of two values of the specific gravity, which match with each other quite closely out of three trials, are reported in Table 1.

#### 3.2 GRADATIONAL AND CONSISTENCY CHARACTERISTICS

The particle-size distribution of the soil samples (except for soil S4) was determined by employing a hydrometer, as per the guidelines provided by ASTM [32]. In addition, a Laser Scanning Diffraction, *LSD*, particle size analyzer (Beckman Coulter's, LS 13 320, USA), available in the Department of Metallurgical Engineering and Materials Science, IIT Bombay, India, which works on the Polarization Intensity Differential Scattering technique and is capable of covering a particle size range of 0.4 to 2000  $\mu\text{m}$ , was employed for the particle size analy-

sis of the soil samples. Though the amount of sample required for the *LSD* is much less ( $=1$  g), compared to that required for the hydrometer test ( $=50$  g), this methodology has been widely employed for establishing the particle-size distribution characteristics of even coarse-grained soils in an extremely short time [33-34]. In this context, earlier researchers have discussed the limitations associated with the hydrometer analysis for establishing the particle-size distribution characteristics of soils with colloids, organic matter, highly dispersive soil and reactive cement admixtures [35-38]. Earlier researchers [36] have successfully established a comparison of the particle-size distribution characteristics of 'quartz glass beads', obtained from the *LSD* and sieve analysis and an excellent matching between the results has been reported. Hence, *LSD* becomes an obvious choice over the hydrometer analysis.

In order to obtain precise results, and to overcome the limitations associated with an extremely small amount of the soil used for the *LSD*, three trials were conducted and the average of the results was considered as the representative value. However, since each technique involves different assumptions, and defines the size of the particles in a different way, the results (i.e., the percentage finer) would depend on the methodology adopted. The particle size distribution characteristics for various soils are presented in Table 1 and it is clear that there is a good agreement between the results obtained using the two methods for most of the soils considered in the study. The consistency limits (Atterberg limits) of the samples were determined in accordance with the guidelines provided by ASTM [39-40]. Consequently, the soil samples were classified based on the Unified Soil Classification System,

Table 1. Physical characteristics of the investigated soils.

Soil	$G$	SSA ( $\text{m}^2/\text{g}$ )	Size fraction (%)			Atterberg limits (%)				USCS
			Clay	Silt	Sand	$LL$	$PL$	$PI$	$SL$	
BT	2.73	629	82	18	-	305	140	165	30	CH
			78	22	0					
WC	2.63	35	54	46	-	54	27	27	17	CH
			59	41	0					
S1	2.63	214	39	61	-	47	21	26	9	CL
			42	36	22					
S2	2.72	135	65	35	-	72	30	42	15	CH
			53	47	0					
S3	2.69	91	55	45	-	45	23	22	8	CL
			41	59	-					
S4	2.65	7	-	2	98	Not applicable				SP

Note: CH: clay of high plasticity; CL: clay of low plasticity; SP: poorly graded sand numerals in italics are hydrometer results

USCS [41]. The test results are presented in Table 1, from which it can be noticed that the soils considered in this study have entirely different characteristics.

### 3.3 SPECIFIC SURFACE AREA

The Specific Surface Area, SSA, of the soil samples was determined by using the Ethylene Glycol Monoethyl Ether, EGME, method, which has been shown to be the most appropriate method for determining the SSA of soils [42-44]. The set-up available in the Environmental Geotechnology Laboratory, Department of Civil Engineering, IIT Bombay, India, was employed for this purpose. A total of 2 g of air-dried soil sample was spread uniformly on the bottom of a glass petri dish, which is 40 mm in internal diameter, 2 mm thick and 20 mm high, and covered with a perforated watch-glass. Six such dishes, with a sample in them, were placed in a vacuum desiccator that contained 250 g of P<sub>2</sub>O<sub>5</sub> and helped to maintain a constant vapor pressure. The sample was evacuated by applying vacuum (0.03 mbar) for 2 h, weighed and replaced in the desiccator. This process was repeated several times and stopped when three consecutive weights were found to be almost same. Later, 6 ml of analytical grade EGME solution was added to the sample and the mixture was swirled, gently, until it became a slurry. This slurry was then placed in the desiccator over a desiccant (mixture of 100 g CaCl<sub>2</sub> and 20 ml EGME) for 12 h, which helped in maintaining constant conditions that are just sufficient to form a monolayer. The initial weight of the slurry along with the glass dish was measured using a precision balance and the dish was replaced in the desiccator for evacuation. The glass dish was taken out of the desiccator, weighed and re-placed in it several times, until it attained a constant weight. The amount of EGME ( $W_a$ , in g) that was absorbed per gram of the sample ( $W_s$ , in g), corresponding to this constant weight condition, was computed by subtracting the dry weight of the sample from the weight of the EGME mixed sample. Subsequently, by employing Eq. 1, the SSA of the sample was determined [42-44] and the results are presented in Table 1.

$$SSA = W_a \cdot (0.000286 \cdot W_s)^{-1} \quad (1)$$

## 4 CHEMICAL CHARACTERIZATION

### 4.1 CHEMICAL COMPOSITION

The chemical composition of the soil samples, in the form of major oxides, was determined using an X-Ray Fluorescence set-up, XRF (Phillips 1410, Netherlands), available at the Sophisticated Analytical and Instrumentation Facility, SAIIF, IIT Bombay, India. A finely powdered soil sample weighing 4 g and 1 g of microcrystalline cellulose were mixed thoroughly with 2 ml of isopropyl alcohol and the mixture was kept below an infrared lamp for slow drying until it became a powder. Subsequently, this powder was poured into an aluminum dish (with an inner diameter of 33 mm and a height of 12 mm) containing methyl-cellulose powder (supplied by Merck Chemicals, India) up to about 70 % of the volume of the dish. To make a pellet, the dish was compressed with the help of a hydraulic jack by applying a load of 15 tonnes. The physical calibration of the XRF set-up, which is conducted to eliminate the error resulting from an uneven and slanting base line, was made using a standard reference material (SRM) supplied by UGCS, USA. While the chemical calibration of the instrument was performed using an international standard reference material, [Fly ash (2689, 2690, 2691), cements (354, 372, 372/1) and soils (SO-2,SO-3,SO-4)], procured from NIST, USA. The chemical composition of the sample was determined by mounting the pellet in the sample holder of the XRF set-up and the results are presented in Table 2.

### 4.2 CATION-EXCHANGE CAPACITY

The cation-exchange capacity, CEC, is the property of the soil by which certain cations adsorbed on the soil particles get replaced by other cations [45-48]. The capacity of a soil to hold cations mainly depends on the

Table 2. Chemical composition (% by weight) of the investigated soils.

Soil	SiO <sub>2</sub>	Al <sub>2</sub> O <sub>3</sub>	Fe <sub>2</sub> O <sub>3</sub>	CaO	K <sub>2</sub> O	Na <sub>2</sub> O	TiO <sub>2</sub>	MgO	P <sub>2</sub> O <sub>5</sub>
BT	42.06	18.90	31.17	1.11	0.35	3.55	1.36	0.96	0.11
WC	37.94	52.84	2.52	1.59	1.84	0.19	2.69	0.20	0.03
S1	37.98	30.70	14.96	8.92	0.91	1.65	2.26	2.16	0.11
S2	42.22	18.53	16.13	11.47	3.73	4.19	1.45	1.73	0.27
S3	39.92	27.81	8.55	11.39	3.51	5.36	0.76	2.27	0.23
S4	66.00	16.99	11.59	0.04	4.39	0.12	0.36	0.22	0.13



pH and the ionic strength of the soil-fluid system. The guidelines presented in the literature [47] were followed to determine the *CEC* of the soil samples used in this study by employing the test set-up available in the Environmental Geotechnology Laboratory, Department of Civil Engineering, IIT Bombay, India.

The soil weighing 1 g was transferred to a 1-ml round-bottom and narrow-neck centrifuge tube and 9 ml of 1N  $\text{CH}_3\text{COONa}$  was added to it. This mixture was shaken on a mechanical shaker for 5 min and later centrifuged until the supernatant was clear. The supernatant was decanted and this process was repeated three times on the residues. Subsequently, 9 ml of 99% isopropyl alcohol was added to the residues and shaking on a mechanical shaker, for 5 min, was performed. This mixture was centrifuged until the supernatant became clear and this procedure was repeated two more times. In addition, 9 ml of  $\text{CH}_3\text{COONH}_4$  was added to the residues and this mixture was shaken in a mechanical shaker for 5 min. This mixture was centrifuged until the supernatant became clear. Following this, the supernatant was decanted into a 100-ml flask and the procedure with the  $\text{CH}_3\text{COONH}_4$  was repeated twice. Finally, the combined supernatant was diluted and brought to 100 ml volume by adding  $\text{CH}_3\text{COONH}_4$ . The  $\text{Na}^+$  concentration was obtained by employing Inductively Coupled Plasma-Atomic Emission Spectrometry (ARCOS, M/s. SPECTRO, Germany). The *CEC* of the sample was computed by employing Eq. 2 and the results are presented in Table 3.

$$CEC = \frac{\text{Concentration of Na} \left( \frac{\mu\text{g}}{\text{ml}} \right) \times 100 \times \text{Vol. of extract (ml)}}{\text{The molar weight of Na} \times 1000 \times \text{wt. of sample (g)}} \quad (2)$$

**Table 3.** Chemical characteristics of the investigated soils.

Soil	pH	EC ( $\mu\text{S/cm}$ )	TDS (ppm)	$\xi$ (mV)	CEC (meq./100g)
BT	7.78	176.4	88	36.4	108.33
WC	7.63	94	47.1	17.5	14.77
S1	7.86	145	72.5	27.6	45.54
S2	7.82	520	260.8	30.6	30.77
S3	7.61	730	364.2	27.6	26.90
S4	7.89	205	101	14.5	3.46

### 4.3 ZETA POTENTIAL

In order to investigate the influence of pore fluid on the particle-to-particle interaction within the soil mass, a determination of the change in the surface-charge

potential of the particles, which is indirectly defined as the zeta potential,  $\xi$ , is quite useful [49-52]. Hence, the  $\xi$  for the soil samples used in this study was determined by employing an automated electrophoresis instrument (Zetasizer-Nano series, Malvern instruments, United Kingdom), available at the Sophisticated Analytical and Instrumentation Facility, SAIF, IIT Bombay, India. This instrument works on the light-scattering technique, which determines the electrophoretic mobility,  $U$ , which is the velocity of a particle in the solution produced by an external electric field of a certain strength. This  $U$  can be used to compute  $\xi$  by employing Helmholtz-Smoluchowski theory, which in the mathematical form can be represented by Eq. 3 [53].

$$\xi = \frac{4\pi\eta U}{\varepsilon} \quad (3)$$

where  $\eta$  is the viscosity of the soil solution (Pa·s),  $\varepsilon$  is the dielectric constant of the soil solution and  $U$  is the electrophoretic mobility [ $\mu\text{m}\cdot\text{cm} / (\text{V}\cdot\text{s})$ ].

Measurements were conducted on 2 ml of soil suspension, by maintaining a liquid-to-solid ratio,  $L/S$ , equal to 100 (corresponding to 25°C), by following the guidelines provided by Kaya et al. [53]. Furthermore, the pH, Electrical Conductivity, *EC*, and Total Dissolved Solids, *TDS*, of the soil were measured by employing a water-quality analyzer (Model PE 136, Elico Ltd., India), available in the Environmental Geotechnology Laboratory, Department of Civil Engineering, IIT Bombay, India, and the results are presented in Table 3.

### 4.4 ORGANIC CONTENT ANALYSIS

The presence of the organic matter, *OM* (in percentage by weight), in the soil samples was determined by using a Carbon, Hydrogen, Nitrogen and Sulphur analyzer (CHNS analyzer, make FLASH EA 1112 series, Thermo Finnigan, Italy), available at the Sophisticated Analytical and Instrumentation Facility, SAIF, IIT Bombay, India. This instrument works on the principle of the "Dumas method", which involves complete and instantaneous oxidation of the sample (4-5 mg weight) by employing "flash combustion" at 900°C. The combustion products ( $\text{CO}_2$ ,  $\text{H}_2\text{O}$ ,  $\text{NO}_2$  and  $\text{SO}_2$ ) were separated by a chromatographic column and detected with the help of a thermal conductivity detector, *TCD*. The *TCD* yields an output signal that is proportional to the concentration of the individual components of the soil mixture. This instrument, which finds its role in determining C, H, N and S in organic compounds, was calibrated by analyzing compounds with K-factors calculations, as suggested by the manufacturer. By using this instrument, the

elements belonging to the CHNS/O group and present in the soils can be detected simultaneously. The value of the *OM* for different soils is listed in Table 4.

**Table 4.** The organic matter (% by weight) in the investigated soils.

Soil	C	H	N	S	Total
WC	0.552	1.144	0.033	NIL	1.729
BT	0.158	1.5	0.064	NIL	1.722
S1	1.393	0.704	0.015	NIL	2.111
S2	2.085	0.47	0.077	NIL	2.632
S3	2.146	0.38	0.029	NIL	2.555
S4	0.958	0.091	0.003	NIL	1.051

#### 4.5 FOURIER TRANSFORM INFRARED SPECTROMETER (FTIR) STUDIES

FTIR studies are found to be quite useful for the identification of the chemical bonds (functional groups) present in the soil, which are representative of the soil contamination [54-55]. Spectrographs of the soils were captured by employing a Fourier Transform Infrared Spectrometer (Nicolet Instruments Corporation, USA; Model: MAGNA 550; Range  $4000\text{ cm}^{-1}$  to  $500\text{ cm}^{-1}$ ), available at the Sophisticated Analytical and Instrumentation Facility, SAIF, IIT Bombay, India. A small quantity of the soil in powder form (weighing 2 mg) was mixed uniformly with KBr and pelletized into a transparent disk by applying a 3 T loading. The pellet was irradiated with the IR beam for the complete range of the wave numbers, mentioned above, and the intensity of the IR radiation that was absorbed and/or transmitted was recorded. Though the amount of sample used for this analysis is limited, the application of FTIR studies for detecting the presence of chemical bonds in the soil samples is well established [54-55].

### 5 MINERALOGICAL CHARACTERIZATION

The mineralogical composition of the soils was determined with the help of an X-ray diffraction spectrometer (Phillips, Eindhoven, Netherlands), available in the Department of Metallurgical Engineering and Materials Science, IIT Bombay, India, which is fitted with a graphite monochromator and employs Cu-K $\alpha$  as the source. The minerals present in the soil sample were identified with the help of the Joint Committee on Powder Diffraction Standards, JCPDS [56] search files, from the diffractograms, and are listed in Table 5. It is clear from the table that the soil samples consist of a wide range of minerals, except for Soils S2 and S3. It is worth mentioning here

**Table 5.** Mineralogical composition of the investigated soils.

Soil	Minerals
BT	Montmorillonite, Muscovite
WC	Kaolinite, Illite
S1	Montmorillonite, Quartz, Calcite
S2, S3	Montmorillonite, Calcite, Muscovite, Quartz
S4	Quartz

that quantification (i.e., the percentage by weight) of various minerals present in the soils can be made using the appropriate software (i.e., Reitveld) [57-58]. However, due to non-availability of such software, the quantification of the amount of various minerals present in the soils used in the present study could not be conducted.

## 6 THERMAL CHARACTERIZATION

### 6.1 LINEAR EXPANSION

The percentage linear expansion, *PLE*, of the soil samples due to heating was determined by employing a dilatometer (Orton, DIL2016 STD, USA) available in the Department of Metallurgical Engineering and Materials Science, IIT Bombay, India. The sample of 12 mm in diameter and 14 mm in length was prepared by pressurizing the finely powdered, air-dried (viz., the ambience being  $27\pm 1^\circ\text{C}$  and  $60\pm 2\%$  relative humidity) soil sample in a mold and by applying a load of 3 tonnes, which helps in binding the soil grains. Subsequently, this sample was placed in the dilatometer and a deformation measuring device was attached to it. Furthermore, the sample was heated up to  $600^\circ\text{C}$ , at a constant rate of  $10^\circ\text{C}/\text{min.}$ , and the *PLE* was data-logged with respect to the temperature,  $\theta$ , and results are shown in Fig. 1.

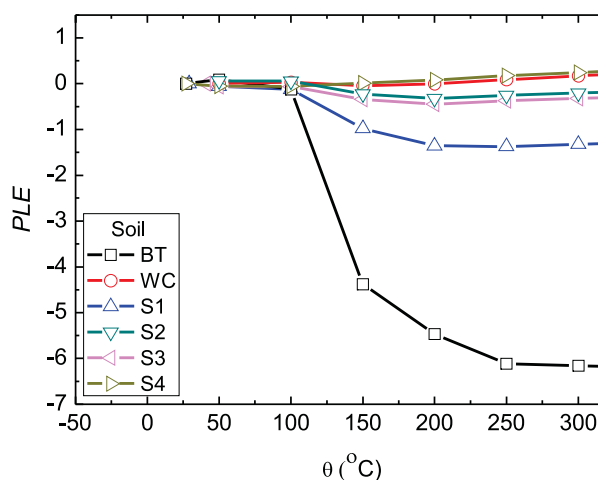


**Figure 1.** Variation of *PLE* with temperature.

## 6.2 THERMO GRAVIMETRIC ANALYSIS (TGA)

Thermo gravimetric analyses of the soil samples were conducted with the help of a thermo gravimetric analyzer (Model Diamond TG/DTA, Perkin Elmer, USA), available at the Sophisticated Analytical and Instrumentation Facility, SAIF, IIT Bombay, India, to determine their response (i.e., the percentage weight loss with respect to the original weight, 20 mg) when exposed to elevated temperatures up to 300°C, by maintaining a rate of heating of 10°C per minute. During the analysis, a controlled environment (i.e., an inert gas, N<sub>2</sub>, flowing at a rate of 600 ml/min, under vacuum 10<sup>-2</sup> Torr) was maintained for monitoring the thermal stability of the sample. It should be noted that this analysis permits the simultaneous quantification of the bound water, biodegradable and humic components in one simple analytical process in the temperature ranges 25 to 190°C, 190 to 450°C and 450 to 650°C, respectively.

## 6.3 DIFFERENTIAL THERMAL ANALYSIS (DTA)

Differential thermal analyses of the soil samples were conducted, maintaining the same conditions as mentioned for the TGA analysis, with the help of a differential thermal analyzer (Model Diamond TG/DTA, Perkin Elmer, USA), available at the Sophisticated Analytical and Instrumentation Facility, SAIF, IIT Bombay, India. This analysis helps in estimating the endothermic or exothermic behaviors of the sample by recording the difference in the temperatures between the sample (weighing 20 mg) and a reference material (viz., Alumina) heated up to 300°C by maintaining the rate of heating as 10°C/min with the help of a set of thermocouples [59-60].

# 7 RESULTS AND DISCUSSION

## 7.1 PHYSICAL APPEARANCE

Figure 2 shows the changes in the physical appearance of the soil samples when exposed to elevated temperatures. It can be seen from the figure that up to  $\theta \leq 250^\circ\text{C}$  there is no appreciable change in the color of the soil sample. However, for  $\theta > 250^\circ\text{C}$  and except for the Soil WC (white colored), the color of the samples changes from brown/grey to brownish/reddish, which can be attributed to increased oxidation and other chemical changes (i.e., shifting of the absorption bands and the disappearance of the absorption features observed in the FTIR spectra, as defined in the following). Kampf et al. [61] and Schwertmann [62] observed a link between the increased

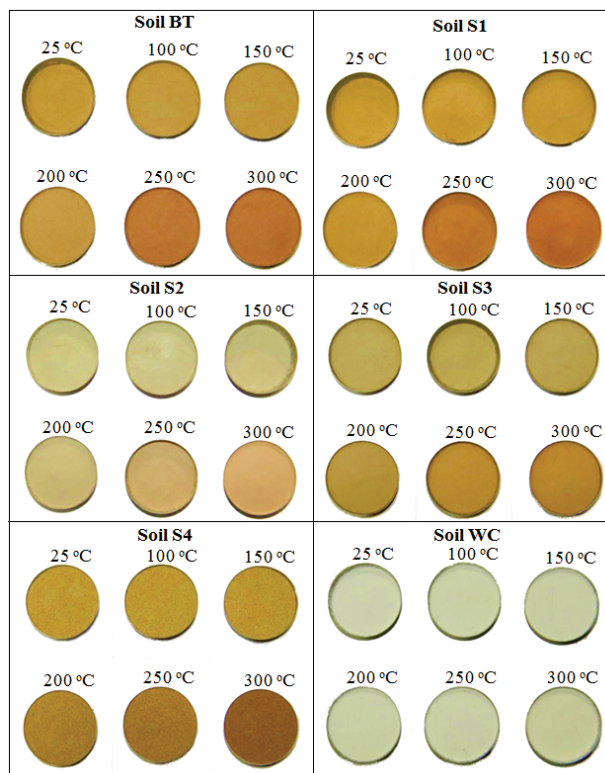


Figure 2. Changes in the color of investigated soils due to heating.

redness and the transformation of iron oxides due to the exposure of the soil to elevated temperatures. In this context, some other researchers [14, 63] suggested that even dark-grey color soils (viz., Soil S2) containing limited organic matter, ferrous and manganese compounds, elemental carbon and hematite would also exhibit a change in the color due to their exposure to elevated temperatures. In contrast, Soil WC, due to the presence of a substantial amount of Al<sub>2</sub>O<sub>3</sub> ( $\approx 52.3\%$ , refer Table 2), does not exhibit any change in color on exposure to elevated temperatures.

## 7.2 SPECIFIC GRAVITY

Figure 3 shows the change in the specific gravity,  $G$ , of different soil samples with respect to the exposure temperature. It is evident from the plot that an increase in  $G$  due to heating is much more for Soils BT, S2 and S3 than for their counterparts (i.e., Soils WC, S1 and S4). The change in  $G$  can be attributed to the shrinkage undergone by the soil particles, due to the complete removal of the absorbed water, as depicted in Fig. 1. At higher temperatures the finer particles tend to agglomerate, which also leads to a change in the  $G$  value. However, the exposure of the soil to elevated temperatures is responsible for a decrease in the clay-sized and

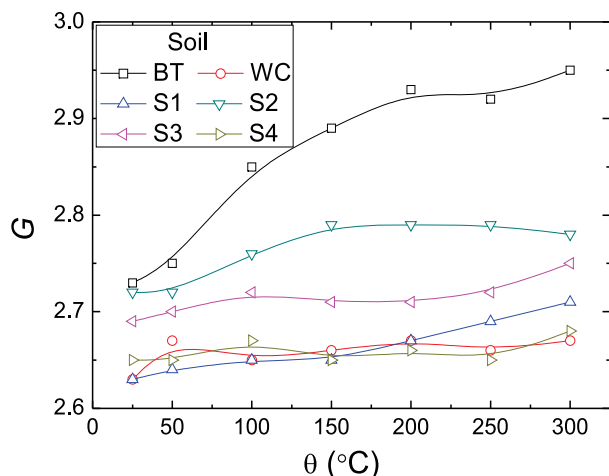


Figure 3. Variation of Specific Gravity of investigated soils with temperature.

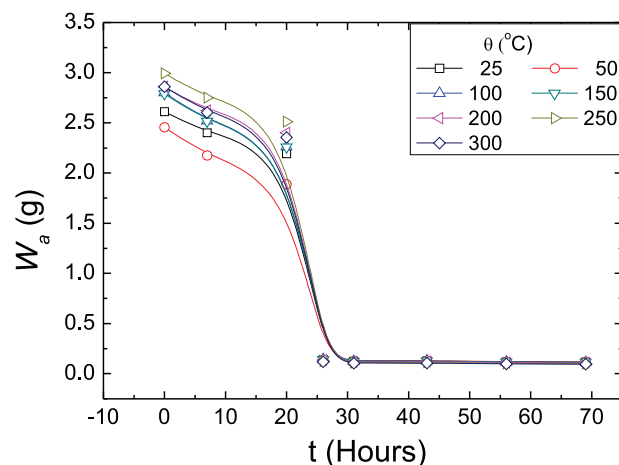


Figure 4. Variation of  $W_a$  with time for Soil S1.

the silt-sized fractions of the soils, except for the Soil S4, which mainly consists of quartz, a mineral insensitive to temperature variations considered in this study. This observation is consistent with the findings reported by Yilmaz [17], which reveal that for  $\theta \geq 100^\circ\text{C}$ , some soils exhibit tremendous changes in the specific gravity, which could be attributed to a loss of moisture, organics, impurities and changes occurring at the elemental level. Incidentally, in contrast to these findings, other researchers [20] have reported a decrease in the specific gravity with an increase in the temperature for highly plastic clays from Turkey.

### 7.3 SPECIFIC SURFACE AREA

Following the methodology for determining the SSA, mentioned earlier, the weight of the *EGME* retained on the soil particles,  $W_a$ , (used for a calculation of the SSA of a soil sample by employing Eq. 1) was recorded with respect to time for all the soils considered in this study. However, for the sake of brevity, the response of Soil S1 is presented in Fig. 4. Following this methodology, the SSA of different soils, treated at temperatures ranging from 25 to  $300^\circ\text{C}$ , was determined and the results are listed in Table 6. The data presented in the table reveals a decrease in the SSA of the soil sample with an increase in the temperature, which is prominent for the Soils WC and S4, as compared to their counterparts (i.e., Soils BT, S1, S2 and S3). This, in general, can be attributed to the depletion of organic matter from the soil due to its exposure to elevated temperatures. Such changes in the SSA can be further substantiated by changes occurring in the particle size of the soils, due to elevated temperatures, as described below.

Table 6. SSA (in  $\text{m}^2/\text{g}$ ) of investigated soils at elevated temperature.

$\theta$ ( $^\circ\text{C}$ )	Soil					
	BT	WC	S1	S2	S3	S4
25	629	35	214	135	91	7
50	623	32	209	135	87	6
	<i>0.95</i>	<i>8.57</i>	<i>2.34</i>	<i>0</i>	<i>4.40</i>	<i>14.29</i>
100	585	31	210	126	88	5
	<i>7.00</i>	<i>11.43</i>	<i>1.87</i>	<i>6.67</i>	<i>3.30</i>	<i>28.57</i>
150	579	25	202	128	81	5
	<i>7.95</i>	<i>28.57</i>	<i>5.61</i>	<i>5.19</i>	<i>10.99</i>	<i>28.57</i>
200	576	24	193	121	78	4
	<i>8.43</i>	<i>31.43</i>	<i>9.81</i>	<i>10.37</i>	<i>14.29</i>	<i>42.86</i>
250	577	19	180	118	75	4
	<i>8.27</i>	<i>45.71</i>	<i>15.89</i>	<i>12.59</i>	<i>17.58</i>	<i>42.86</i>
300	572	12	170	92	72	4
	<i>9.06</i>	<i>65.71</i>	<i>20.56</i>	<i>31.85</i>	<i>20.88</i>	<i>42.86</i>

Note: Numerals in italics represent the % change with respect to the value at  $25^\circ\text{C}$

### 7.4 PARTICLE SIZE ANALYSIS

The results of the particle size analysis, obtained by resorting to *LSD*, on the soil samples exposed to different temperatures, are shown in Fig. 5. From the trends in the figure, it is clear that all the soils, except for Soil S4, exhibit a change in the particle diameter (i.e., there is a scatter around the dotted line, which represents the soil at normal temperature) with an increase in the exposure temperature. In general, it has been noted that at higher temperatures (particularly

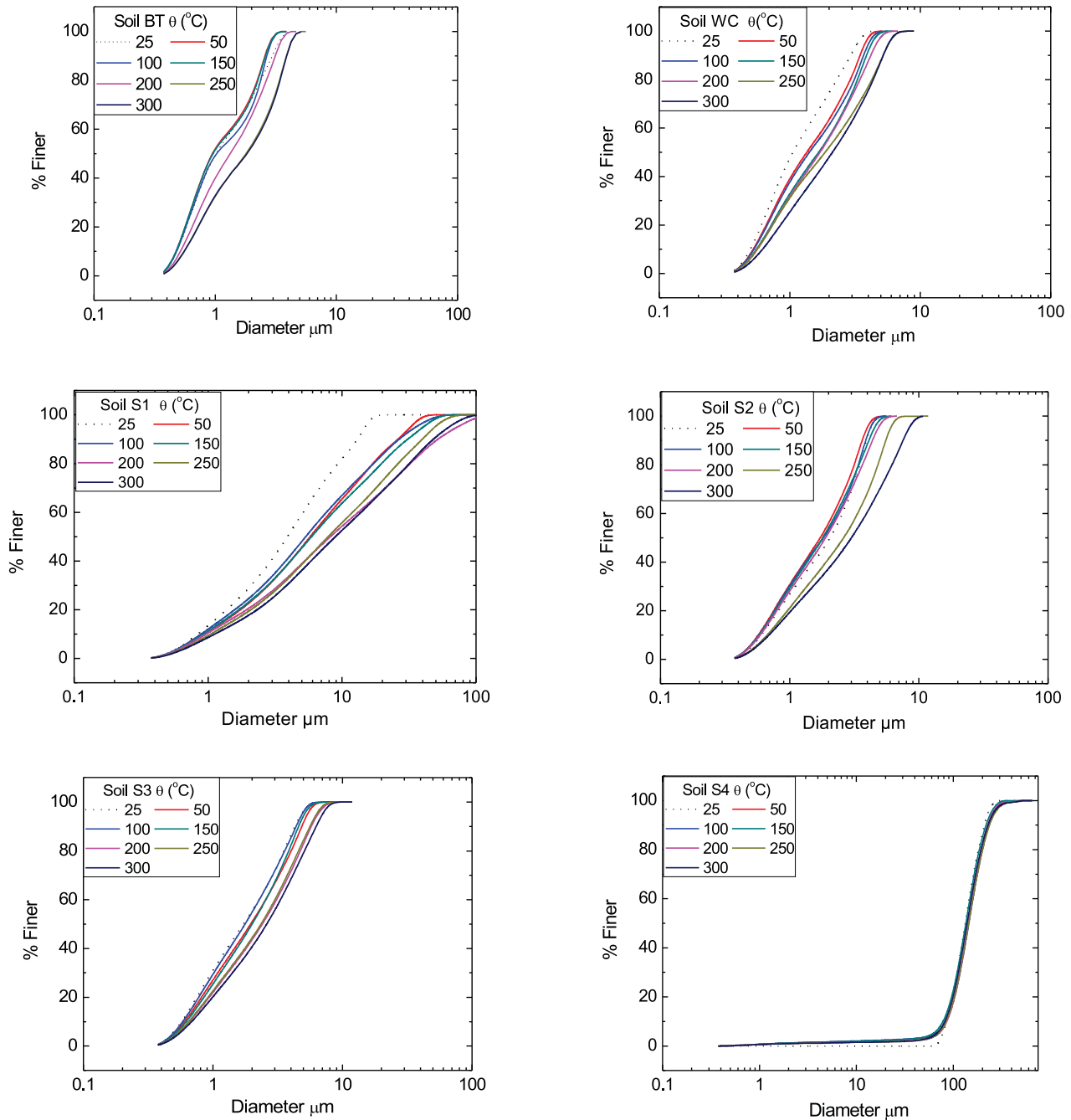


Figure 5. Variation of the particle size distribution characteristics of the investigated soils (obtained from *LSD*) with temperature.

for  $\theta > 200^{\circ}\text{C}$ ) the tendency of the soil particles is to expand. However, this expansion is observed to be much less for Soil S4 (which is a sandy soil) than for its counterparts.

Based on the *LSD* analysis, the particle sizes of the soils corresponding to the clay-sized ( $< 2 \mu\text{m}$ ) and the silt-sized (2 to 75  $\mu\text{m}$ ) fractions were determined and plotted with respect to the temperature,  $\theta$ , (refer Fig.

6). It is clear from the trends presented in Fig. 6 that, in general, except for Soil S4, the clay-sized fraction decreases while the silt-sized fraction increases with an increase in temperature. This further substantiates the findings, as reported above, that exposure of the soil to elevated temperatures results in an increase in its particle size. However, the Soil S4 with passive minerals (viz., predominance of quartz in Soil S4) was found to be insensitive to temperature variations.

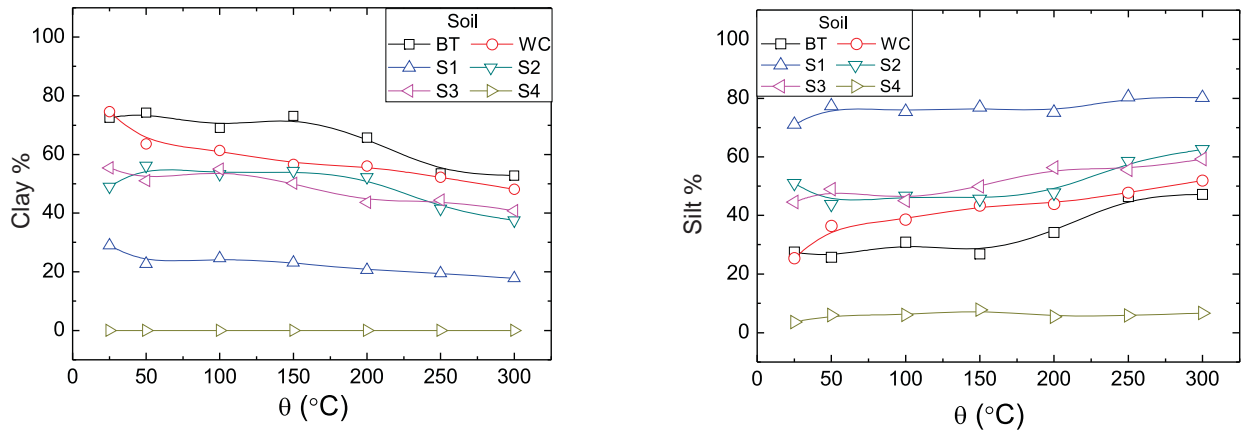


Figure 6. Variation of the percentage clay and silt fractions of the investigated soils with temperature.

## 7.5 CATION-EXCHANGE CAPACITY

The Cation-exchange capacity, *CEC*, of the soil samples is listed in Table 7. The numerals in italics represent the percentage change in the *CEC* with respect to its value at 25°C. It can be seen that the *CEC* of the soil samples decreases as the temperature increases [45-48]. This can be attributed to a reduction in the exchangeable cations and a loss of organic matter present in the soil. A decrease in the *CEC* value of the heated soil sample can also be justified by an increase in the particle size and a decrease in the *SSA* when soil is exposed to high temperatures, as discussed above.

Table 7. *CEC* (in meq./100g) of the investigated soils at elevated temperatures.

$\theta$ (°C)	Soil					
	BT	WC	S1	S2	S3	S4
25	108.33	14.77	45.54	30.77	26.90	3.46
50	105.28	14.35	43.68	30.18	26.35	3.42
	<i>2.82</i>	<i>2.84</i>	<i>4.08</i>	<i>1.92</i>	<i>2.04</i>	<i>1.16</i>
100	104.67	13.97	42.49	29.92	23.70	3.32
	<i>3.38</i>	<i>5.42</i>	<i>6.70</i>	<i>2.76</i>	<i>2.04</i>	<i>4.05</i>
150	101.19	13.81	41.84	29.31	23.03	3.31
	<i>6.59</i>	<i>6.50</i>	<i>8.12</i>	<i>4.74</i>	<i>14.39</i>	<i>4.34</i>
200	96.75	11.55	29.71	29.14	20.28	3.28
	<i>10.69</i>	<i>21.80</i>	<i>34.76</i>	<i>5.30</i>	<i>24.61</i>	<i>5.20</i>
250	95.68	11.11	28.10	28.10	19.74	2.07
	<i>11.68</i>	<i>24.78</i>	<i>38.30</i>	<i>8.68</i>	<i>26.62</i>	<i>40.17</i>
300	95.28	10.97	27.42	28.10	19.68	1.61
	<i>12.05</i>	<i>25.73</i>	<i>39.79</i>	<i>8.68</i>	<i>26.84</i>	<i>53.47</i>

Note: Numerals in italics represent the % change with respect to the value at 25°C

## 7.6 ZETA POTENTIAL

The changes in the zeta-potential,  $\xi$ , with respect to the temperature,  $\theta$ , are presented in Table 8. A decrease in the particle mobility (i.e.,  $\xi$  becomes less negative) was observed when the temperature increases from 25 to 300°C. This is consistent with the observations reported by Chorom and Rengasamy [64]. A reduction in  $\xi$  when the soil is subjected to heating, as depicted in Table 8, can be attributed to the charge reduction caused by the reduction in the *CEC* (see Table 7) and the structural changes in the crystal lattice due to an increase in the *d*-spacing, as explained in the following (section *XRD*

Table 8. Zeta-Potential,  $\xi$ , (- mV) of the investigated soils at elevated temperatures.

$\theta$ (°C)	Soil					
	BT	WC	S1	S2	S3	S4
25	36.4	17.5	27.6	30.6	27.6	14.5
50	33.4	17.5	27.4	30.8	26.4	14.4
	<i>8.24</i>	<i>0</i>	<i>0.72</i>	<i>-0.65</i>	<i>4.35</i>	<i>0.69</i>
100	34.4	16.6	26.6	30.1	26.2	14.3
	<i>5.49</i>	<i>5.14</i>	<i>3.62</i>	<i>1.63</i>	<i>5.07</i>	<i>1.38</i>
150	34.1	15.9	26.2	29.6	25.5	14.3
	<i>6.32</i>	<i>9.14</i>	<i>5.07</i>	<i>3.27</i>	<i>7.61</i>	<i>1.38</i>
200	34.1	14.2	25.9	29.5	25.3	13.8
	<i>6.32</i>	<i>18.86</i>	<i>6.16</i>	<i>3.59</i>	<i>8.33</i>	<i>4.83</i>
250	33.3	12.3	25.7	28.1	24.4	12.7
	<i>8.51</i>	<i>29.71</i>	<i>6.88</i>	<i>8.17</i>	<i>11.59</i>	<i>12.41</i>
300	34.6	11.0	23.9	22.9	22.9	11.4
	<i>4.95</i>	<i>37.14</i>	<i>13.41</i>	<i>25.16</i>	<i>17.03</i>	<i>21.38</i>

Note: Numerals in italics represent the % change with respect to the value at 25°C

analysis), and an expansion of the soil minerals with temperature (refer Fig. 1). Furthermore, the  $\xi$  of the soil can decrease due to a decrease in the various attributes of the soil (viz., electrical conductivity, specific surface area and particle size distribution).

## 7.7 FOURIER TRANSFORM INFRARED SPECTROMETER (FTIR) ANALYSIS

The FTIR spectral characteristics of the soil samples were obtained by plotting the transmittance (in %) with respect to the wave number,  $\text{cm}^{-1}$ , as depicted

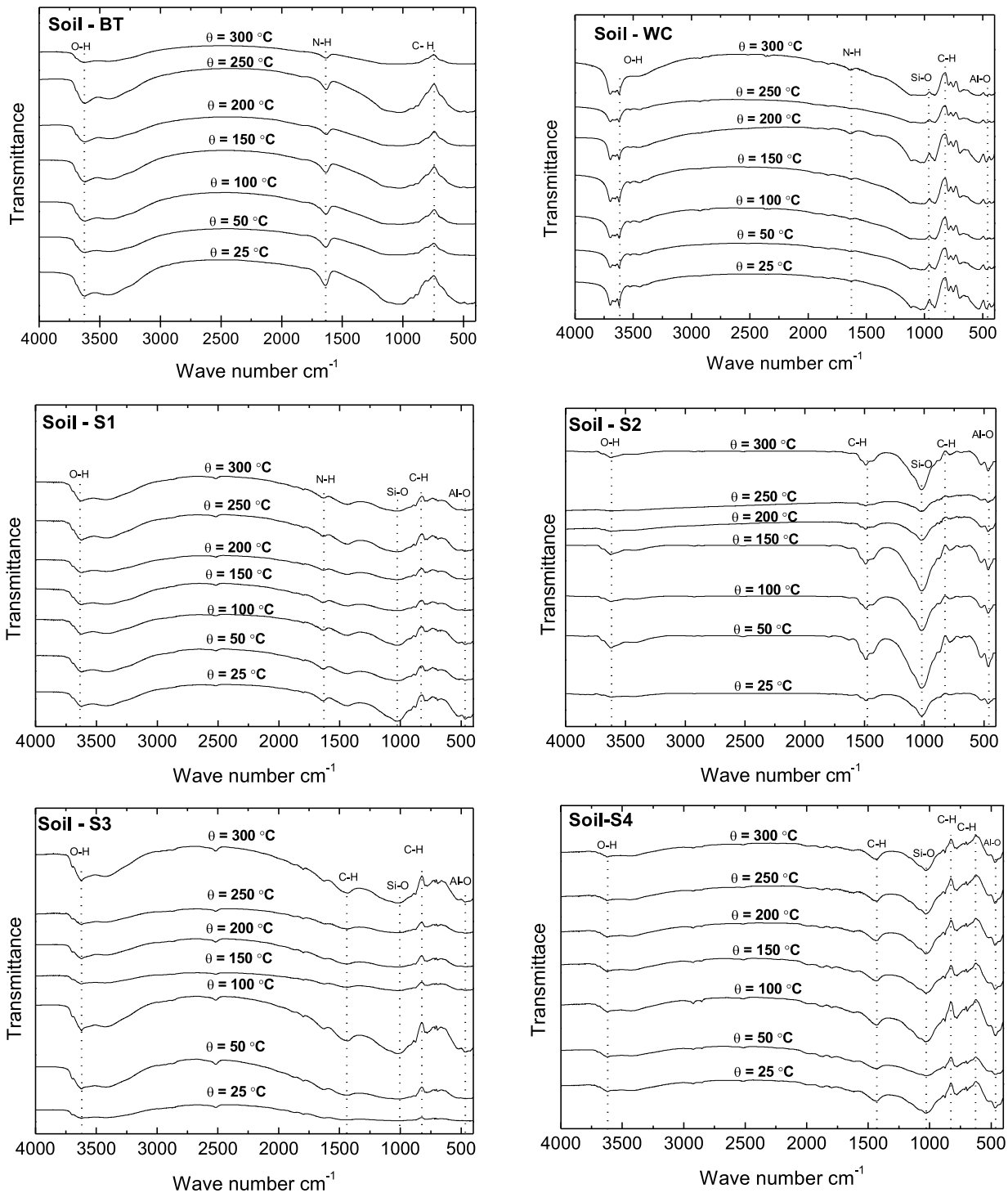


Figure 7. FTIR spectra of soils heated at the investigated temperatures.

in Fig. 7. The resultant trend shows that there is not much variation in the spectral characteristics of the samples due to their exposure to elevated temperatures. Furthermore, this analysis reveals that the O-H bonds (3628, 3615, 3635, 3613, 3631 and 3622  $\text{cm}^{-1}$  for Soils BT, WC, S1, S2, S3 and S4, respectively), the N-H bonds (1636, 1635, 1627, 1030  $\text{cm}^{-1}$  for Soils BT, WC, S1 and S4, respectively), the C-H bonds (740, 831, 825, 833 & 1471, 828 & 1440, 829 & 640  $\text{cm}^{-1}$  for Soils BT, WC, S1, S2, S3 and S4, respectively), and the Si-O and Al-O bonds (1000-1260  $\text{cm}^{-1}$  and 400-1000  $\text{cm}^{-1}$ , for soils WC, S1, S2, S3 and S4, respectively) are present in the soils considered in this study. The existence of the O-H bond is due to the hygroscopic moisture, which is present in the samples both before and after the exposure to elevated temperatures, whereas the C-H and C-N bonds are mainly due to the presence of organic matter in the soil, which might be eliminated completely corresponding to  $\theta \geq 300^\circ\text{C}$ . However, it should be noted that complete removal of the C-H and C-N bonds occurs at temperatures higher than  $300^\circ\text{C}$ . The peaks in the FTIR plots, corresponding to the temperature range considered in this study, indicate 'flattening' (see Fig. 7), which represents the sequential removal of the C-H and C-N bonds.

## 7.8 X-RAY DIFFRACTION ANALYSIS

The six soil samples were exposed to  $300^\circ\text{C}$ , sequentially in steps of  $50^\circ\text{C}$ , and their XRD patterns are presented in Fig. 8. From these patterns it can be clearly observed that the peaks are shifted, towards the left, with an increase in the exposure temperature. This indicates a decrease in  $2\phi$  (where  $\phi$  is the angle of incidence of the X-rays) with an increase in temperature, which leads to a noticeable increase in the Full Width Half Maximum, *FWHM* and *d*-spacing (in Å). According to Bragg's law ( $\lambda = 2d \cdot \sin\phi$ ), the *d*-spacing has an inverse relation with  $2\phi$ , where  $\lambda$  is the wavelength and *d* is the lattice spacing.

It should be noted that the shift in the peaks and the change in the *d*-spacing (refer Table 9) are indications of the structural transformation(s) in the soil due to its exposure to elevated temperatures [65]. Furthermore, from Fig. 8, it can be seen that the peak position  $2\phi$  is different for various types of soils. However, the soils with the same mineralogy (viz., Soils S2 and S3) exhibit similar peaks as well as a similar shift in peaks with respect to the temperature. It should also be noted that the intensities (peak areas) of the different peaks, for a mineral, commonly vary due to the specific structural and compositional effects of the unit cell on the diffracted beam of the X-ray. Hence, due to an increase in temperature there is an increase in the thermal vibration of the lattice, which can be attributed to a decrease in the intensity of the diffracted beam [66]. These changes in the crystallographic characteristics strongly influence the physical and chemical properties of the soil. Thus, the changes in *d*-spacing can be attributed to the expansion of the minerals due to the exposure of the soil to elevated temperatures.

## 7.9 LINEAR EXPANSION

It can be observed from the trends shown in Fig. 1 that with an increase in temperature,  $\theta$ , the *PLE* either decreases (a negative value corresponds to shrinkage) or increases (a positive value corresponds to expansion), depending upon the soil type. The Soils BT, S1, S2 and S3 exhibit shrinkage, which could be attributed to a reduction in the double layer, due to a loss of hygroscopic moisture, from the soils containing montmorillonite as active minerals. In contrast, the Soils S4 and WC, containing passive minerals (viz., quartz and kaolinite), exhibit expansion due to heating. It is worth mentioning here that the hygroscopic moisture, which is the water held tightly on the surface of soil particles (due to the presence of active minerals), does not evaporate at normal temperatures [67].

Table 9. The *d*-spacings of various samples at elevated temperatures.

$\theta$ ( $^\circ$ )	<i>d</i> -spacing (nm)					
	BT	WC	S1	S2	S3	S4
30	0.197373	0.358977	0.335119	0.337032	0.339574	0.334133
50	0.197344	0.359352	0.335226	0.337191	0.339729	0.334166
100	0.197457	0.359623	0.33543	0.337381	0.339932	0.334382
150	0.197544	0.359958	0.335621	0.337523	0.340088	0.334499
200	0.197587	0.360226	0.335873	0.337826	0.340334	0.334717
250	0.197678	0.360693	0.336159	0.338061	0.340675	0.335048
300	0.197559	0.360843	0.336405	0.338402	0.340904	0.335307



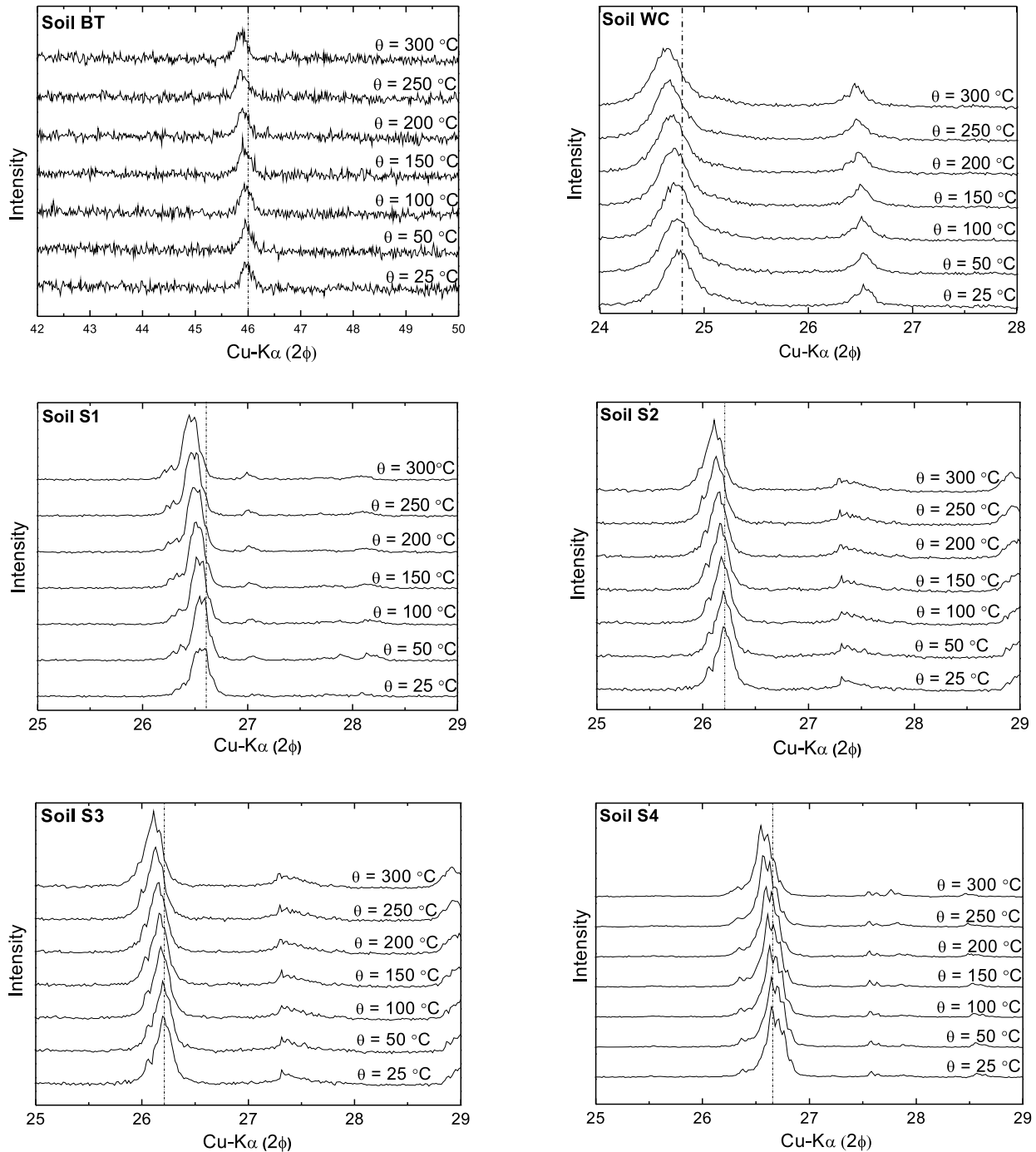


Figure 8. X-Ray Diffractograms of the investigated soils heated at different temperatures.

## 7.10 THERMO GRAVIMETRIC ANALYSIS (TGA)

The results of the TGA for different soil samples in an inert atmosphere (i.e., nitrogen gas,  $N_2$ ) are depicted in

Fig. 9. The samples were subjected to a thermal treatment only up to 300°C, in view of the fact that even in deep geological formations (repositories) the rise in temperature will not exceed 300°C. From the trends shown in Fig. 9, it is clear that at 50°C, as expected, no

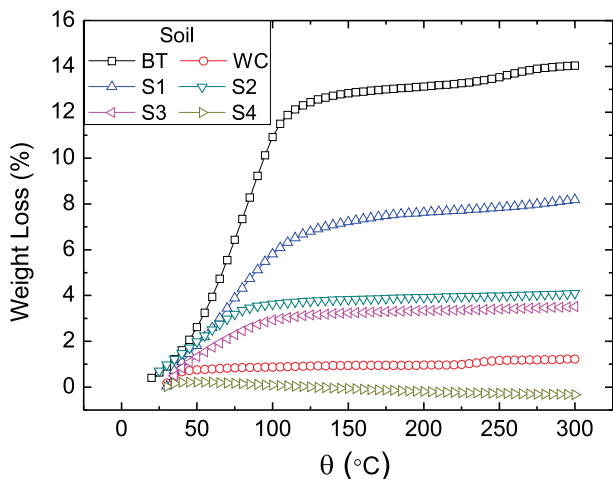


Figure 9. Variation of the weight loss of the investigated soils with temperature.

appreciable change in the weight of the soil is observed except for the soil BT. This can be attributed to the fact that the thermal energy corresponding to this temperature is not sufficient to cause a significant weight loss of the soil sample. However, a very rapid weight loss in the soil sample was observed corresponding to 50–100°C, which can be attributed to the loss of weakly bonded hygroscopic moisture content, sorbed on the soil particles. While, between 100 to 300°C, a steady weight loss was observed, which might be attributed to the loss of the adsorbed water from the interlayer (containing cations) of the soil particles. Incidentally, it can also be observed from the figure that the weight loss for  $\theta > 150^\circ\text{C}$  is almost constant, except for the Soil S4, due to its mineralogy and particle size.

In general, Fig. 9 substantiates the fact that the loss of weight is much more for the Soil BT than for its counterparts, which could be attributed to the presence of a higher clay fraction and active minerals (as listed in Tables 1 and 5) that would result in a larger hygroscopic moisture content [67]. Usually, a loss in weight of the soil sample can be attributed to the escape of volatiles and moisture, when  $\text{N}_2$  (inert atmosphere) is used for combustion. Thus, the loss of weight of these soils can be attributed to a release of moisture and the oxidation of carbon compounds present in them. Incidentally, the Soil WC, though it contains a higher percentage of clay, exhibits a low percentage of weight loss due to the presence of the passive mineral (Kaolinite, refer Table 5). Furthermore, Soil S4 (i.e., the fine sand) exhibits a smaller percentage of the weight loss due to its passive nature as listed in Table 5 (viz., the presence of the passive mineral, quartz) and the negligible percentage of clay content.

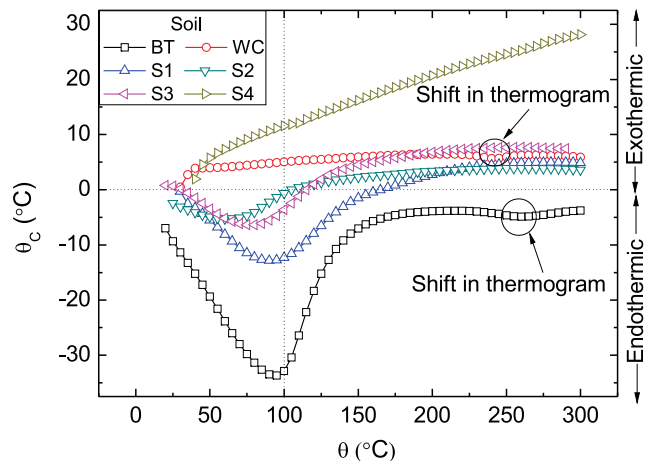


Figure 10. Variation of the temperature difference between the reference material and the soils at elevated temperatures.

## 7.11 DIFFERENTIAL THERMAL ANALYSIS (DTA)

The results obtained from the *DTA* for the soils in an inert atmosphere (with  $\text{N}_2$ ) are plotted as a variation in temperature with respect to the reference material (i.e., Alumina), designated as  $\theta_c$ , versus the exposure temperature,  $\theta$ , as shown in Fig. 10. It can be seen from this figure that the combustion of the soil may result in both exothermic as well as endothermic reactions, due to the physical and chemical changes occurring in it. In general, for soils, endothermic reactions occur due to dehydration, dehydroxylation, structural decomposition, sintering and melting, or evaporation and sublimation, whereas exothermic reactions may occur due to oxidation/burning of the organic matter, iron oxidation, or the crystallization of amorphous material [68]. In this context, it can be seen from Fig. 10 that the Soils BT, S1, S2 and S3 exhibit a more endothermic reaction as compared to their counterparts (viz., Soils WC and S4). This can be attributed to the lower heat-holding capacity of the Soils WC and S4, which exhibit a lower percentage weight loss as compared to their counterparts (see Fig. 9). Furthermore, Soils BT and S1 exhibit an endothermic reaction (i.e., heat absorption) up to 100°C due to the presence of hygroscopic moisture and thereafter a reduction in the endothermic reaction due to the loss of moisture. According to Barshad [69], the removal of the crystal lattice water (dehydroxylation) causes a complete destruction of the mineral structure and hence the dehydration reactions are endothermic. Furthermore, a slight shift from the regular trend has been observed in the thermogram of the Soils BT and WC, as shown in Fig. 10. This reveals the structural change undergone

by the crystal structure of these soils at  $\theta \approx 250^\circ\text{C}$ , which can be observed by a large shift in the peaks at  $250^\circ\text{C}$ , as shown in Fig. 8. The structural changes can also be attributed to the process of drying, which results in the shrinkage (refer Fig. 1) and formation of fissures that could introduce thermal resistance in the fine-grained soils. Furthermore, the fragmentation of these soils leads to the generation of air gaps, which is responsible for a decrease in the thermal conductivity.

## CONCLUSIONS

Based on a critical synthesis of the results and the discussion presented in the preceding sections, the following can be concluded.

1. The change in the color of the soil for  $\theta \leq 250^\circ\text{C}$  can be attributed to the depletion of the organic matter, while for  $\theta > 250^\circ\text{C}$  the same can be attributed to increased oxidation and chemical changes, except for the soil WC.
2. An increase in the specific gravity and a decrease in the specific surface area of the soil, due to its exposure to elevated temperatures, was observed. This can be attributed to a depletion in the moisture and agglomeration of the fine organic matter present in the soil.
3. It has been observed that, except for the soils with passive minerals, the clay-sized fraction decreases, while the silt-sized fraction increases with an increase in temperature. This further substantiates the fact that the exposure of the soil to elevated temperatures results in an increase in its particle size.
4. The decrease in the specific surface area of the soil can be further substantiated by an increase in its particle size due to its exposure to elevated temperatures. This phenomenon was demonstrated by laser scanning diffraction analyses.
5. A reduction in exchangeable cations and a loss of organic matter results in a decrease in the cation-exchange capacity of the soils when they are exposed to higher temperatures.
6. A reduction in the zeta-potential of the soil has been noted due to its exposure to elevated temperatures.
7. The study demonstrates that with an increase in exposure temperature, there is a change in the lattice spacing, which indicates structural transformation. These changes in the crystallographic characteristics strongly influence the physical and chemical properties of the soil.
8. It has been observed that with an increase in temperature, the soils containing passive minerals (viz., quartz and kaolinite), exhibit an expansion. In

contrast, soils containing active minerals (viz., montmorillonite) shrink, due to the loss of hygroscopic moisture.

In the authors' opinion, these changes to the soil properties, due to the exposure to elevated temperatures, would be quite important and crucial for designing various structures (viz., liners of waste landfills and cores of the dams, which are primarily constructed from fine-grained soils, treatment and the stabilization of highly contaminated soils and dredged sediments, the stabilization of weak foundation soils, the construction of roads and airfields, based on thermal stabilization).

## REFERENCES

- [1] Li, Y., Wang, L. and Liu, L. (2011). Study on constructional reinforcement for the foundation of blast furnace due to temperature effect. *International Conference on Civil Engineering and Transportation, ICCET*, Vol. 94-96, pp. 1545-1548.
- [2] Gangadhara Rao, M.V.B.B. and Singh, D.N. (1999). A generalized Relationship to Estimate Thermal Resistivity of Soils. *Canadian Geotechnical Journal*, Vol. 36, No. 4, pp. 767-773.
- [3] Varlakov, A., Sobolev, I., Barinov, A., Dmitriev, S., Karlin, S. and Flit, V. (1997). Method of treatment of radioactive silts and soils. Proceedings of the MRS Fall Meeting, Moscow, Russia, *Materials Research Society*, Pittsburgh, PA, pp. 591-594.
- [4] Farag, I. (1993). Simulating hazardous waste incineration. *Chemical Engineer*, Issue-538, pp. 11-16.
- [5] Ma, C. and Hueckel, T. (1992). Stress and pore pressure in saturated clay subjected to heat from radioactive waste: a numerical simulation. *Canadian Geotechnical Journal*, Vol. 29, pp. 1087-1094.
- [6] Alcocer, C. and Chowdhury, H. (1993). Experimental study of an environmental remediation of Gulf Coast crude-oil contaminated soil using low temperature thermal treatment. *Proceedings of the Western Regional Meeting, Louisiana, Society of Petroleum Engineers*, Richardson, pp. 723-724.
- [7] Akinmusuru, J. (1994). Thermal conductivity of earth blocks. *Journal of Materials in Civil Engineering*, Vol. 6, No. 3, pp. 341-351.
- [8] Joshi, R., Achari, G.C., Horsfield, D. and Nagaraj, T. (1994). Effect of heat treatment on strength of clays. *Journal of Geotechnical Engineering*, Vol. 120, No. 6, pp. 1080-1088.
- [9] Yang, L. and Farouk, B. (1995). Modelling of solid particles flow and heat transfer in rotary kiln calciners. *Proceedings of the 30<sup>th</sup> National Heat*

- Transfer Conference*, Portland, Oregon, American Society of Mechanical Engineers, New York, NY, pp. 11-19.
- [10] Krishnaiah, S. and Singh, D.N. (2006). Determination of Thermal Properties of Soils in a Geotechnical Centrifuge. *Journal of Testing and Evaluation*, ASTM, Vol. 34, No. 4, pp. 1-8.
- [11] Litvinov, I.M. (1906). Stabilization of settling and weak clayey soils by thermal treatment. *Highway research board special report 60*, National Research Council, Washington, DC, pp. 94-112.
- [12] Mitchell, J.K. (1969). Temperature effects on the engineering properties and behavior of soils. *Highway Research Board Special Report 103*, Washington, DC, pp. 9-28.
- [13] Ketterings, Q.M., Bigham, J.M. and Laperrche, V. (2000). Changes in soil mineralogy and texture caused by slash and burn fires in Sumatra, Indonesia. *Soil Science Society of American Journal*, Vol. 64, pp. 1108-1117.
- [14] Ulery, A.L. and Graham, R.C. (1993). Forest fire effects on soil color and texture. *Soil Science Society of American Journal*, Vol. 57, pp. 135-140.
- [15] Sertsu, S.M. and Sanchez, P.A. (1978). Effects of heating on some changes in soil properties in relation to an Ethiopian land management practice. *Soil Science Society of American Journal*, Vol. 42, pp. 940-944.
- [16] Fernandez, I., Cabaneiro, A. and Carballas, T. (1997). Organic matter changes immediately after a wildfire in an Atlantic forest soil comparison with laboratory soil heating. *Soil Biology Biochemistry*, Vol. 29, pp. 1-11.
- [17] Yilmaz, G. (2011). The effects of temperature on the characteristics of Kaolinite and Bentonite. *Academic Journals, Scientific Research and Essays*, Vol. 6, No. 9, pp. 1928-1939.
- [18] Utkaeva, V. F. (2007). Specific surface area and wetting heat of different soil types in European Russia. ISSN 1064-2293, *Eurasian Soil Science*, Pleiades Publishing, Ltd., Vol. 40, No. 11, pp. 1193-1202.
- [19] Abu-Zreig, M.M., Al-Akhras, N.M. and Attom, M.F. (2001). Influence of heat treatment on the behavior of clayey soils. *Applied Clay Science*, Vol. 20, pp. 129-135.
- [20] Tan, O., Yilmaz, L. and Zaimoglu, A.S. (2004). Variation of some engineering properties of clays with heat treatment. *Materials Letters*, Vol. 58, No. 7-8, pp. 1176-1179.
- [21] Sultan, N., Delage, P. and Cui, Y.J. (2002). Temperature effects on the volume change behavior of Boom clay. *Engineering Geology*, Vol. 64, pp. 135-145.
- [22] Parlak, M. (2011). Effect of heating on some physical, chemical and mineralogical aspects of forest soil. *Bartın Orman Fakultesi Dergisi*, Cilt: 13, Sayı, 19, pp. 143-152.
- [23] Ghuman, B.S. and Lal, R. (1989). Soil temperature effects of biomass burning in windrows after clearing a tropical rainforest. *Field Crops Research*, Vol. 22, pp. 1-10.
- [24] Certini, G. (2005). Effects of fire on properties of forest soils. *A review of Oecologia*, Vol. 143, pp. 1-10.
- [25] Hatten, J., Zabowski, D., Scherer, G. and Dolan, E.A. (2005). Comparison of soil properties after contemporary wildfire and fire suppression. *Forest Ecology and Management*, Vol. 220, No. 1-3, pp. 227-241.
- [26] Moritz, L. and Gabriellsson, A. (2000). Temperature effect on the properties of clay. *Soft ground Technology conference*, ASCE, pp. 304-314.
- [27] Tanaka, N., Graham, J. and Crilly, T. (1997). Stress-strain behaviour of reconstituted illitic clay at different temperatures. *Engineering Geology*, Vol. 47, pp. 339-350.
- [28] Zhang, Y., Miao, L., and Wang, F. (2011). Study on the engineering properties of the stabilized mucky clay as backfill material in highway embankment projects. *Geo-Frontiers 2011: Advances in Geotechnical Engineering*, ASCE, pp. 1365-1371.
- [29] Booker, J.R., and Savvidou, C., (1985). Consolidation Around a point heat source. *International Journal of Numerical and Analytical Methods in Geomechanics*, Vol. 9, pp. 173-184.
- [30] Varlakov, A., Sobolev, I., Barinov A., Dmitriev S., Karlin S., Flit V. (1997). Method of Treatment of Radioactive Silts and Soils. *Proceedings of the MRS Fall Meeting*, Moscow, Russia, Materials Research Society, Pittsburgh, PA, 591-594.
- [31] ASTM D 5550-06, Standard test method for specific gravity of soil solids by gas pycnometer. *Annual Book of ASTM Standard*, 04.08, ASTM, Philadelphia, USA.
- [32] ASTM D 422-63, Standard test method for particle size analysis of soils. *Annual Book of ASTM Standards*, 04.08, ASTM, Philadelphia, USA, 1994.
- [33] Eshel, G., Levy, G.J, Mingelgrin, U. and Singer M.J. (2004). Critical evaluation of the use of laser diffraction for particle-size distribution analysis. *Soil Science Society American Journal*, Vol. 68, pp. 736-743.
- [34] Stanley, J.V. and Leon Y.S. (1997). Particle-size analysis of soils using laser light scattering and X-Ray absorption technology. *Geotechnical Testing Journal*, Vol. 20, No. 1, pp. 63-73.
- [35] Beverwijk, A. (1967). Particle size analysis of soils

- by means of the hydrometer method. *Sediment. Geol.*, Vol. 1, pp. 403-406.
- [36] Konert, M., and Vandenberghe, J. (1997). Comparison of laser grain size analysis with pipette and sieve analysis: a solution for the underestimation of the clay fraction. *Sedimentology*, Vol. 44, pp. 523-535.
- [37] Bah, A.R., Kravchuk, O., and Kirchhof, G. (2009). Fitting performance of particle-size distribution models on data derived by conventional and laser diffraction techniques. *Soil Science Society America Journal*, Vol. 73, pp. 1101-1107.
- [38] Shanthakumar, S., Singh, D.N. and Phadke, R.C. (2010). Methodology for Determining Particle-Size Distribution Characteristics of Fly Ashes. *Journal of Materials in Civil Engineering*, ASCE, VOL. 22(5), pp. 435-442.
- [39] ASTM D 4318-93, Standard test method liquid limit, plastic limit and plasticity index of soils. *Annual Book of ASTM Standards*, 04.08, ASTM, Philadelphia, USA, 1994.
- [40] ASTM D 427, Test Method for shrinkage factors of soils by the mercury method. *Annual Book of ASTM Standards*, 04.08, ASTM, Philadelphia, USA.
- [41] ASTM D 2487-10, Standard practice for classification of soils for engineering purposes (Unified Soil Classification System). *Annual Book of ASTM Standards*, 04.08, ASTM, Philadelphia, USA.
- [42] Carter, D.L., Mortland, M.M. and Kemper, W.D. (1986). Specific Surface-Methods of Soil Analysis, *American Society of Agronomy*, USA, pp. 412-423.
- [43] Cerato, A.B. and Lutenegeger, A.J. (2002). Determination of surface area of fine grained soils by the ethylene glycol mono-ethyl ether (EGME) method. *Geotechnical Testing Journal*, ASTM, Vol. 25, No. 3, pp. 1-7.
- [44] Arnepalli, D.N., Shanthakumar, S., Hanumantha, Rao, B. and Singh, D.N. (2008). Comparison of methods for determining specific-surface area of fine-grained soils. *Geotech Geol Eng*, Vol. 26, pp. 121-132.
- [45] Kyziol, J., (2002). Effect of physical properties and cation exchange capacity on sorption of heavy metals onto peats. *Journal of Environmental Studies*, Vol. 11(6), pp. 713-718.
- [46] Liu, X. and Lu, X. (2011). Correlation between Bentonite's Cation Exchange Capacity (CEC) activated clay quality indexes and activation strength. *Applied Mechanics and Materials*, Vol. 99-100, pp. 1031-1034.
- [47] IS 2720 Part XXIV (1976). Methods of test for soils determination of cation exchange capacity. *Indian Standards Institute*, New Delhi, India.
- [48] Sparks, D.L. (1986). *Soil Physical Chemistry*, CRC Press, Boca Raton
- [49] West, L.J. and Stewart, D.L. (1995). Effect of zeta potential on soil electrokinesis. *Proceedings of Geoenvironment*, ASCE Special Publication, pp. 1535-1549.
- [50] Vane, L.M. and Zhang, G.M. (1997). Effects of aqueous phase properties on clay particle zeta potential and electro-osmotic permeability: Implications for electro kinetic soil remediation processes. *Journal of Hazardous Materials*, Vol. 55, No. 1-3, pp. 1-22.
- [51] Yukselen, Y. and Kaya, A. (2003). Zeta potential of Kaolinite in the presence of alkali, alkaline earth and hydrolyzable metal ions. *Journal of Water, Air and Soil Pollution*, Vol. 145, No. 1-4, pp. 155-168.
- [52] Kaya, A., Oren, A.H. and Yukselen, Y. (2003). Settling behaviour and zeta potential of Kaolinite in aqueous media. *Proceedings of the Thirteenth International Offshore and Polar Engineering Conference Honolulu*, Hawaii, USA, pp. 407- 412.
- [53] Kaya, A. and Yukselen, Y. (2005). Zeta potential of clay minerals and quartz contaminated by heavy metals. *Canadian Geotechnical Journal*. Vol. 42, No. 5, pp. 1280-1289.
- [54] Cox, R.J., Peterson, H.L., Young, J., Cusik, C. and Espinoza, E.O. (2000). The forensic analysis of soil organic by FTIR. *Forensic science International*, Vol. 108, pp. 107-116.
- [55] Ivan, S., Pavel, D., Stefan, D.H., Mataix-Solera, J. and Vlasta, S. (2008). Thermal destruction of soil water repellency and associated changes to soil organic matter as observed by FTIR spectroscopy. *Catena*, Vol. 74, pp. 205-211.
- [56] JCPDS (1994). Power diffraction file, 44, 7354-CD ROM (PDF 1-44), International Centre for Diffraction Data, Pennsylvania
- [57] Young, R.A. (2002). *The Rietveld Method*. International Union of Crystallography, *Oxford University Press*, New York, NY, USA.
- [58] Young, R.A., Larson, A.C., and Paiva-Santos, C.O. (2000). User's guide to program DBWS-9807a for Rietveld analysis of X-ray and neutron powder diffraction patterns. *Georgia Institute of Technology*, Atlanta, GA, USA.
- [59] Grim, R. E., and Rowland, R. A. (1944). Differential thermal analysis of clays and shales, control and prospecting method. *American Ceramic Society Journal*, Vol. 27, pp. 65-76.
- [60] Allaway, W. H. (1948). Differential thermal analyses of clays treated with organic cations as an aid in the study of soil colloids. *Soil Science Society of America Proc*, Vol. 13, pp. 183-188.

- [61] Kampf, N., Scheinost, A.C. and Schulze, D.G. (2000). Oxide minerals. In: M.E. Sumner (Ed.), *Handbook of Soil Science*, CRC Press: Boca Raton, Fl., pp. 125-165.
- [62] Schwertmann, U. (1984). The double dehydroxylation peak of goethite, *Thermochimica Acta*, Vol. 78, No. 1-3, pp. 39-46.
- [63] Altınbaş, U. (1982). A study of the some properties of the raw material used in the ceramic industry at different temperatures. *Review of the Faculty of Agriculture*, University of Ege, Vol. 460, pp. 1-40.
- [64] Chorom, M. and Rengasamy, P. (1996). Effect of heating on swelling and dispersion of different cationic forms of a smectite. *Clay and Clay Minerals*, Vol. 44, No. 6, pp. 783-790.
- [65] Khameneh, A.S., Heydarzadeh, S.M. and Hadavi, S.M.M. (2004). The Effect of the Heat Treatment on Residual Stresses in HVOF Sprayed WC-Co Coating. *Materials Science Forum*, Vol. 465, No. 466, pp. 427-432.
- [66] Cullity, B.D. and Stock, S.R. (2001). *Elements of X-Ray Diffraction*. 3<sup>rd</sup> Ed., Prentice-Hall Inc., ISBN 0-201-61091-4, pp. 167-171.
- [67] Shah, P.H. and Singh, D.N. (2006). Methodology for Determination of Hygroscopic Moisture Content of Soils. *Journal of ASTM International*, Vol. 3, No. 2, pp. 1-14.
- [68] Smykatz-Kloss, W., (1982). Application of differential thermal analysis in mineralogy. *Journal of Thermal Analysis*, Vol. 23, No. 1-2, pp. 15-44.
- [69] Barshad, I. (1995). Thermal analysis techniques for mineral identification and mineralogical composition. *Methods of soil analysis, Agronomy*, American Society of Agronomy, Madison, Wisc. No. 9, Chapter 50.

# NAVODILA AVTORJEM

## VSEBINA ČLANKA

Članek naj bo napisan v naslednji obliki:

- Naslov, ki primerno opisuje vsebino članka in ne presega 80 znakov.
- Izvleček, ki naj bo skrajšana oblika članka in naj ne presega 250 besed. Izvleček mora vsebovati osnove, jedro in cilje raziskave, uporabljeno metodologijo dela, povzetek izidov in osnovne sklepe.
- Največ 6 ključnih besed, ki bi morale biti napisane takoj po izvlečku.
- Uvod, v katerem naj bo pregled novejšega stanja in zadostne informacije za razumevanje ter pregled izidov dela, predstavljenih v članku.
- Teorija.
- Eksperimentalni del, ki naj vsebuje podatke o postavitvi preiskusa in metode, uporabljene pri pridobitvi izidov.
- Izidi, ki naj bodo jasno prikazani, po potrebi v obliki slik in preglednic.
- Razprava, v kateri naj bodo prikazane povezave in posplošitve, uporabljene za pridobitev izidov. Prikazana naj bo tudi pomembnost izidov in primerjava s poprej objavljenimi deli.
- Sklepi, v katerih naj bo prikazan en ali več sklepov, ki izhajajo iz izidov in razprave.
- Vse navedbe v besedilu morajo biti na koncu zbrane v seznamu literature, in obratno.

## DODATNE ZAHTEVE

- Vrstice morajo biti zaporedno oštevilčene.
- Predložen članek ne sme imeti več kot 18 strani (brez tabel, legend in literature); velikost črk 12, dvojni razmik med vrsticami. V članek je lahko vključenih največ 10 slik. Isti rezultati so lahko prikazani v tabelah ali na slikah, ne pa na oba načina.
- Potrebno je priložiti imena, naslove in elektronske naslove štirih potencialnih recenzentov članka. Urednik ima izključno pravico do odločitve, ali bo te predloge upošteval.

## ENOTE IN OKRAJŠAVE

V besedilu, preglednicah in slikah uporabljajte le standardne označbe in okrajšave SI. Simbole fizikalnih veličin v besedilu pišite poševno (npr.  $v$ ,  $T$  itn.). Simbole enot, ki so sestavljene iz črk, pa pokončno (npr. Pa, m itn.). Vse okrajšave naj bodo, ko se prvič pojavijo, izpisane v celoti.

## SLIKE

Slike morajo biti zaporedno oštevilčene in označene, v besedilu in podnaslovu, kot sl. 1, sl. 2 itn. Posnete naj

bodo v katerem koli od razširjenih formatov, npr. BMP, JPG, GIF. Za pripravo diagramov in risb priporočamo CDR format (CorelDraw), saj so slike v njem vektorske in jih lahko pri končni obdelavi preprosto povečujemo ali pomanjšujemo.

Pri označevanju osi v diagramih, kadar je le mogoče, uporabite označbe veličin (npr.  $v$ ,  $T$  itn.). V diagramih z več krivuljami mora biti vsaka krivulja označena. Pomen oznake mora biti razložen v podnaslovu slike.

Za vse slike po fotografskih posnetkih je treba priložiti izvirne fotografije ali kakovostno narejen posnetek.

## PREGLEDNICE

Preglednice morajo biti zaporedno oštevilčene in označene, v besedilu in podnaslovu, kot preglednica 1, preglednica 2 itn. V preglednicah ne uporabljajte izpisanih imen veličin, ampak samo ustrezne simbole. K fizikalnim količinam, npr.  $t$  (pisano poševno), pripišite enote (pisano pokončno) v novo vrsto brez oklepajev. Vse opombe naj bodo označene z uporabo dvignjene številke<sup>1</sup>.

## SEZNAM LITERATURE

### navedba v besedilu

Vsaka navedba, na katero se sklicujete v besedilu, mora biti v seznamu literature (in obratno). Neobjavljeni rezultati in osebne komunikacije se ne priporočajo v seznamu literature, navedejo pa se lahko v besedilu, če je nujno potrebno.

### oblika navajanja literature

**V besedilu:** Navedite reference zaporedno po številkah v oglatih oklepajih v skladu z besedilom. Dejanski avtorji so lahko navedeni, vendar mora obvezno biti podana referenčna številka.

Primer: »..... kot je razvidno [1,2]. Brandl and Blovsky [4], sta pridobila drugačen rezultat...«

**V seznamu:** Literaturni viri so oštevilčeni po vrstnem redu, kakor se pojavijo v članku. Označimo jih s številkami v oglatih oklepajih.

*Sklicevanje na objave v revijah:*

- [1] Desai, C.S. (2007). Unified DSC constitutive model for pavement materials with numerical implementation. *Int. J. of Geomech.*, Vol. 7, No. 2, pp. 83-101.

*Sklicevanje na knjigo:*

- [2] Šuklje, L. (1969). Rheological aspects of soil mechanics. Wiley-Interscience, London

Sklicevanje na poglavje v monografiji:

- [3] Mettam, G.R., Adams, L.B., 1999. How to prepare an electronic version of your article, in: Jones, B.S., Smith, R.Z. (Eds.), *Introduction to the Electronic Age*. E-Publishing Inc., New York, pp. 281–304.

Sklicevanje na objave v zbornikih konferenc:

- [4] Brandl, H. and Blovsky, S. (2005). Slope stabilization with socket walls using the observational method. *Proc. Int. conf. on Soil Mechanics and Geotechnical Engineering, Bratislava*, pp. 2485-2488.

Sklicevanje na spletne objave:

- [5] Kot najmanj, je potrebno podati celoten URL. Če so poznani drugi podatki (DOI, imena avtorjev, datumi, sklicevanje na izvirno literaturo), se naj prav tako dodajo.

## PODATKI O AVTORJIH

Članku priložite tudi podatke o avtorjih: imena, nazive, popolne poštno naslove, številke telefona in faksa,

naslove elektronske pošte. Navedite kontaktno osebo.

## SPREJEM ČLANKOV IN AVTORSKE PRAVICE

Uredništvo si pridržuje pravico do odločanja o sprejemu članka za objavo, strokovno oceno mednarodnih recenzentov in morebitnem predlogu za krajšanje ali izpopolnitev ter terminološke in jezikovne korekture. Z objavo preidejo avtorske pravice na revijo ACTA GEOTECHNICA SLOVENICA. Pri morebitnih kasnejših objavah mora biti AGS navedena kot vir.

Vsa nadaljnja pojasnila daje:

Uredništvo  
ACTA GEOTECHNICA SLOVENICA  
Univerza v Mariboru,  
Fakulteta za gradbeništvo  
Smetanova ulica 17, 2000 Maribor, Slovenija  
E-pošta: ags@uni-mb.si

# INSTRUCTIONS FOR AUTHORS

## FORMAT OF THE PAPER

The paper should have the following structure:

- A Title, which adequately describes the content of the paper and should not exceed 80 characters;
- An Abstract, which should be viewed as a mini version of the paper and should not exceed 250 words. The Abstract should state the principal objectives and the scope of the investigation and the methodology employed; it should also summarise the results and state the principal conclusions;
- Immediately after the abstract, provide a maximum of 6 keywords;
- An Introduction, which should provide a review of recent literature and sufficient background information to allow the results of the paper to be understood and evaluated;
- A Theoretical section;
- An Experimental section, which should provide details of the experimental set-up and the methods used to obtain the results;
- A Results section, which should clearly and concisely present the data, using figures and tables where appropriate;
- A Discussion section, which should describe the relationships shown and the generalisations made possible by the results and discuss the significance of the results, making comparisons with previously published work;

- Conclusions, which should present one or more conclusions that have been drawn from the results and subsequent discussion;
- A list of References, which comprises all the references cited in the text, and vice versa.

## Additional requirements for manuscripts

- Use double line-spacing.
- Insert continuous line numbering.
- The submitted text of Research Papers should cover no more than 18 pages (without Tables, Legends, and References, style: font size 12, double line spacing). The number of illustrations should not exceed 10. Results may be shown in tables or figures, but not in both of them.
- Please submit, with the manuscript, the names, addresses and e-mail addresses of four potential referees. Note that the editor retains the sole right to decide whether or not the suggested reviewers are used.

## UNITS AND ABBREVIATIONS

Only standard SI symbols and abbreviations should be used in the text, tables and figures. Symbols for physical quantities in the text should be written in *Italics* (e.g. *v*, *T*, etc.). Symbols for units that consist of letters should be in plain text (e.g. Pa, m, etc.). All abbreviations should be spelt out in full on first appearance.



## FIGURES

Figures must be cited in consecutive numerical order in the text and referred to in both the text and the caption as Fig. 1, Fig. 2, etc. Figures may be saved in any common format, e.g. BMP, JPG, GIF. However, the use of CDR format (CorelDraw) is recommended for graphs and line drawings, since vector images can be easily reduced or enlarged during final processing of the paper.

When labelling axes, physical quantities (e.g.  $v$ ,  $T$ , etc.) should be used whenever possible. Multi-curve graphs should have individual curves marked with a symbol; the meaning of the symbol should be explained in the figure caption. Good quality black-and-white photographs or scanned images should be supplied for the illustrations.

## TABLES

Tables must be cited in consecutive numerical order in the text and referred to in both the text and the caption as Table 1, Table 2, etc. The use of names for quantities in tables should be avoided if possible: corresponding symbols are preferred. In addition to the physical quantity, e.g.  $t$  (in Italics), units (normal text), should be added on a new line without brackets.

Any footnotes should be indicated by the use of the superscript<sup>1</sup>.

## LIST OF REFERENCES

### citation in text

Please ensure that every reference cited in the text is also present in the reference list (and vice versa). Any references cited in the abstract must be given in full. Unpublished results and personal communications are not recommended in the reference list, but may be mentioned in the text, if necessary.

### reference style

**Text:** Indicate references by number(s) in square brackets consecutively in line with the text. The actual authors can be referred to, but the reference number(s) must always be given:

Example: "... as demonstrated [1,2]. Brandl and Blovsky [4] obtained a different result ..."

**List:** Number the references (numbers in square brackets) in the list in the order in which they appear in the text.

### Reference to a journal publication:

- [1] Desai, C.S. (2007). Unified DSC constitutive model for pavement materials with numerical implementation. *Int. J. of Geomech.*, Vol. 7, No. 2, pp. 83-101.

### Reference to a book:

- [2] Šuklje, L. (1969). Rheological aspects of soil mechanics. Wiley-Interscience, London

### Reference to a chapter in an edited book:

- [3] Mettam, G.R., Adams, L.B. (1999). How to prepare an electronic version of your article, in: Jones, B.S., Smith, R.Z. (Eds.), *Introduction to the Electronic Age*. E-Publishing Inc., New York, pp. 281–304.

### Conference proceedings

- [4] Brandl, H. and Blovsky, S. (2005). Slope stabilization with socket walls using the observational method. *Proc. Int. conf. on Soil Mechanics and Geotechnical Engineering, Bratislava*, pp. 2485-2488.

### Web references:

- [5] As a minimum, the full URL should be given and the date when the reference was last accessed. Any further information, if known (DOI, author names, dates, reference to a source publication, etc.), should also be given.

## AUTHOR INFORMATION

The following information about the authors should be enclosed with the paper: names, complete postal addresses, telephone and fax numbers and E-mail addresses. Indicate the name of the corresponding author.

## ACCEPTANCE OF PAPERS AND COPYRIGHT

The Editorial Committee of the Slovenian Geotechnical Review reserves the right to decide whether a paper is acceptable for publication, to obtain peer reviews for the submitted papers, and if necessary, to require changes in the content, length or language.

On publication, copyright for the paper shall pass to the ACTA GEOTECHNICA SLOVENICA. The AGS must be stated as a source in all later publication.

For further information contact:

---

Editorial Board  
 ACTA GEOTECHNICA SLOVENICA  
 University of Maribor,  
 Faculty of Civil Engineering  
 Smetanova ulica 17, 2000 Maribor, Slovenia  
 E-mail: ags@uni-mb.si

## NAMEN REVIJE

Namen revije ACTA GEOTECHNICA SLOVENICA je objavljavanje kakovostnih teoretičnih člankov z novih pomembnih področij geomehanike in geotehnike, ki bodo dolgoročno vplivali na temeljne in praktične vidike teh področij.

ACTA GEOTECHNICA SLOVENICA objavlja članke s področij: mehanika zemljin in kamnin, inženirska geologija, okoljska geotehnika, geosintetika, geotehnične konstrukcije, numerične in analitične metode, računalniško modeliranje, optimizacija geotehničnih konstrukcij, terenske in laboratorijske preiskave.

Revija redno izhaja dvakrat letno.

## AVTORSKE PRAVICE

Ko uredništvo prejme članek v objavo, prosi avtorja(je), da prenese(jo) avtorske pravice za članek na izdajatelja, da bi zagotovili kar se da obsežno razširjanje informacij. Naša revija in posamezni prispevki so zaščiteni z avtorskimi pravicami izdajatelja in zanje veljajo naslednji pogoji:

### fotokopiranje

V skladu z našimi zakoni o zaščiti avtorskih pravic je dovoljeno narediti eno kopijo posameznega članka za osebno uporabo. Za naslednje fotokopije, vključno z večkratnim fotokopiranjem, sistematičnim fotokopiranjem, kopiranjem za reklamne ali predstavitvene namene, nadaljnjo prodajo in vsemi oblikami nedobičkonosne uporabe je treba pridobiti dovoljenje izdajatelja in plačati določen znesek.

Naročniki revije smejo kopirati kazalo z vsebino revije ali pripraviti seznam člankov z izvlečki za rabo v svojih ustanovah.

### elektronsko shranjevanje

Za elektronsko shranjevanje vsakršnega gradiva iz revije, vključno z vsemi članki ali deli članka, je potrebno dovoljenje izdajatelja.

## ODGOVORNOST

Revija ne prevzame nobene odgovornosti za poškodbe in/ali škodo na osebah in na lastnini na podlagi odgovornosti za izdelke, zaradi malomarnosti ali drugače, ali zaradi uporabe kakršnekoli metode, izdelka, navodil ali zamisli, ki so opisani v njej.

## AIMS AND SCOPE

ACTA GEOTECHNICA SLOVENICA aims to play an important role in publishing high-quality, theoretical papers from important and emerging areas that will have a lasting impact on fundamental and practical aspects of geomechanics and geotechnical engineering.

ACTA GEOTECHNICA SLOVENICA publishes papers from the following areas: soil and rock mechanics, engineering geology, environmental geotechnics, geosynthetic, geotechnical structures, numerical and analytical methods, computer modelling, optimization of geotechnical structures, field and laboratory testing.

The journal is published twice a year.

## COPYRIGHT

Upon acceptance of an article by the Editorial Board, the author(s) will be asked to transfer copyright for the article to the publisher. This transfer will ensure the widest possible dissemination of information. This review and the individual contributions contained in it are protected by publisher's copyright, and the following terms and conditions apply to their use:

### photocopying

Single photocopies of single articles may be made for personal use, as allowed by national copyright laws. Permission of the publisher and payment of a fee are required for all other photocopying, including multiple or systematic copying, copying for advertising or promotional purposes, resale, and all forms of document delivery.

Subscribers may reproduce tables of contents or prepare lists of papers, including abstracts for internal circulation, within their institutions.

### electronic storage

Permission of the publisher is required to store electronically any material contained in this review, including any paper or part of the paper.

## RESPONSIBILITY

No responsibility is assumed by the publisher for any injury and/or damage to persons or property as a matter of product liability, negligence or otherwise, or from any use or operation of any methods, products, instructions or ideas contained in the material herein.